D5.5 Agri-PV demonstrators testing programs: first year of activity

Symbiosyst

Horizon Europe EU project
Grant Agreement No. 101096352



Funded by the European Union

Views and opinions expressed are however those of the author(s) only and do not necessarily reflect those of the European Union or CINEA. Neither the European Union nor the granting authority can be held responsible for them. As of 5th of November 2026 this report has been submitted to the EC but its content has not been approved yet.

Document control sheet

Project	**SYMBIOSYST – Create a Symbiosis where PV and agriculture can have a mutually beneficial relationship**

Topic identifier	HORIZON-CL5-2022-D3-01-06
Grant Agreement N°	101096352
Coordinator	ACCADEMIA EUROPEA DI BOLZANO (EURAC)
Duration	01/01/2023 – 31/12/2026
Work package N°	WP5
Work package title	Demonstration of novel agri-PV solutions
Work package leader	EF SOLARE ITALIA
Task n°	5.4- 5.5
Task leader	EFSOLARE
Document title	Agri-PV demonstrators testing program: first year of activity
Lead Beneficiary	LAIMBURG
Dissemination level	PUBLIC
Authors	Stefano Modugno (LAIMBURG)
Contributors	Pietro Felici (EF solare), Ramon Salcedo (UPC), Barry Marrevjik van (KUBO)
Reviewer(s)	Maarten Hertog (KUL)
Issue date	30/04/2026

Acknowledgements

The work described in this publication has received funding from the European Union Horizon Europe research and innovation program under grant agreement Nº 101096352.

Disclaimer

This work may rely on data from sources external to the members of the SYMBIOSYST project Consortium. Members of the Consortium do not accept liability for loss or damage suffered by any third party as a result of errors or inaccuracies in such data. The information in this document is provided “as is” and no guarantee or warranty is given that the information is fit for any particular purpose. The user thereof uses the information at its sole risk, and no member of the SYMBIOSYST Consortium shall be liable for any use that may be made of the information.

Executive Summary

The SYMBIOSYST project, funded by the European Commission under the Horizon Europe Programme, aims to advance the integration of photovoltaic (PV) systems into agricultural environments by developing tailored agri-PV solutions capable of simultaneously supporting renewable energy production and agricultural productivity. The project focuses on both greenhouse and open-field applications, with demonstrators implemented in Italy, Spain and in the Netherlands to test these solutions under diverse climatic and agronomic conditions. The installations support both vegetable crops and fruit production systems, combining conventional and innovative training approaches with PV modules mounted on adjustable tracking structures. During the initial phase of the project, extensive work was carried out to define the technical specifications required for the design and deployment of the demonstrators. In parallel, advanced modelling tools were developed to support the effective integration of PV systems into agricultural systems. These modelling activities addressed both open-field agri-PV configurations and greenhouse applications, with particular attention to optimizing module placement, height, and tracking strategies in order to balance energy generation with crop performance. The integration approaches were designed to be applicable to both newly established systems and existing agricultural infrastructures.
Following the completion of the design and modelling phase, the construction and commissioning of the agri-PV demonstrators in Bolzano (Italy) and in Barcelona (Spain) were successfully completed during 2025 in accordance with the predefined technical specifications. Their commissioning marked the transition from design to implementation, enabling the start of field monitoring and validation activities. SYMBIOSYST project also includes demonstrator located in Scalea (Italy), already built by EF Solare Italia S.p.A (partner of the project). Within the scope of this initiative, in this demo, the tracking system was upgraded—through EF Solare's own budget, independent from the Symbiosyst funding—thanks to the installation of new, more efficient and higher-power bifacial photovoltaic modules.

Tasks 5.4 and 5.5, described in this deliverable, focus on demonstrating and monitoring the innovative agri-PV solutions developed in WP2 and WP3, following installation activities conducted under Task 5.3. Between months 24 and 36 of the project (2025), an extensive monitoring campaign was carried out to evaluate environmental conditions, crop performance, and energy production within the demonstrators. The collected data will contribute to validating and refining the models developed in WP2 and will provide essential inputs for the use case analyses in WP7. Monitoring activities will continue until the end of the project (month 48), ensuring the collection of multi-season data necessary to assess the long-term agronomic and technical performance of the agri-PV systems.

At the Scalea demonstrator (Italy), the tracker-based system with bifacial modules confirmed reliable energy production and continuous off-grid operation. From an agronomic standpoint, lemon trees cultivated beneath the PV structures showed no signs of reduced performance compared to the open field. Key physiological indicators — including leaf area, stomatal conductance, and leaf water potential — all pointed to improved plant water status under partial shading, while photosynthetic efficiency remained comparable between the two systems. Soil moisture dynamics were more stable beneath the agrivoltaic canopy, and the automated matric-potential-based irrigation protocol contributed to improved water use efficiency across the season.

At the Bolzano demonstrator (Italy), the first year of monitoring of an apple orchard integrated with PV structures revealed a significant modification of the orchard microclimate, with clear effects on soil water dynamics and fruit quality. Soil moisture monitoring indicated slower drying rates and prolonged water availability under the panels, suggesting potential gains in water use efficiency. However, tree-level yield was approximately 15% lower under agri-PV conditions, driven primarily by a reduced number of fruits per tree. Fruit quality analyses showed reduced red coloration, lower soluble solids content, higher acidity, and delayed starch degradation, suggesting that shading may induce a delay in physiological maturity rather than a direct impairment of plant health. Future campaigns will aim to disentangle the effects of shading on fruit maturation from those related to phenological shifts induced prior to PV installation.

At the Barcelona demonstrator (Spain), lettuce crops grown under opaque panels, semi-transparent panels, and open-field control conditions reached comparable final values at harvest across all evaluated parameters, including plant height, biomass, and architectural indicators. Although some differences emerged at intermediate growth stages, these were not maintained at harvest, suggesting that lettuce is capable of compensating for differences in incident radiation within the range of conditions tested. These results indicate that agrivoltaic shading did not substantially alter crop development patterns or commercial quality under the evaluated conditions, though further seasonal campaigns will be needed to confirm the robustness of these findings.

At the Schipluiden demonstrator (The Netherlands), investigations focused on greenhouse-integrated PV systems and the quantification of shading effects on crop light availability. As no crops were cultivated within the demonstrator, all agronomic assessments are fully model-driven. PV-induced shading was found to be measurable, predictable, and linearly scalable with panel density. Diffuse glass significantly improved light uniformity and modelling reliability, while clear glass increased total PAR but introduced undesirable variability. Modelling based on Daily Light Integral (DLI) indicated expected yield reductions of 4–15% depending on crop type and PV density, though LED supplementation was found capable of fully compensating DLI deficits when properly configured. These findings suggest that PV densities of 6–12% are technically feasible within greenhouse systems, provided that diffuse glass is adopted and LED strategies are tailored to crop-specific light requirements.

Table of contents

Document control sheet 2

Acknowledgements 3

Disclaimer 3

Executive Summary 4

Table of contents 6

Table of Figures 8

List of tables 13

1. Introduction 14

1.1. Description of the Deliverable Contents 14

1.2. Abbreviation List 15

2. Agri-PV demonstrator - Bolzano (IT) 17

2.1. Site description and experimental design 17
Agri-PV system layout and treatments 17
Auxiliary systems and agronomic management and monitoring 20

Hail-Net protection 24

2.2. Results of the first year of activity 28
Physiological traits 28
Pimprenelle analysis for internal quality analysis 37
AWETA optical fruit grader for apple fruit quality 41
Yield 42
Meteorological data-analysis 54
Soil water status and irrigation efficiency assessment 59

2.3. Conclusion and Perspectives 61

3. Agri-PV demonstrator – Barcelona (SP) 62

3.1. Site description and experimental design 62
Location of the experiment 62
Pilot plant plot 62
Laboratories 64
Description of the photovoltaic panels 64
Microclimate monitoring 65
Plant material 67
Experimental layout 68
Structure of the subplots 68
Arrangement of beds and replication blocks 70
Experiment management 71
Plot and facility preparation 71
Planting and management of plant material 73
Growth evolution and monitoring 75
Biomass measurements 77

Fresh weight 77
Dry weight 78

3.2. Results of the first year of activity *80*
Vertical crop development 81
Diameters and plant architecture 88
Biomass production 101

3.3. Conclusion and Perspectives *107*

4. Agri-PV demonstrator - Scalea (IT) **108**

4.1. Site description and experimental design *108*
Experimental design 108

4.2. Results of the first year of activity *112*
Behaviour of the Agrivoltaic System from the Electrical and Energy Perspective 112
Agricultural results 113

4.3. Conclusion and Perspectives *118*

5. Agri-PV demonstrator - Schipluiden (NL) **119**

5.1. Site description and experimental design *119*
Demonstrator Setup (Lotsweg Greenhouse) 119
Monitoring, Data Collection & Methodology 120

5.2 Results of the first year of activity *121*
Light Entry Analysis (First-Year Results) 121
Spatial Radiation Distribution (Zone-Based Analysis) 124
Crop Impact and Modelling Approach 125
LED Supplementation and Compensation Strategies 127

5.2. Conclusions and Perspectives *129*

Table of Figures

Figure 2.1 Agri-PV demonstrator in Bolzano (IT). 17
Figure 2.2 New plant sector with multileader (guyot) training system. 19
Figure 2.3 Bifacial 80 HC PV modules semi-transparent modules by Aleo in the Bolzano's demonstrator. 19
Figure 2.4 Schematic layout of the agri-PV demonstrator in Bolzano and its sectors. 20
Figure 2.5 Spatial arrangement of reference and agri-PV monitoring stations at the Bolzano site, including sensor positions for agricultural and photovoltaic components. 22
Figure 2.6 Netafim MegaNet™ 15D 23
Figure 2.7 Schematic layout of the anti-frost irrigation system. Red dots denote the pre-existing sprinkler locations, whereas green dots identify the newly installed sprinklers. 23
Figure 2.8 Anti-frost system installed in the Bolzano demonstrator. 24
Figure 2.9 Hail nets installed in the new plant orchard in Bolzano demo 25
Figure 2.10 Layout of the irrigation system, showing the subdivision of the orchard into five irrigation zones. 27
Figure 2.11 (1) ELMED TSN Tensiometer installed; (2) Milesight UC 511 controller; (3) Irritec solenoid valve installed in the Bolzano demonstrator. 28
Figure 2.12 Illustrates the distribution of mean shoot length per tree across treatments. Each point represents the average shoot length of an individual tree, while boxplots summarise variability among trees within each treatment. 29
Figure 2.13 Illustrates the distribution of the sum of shoot length per tree across treatments. Each point represents the sum of the shoot length of an individual tree, while boxplots summarise variability among trees within each treatment. 30
Figure 2.14 Representative scanned apple leaves used for the determination of leaf area. Leaves were arranged on a flat contrasting background and digitally acquired prior to image analysis. 31
Figure 2.15 Specific Leaf Area (SLA, $cm^2\ g^{-1}$) across treatments: Control (C), Inter-row (I), and Under-panel (P). Boxplots represent the interquartile range, the horizontal line indicates the median, and points represent individual composite samples (each sample consisting of 10 leaves). Different letters indicate statistically significant differences among treatments according to Tukey's post-hoc test ($p < 0.05$). 32
Figure 2.16 Pimprenelle II machine for quality analysis. 34
Figure 2.17 Apple slices treated with Lugol for the starch test. 35
Figure 2.18 Boxplot of starch index across the treatments. Control (C), Inter-row (I), and Under-panel (P). Boxes represent the interquartile range, the horizontal line indicates the median, and points represent individual fruit measurements. 36
Figure 2.19 The distribution of SSC values across treatments. Control (C), Inter-row (I), and Under-panel (P). Boxes represent the interquartile range, the horizontal line indicates the median, and points represent individual fruit measurements. 38
Figure 2.20 The distribution of fruit firmness values across treatments. Control (C), Inter-row (I), and Under-panel (P). Boxes represent the interquartile range, the horizontal line indicates the median, and points represent individual fruit measurements 39
Figure 2.21 The distribution of acidity values (malic acid g/L) across treatments. Control (C), Inter-row (I), and Under-panel (P). Boxes represent the interquartile range, the horizontal line indicates the median, and each point corresponds to one sample mean (n = 4 per treatment). 40
Figure 2.22 Boxplot of fruit number (n) at tree level. Control (C), Inter-row (I), and Under-panel (P). Boxes represent the interquartile range, the horizontal line indicates the median, and points represent tree-level mean values. 43

Figure 2.23 Boxplot of the mean fruit weight (g). Boxes represent the interquartile range, the horizontal line indicates the median, and points represent tree-level mean values. Control (C), Inter-row (I), and Under-panel (P)..... 44
Figure 2.24 Scatter plot showing the relationship between fruit number per tree and mean fruit weight (g) for each treatment (C = control, I = inter-row, P = panel-row). Lines represent linear regression fits with 95% confidence intervals. 46
Figure 2.25 Boxplot of the mean fruit diameter (mm). Boxes represent the interquartile range, the horizontal line indicates the median, and points represent tree-level mean values. Control (C), Inter-row (I), and Under-panel (P)..... 47
Figure 2.26 Boxplot of the tree-level yield (kg/tree). Boxes represent the interquartile range, the horizontal line indicates the median, and points represent tree-level mean values. Control (C), Inter-row (I), and Under-panel (P)..... 49
Figure 2.27 Boxplot of the tree-level mean blush area (% of fruit surface red coloured area). Boxes represent the interquartile range, the horizontal line indicates the median, and points represent tree-level mean values. Control (C), Inter-row (I), and Under-panel (P). 50
Figure 2.28 Boxplot of the tree-level mean blush color (index indicating the intensity of the red color). Boxes represent the interquartile range, the horizontal line indicates the median, and points represent tree-level mean values. Control (C), Inter-row (I), and Under-panel (P). 52
Figure 2.29 Boxplot of the tree-level mean fruit density. Boxes represent the interquartile range, the horizontal line indicates the median, and points represent tree-level mean values. Control (C), Inter-row (I), and Under-panel (P)..... 53
Figure 2.30 Seasonal temperature throughout the growing season summary in the multileader (newerplant) section. C = control, P5 = plant under the panels with 5% transparency, I5= plants in the inter-row between panels with 5% transparency, P40 = plants under the panels with 40% transparency, I40= plants in the inter-row between panels with 40% transparency)..... 55
Figure 2.31 Daily ΔTmean time series in the multileader (newerplant) section. C = control, P5 = plant under the panels with 5% transparency, I5= plants in the inter-row between panels with 5% transparency, P40 = plants under the panels with 40% transparency, I40= plants in the inter-row between panels with 40% transparency)..... 55
Figure 2.32 Daily temperature anomalies (ΔT) relative to the Control R1 were computed and compared across treatments using the Kruskal-Wallis test followed by Dunn's post-hoc test with Bonferroni correction. 56
Figure 2.33 Seasonal temperature throughout the growing season summary in the spindle (olderplant) section. C = control, P = plant under the panels, I= plants in the inter-row between panels. 57
Figure 2.34 Daily ΔTmean time series in the Spindle (olderplant) section. C = control, P = plant under the panels, I= plants in the inter-row between panels. 57
Figure 2.35 Daily temperature anomalies (ΔT) relative to the Control R1 were computed and compared across treatments using the Kruskal-Wallis test followed by Dunn's post-hoc test with Bonferroni correction. 58
Figure 2.36 Soil water tension dynamics (mbar) for the control (C), inter-row (I), and under-panel (P) treatments. 60
Figure 3.1 Aerial view of Agropolis (left) and facilities (right). 63
Figure 3.2 Agrivoltaic pilot plant at Agropolis. 63
Figure 3.3 Laboratory facilities at Agropolis (a) and EEABB–UPC (b) 64
Figure 3.4 Photovoltaic panel arrangements with different transparency levels: (a) 40 % transmittance and (b) 5 % transmittance..... 65
Figure 3.5 Environmental sensing in the agrivoltaic plots: (a) PAR radiation measurement; (b) soil monitoring at crop level. 66
Figure 3.6 Mobile robot operating under the agrivoltaic structure (left); RGB-based scene analysis of crop rows (right). 67

Figure 3.7 Crop cultivation at Agropolis to evaluate the performance of two lettuce varieties and one broccoli variety within an agrivoltaic system: a) Randomized experimental plots; b) close-up of the Maravilla lettuce variety; c) close-up of the broccoli crop. 68
Figure 3.8 Experimental layout of crop rows across agrivoltaic sections and open-field control for the summer (a) and autumn (b) 2025 cropping cycles, showing the spatial distribution of evaluated and non-evaluated crop rows, crop species and cultivars, and the relative position of the photovoltaic structures within each section. 69
Figure 3.9 Organization of crop rows for the two single blocks of the summer cycle (a) and one representative block of the autumn cycle (b). 71
Figure 3.10 Plot preparation under the agrivoltaic structure: (a) mechanized soil tillage and bed formation using conventional tractor operations; (b) final arrangement of prepared beds with mulching installed beneath the photovoltaic structure. 72
Figure 3.11 Installation of perimeter fencing for crop protection around the agrivoltaic structure. 73
Figure 3.12 Transplanting work: a) alignment and spacing of seedlings along mulched crop rows and b) placement of seedlings within the prepared beds. 74
Figure 3.13 Sampling organization according to cropping cycles, for the two available block types in the summer cycle (a) and one representative block of the autumn cycle (b). 76
Figure 3.14 Field measurements during a crop monitoring session. 77
Figure 3.15 On-site fresh weight determination of harvested lettuce. 78
Figure 3.16 Post-harvest handling and sample preparation of lettuce and broccoli for laboratory analysis. 78
Figure 3.17 Equipment used for weight determination: a) precision balance for weight measurements and b) forced-air drying oven with labelled samples. 79
Figure 3.18 Mean plant height at the end of the summer cycle for Lettuce (cv. Francesca) under opaque panels (blue), semi-transparent panels (red), and open-field conditions (green). Different letters indicate significant differences between sampling dates within the same treatment (Tukey's test, $p < 0.05$). 81
Figure 3.19 Mean plant height at the end of the autumn cycle for lettuce (cv. Francesca) under opaque panels (blue), semi-transparent panels (red), and open-field conditions (green). Bars express standard deviations. Letters indicate homogeneous groups obtained by the Tukey's test ($p < 0.05$). 82
Figure 3.20 Mean relative height growth at mid-cycle of the summer season for Lettuce (cv. Francesca) under opaque panels (blue), semi-transparent panels (red), and open-field conditions (green). Bars express standard deviations. Letters indicate homogeneous groups obtained by the Tukey's test ($p < 0.05$). 82
Figure 3.21 Mean relative height growth at mid-cycle of the autumn season for Lettuce (cv. Francesca) under opaque panels (blue), semi-transparent panels (red), and open-field conditions (green). Bars express standard deviations. Letters indicate homogeneous groups obtained by the Tukey's test ($p < 0.05$). 83
Figure 3.22 Mean plant height at the end of the autumn cycle for lettuce (cv. Maravilla) under opaque panels (blue), semi-transparent panels (red), and open-field conditions (green). Bars express standard deviations. Letters indicate homogeneous groups obtained by the Tukey's test ($p < 0.05$). 83
Figure 3.23 Mean plant height at the end of the autumn cycle for lettuce (cv. Maravilla) under opaque panels (blue), semi-transparent panels (red), and open-field conditions (green). Bars express standard deviations. Letters indicate homogeneous groups obtained by the Tukey's test ($p < 0.05$). 84
Figure 3.24 Relative height growth at mid-cycle of the autumn season for lettuce (cv. Maravilla) under opaque panels (blue), semi-transparent panels (red), and open-field conditions (green). Bars express standard deviations. Letters indicate homogeneous groups obtained by the Tukey's test ($p < 0.05$). 85
Figure 3.25 Relative height growth at mid-cycle of the autumn season for lettuce (cv. Maravilla) under opaque panels (blue), semi-transparent panels (red), and open-field conditions (green). Bars express standard deviations. Letters indicate homogeneous groups obtained by the Tukey's test ($p < 0.05$). 86
Figure 3.26 Mean plant height at the end of the autumn cycle for broccoli under opaque panels (blue), semi-transparent panels (red), and open-field conditions (green). Bars express standard deviations. Bars express standard deviations. Letters indicate homogeneous groups obtained by the Tukey's test ($p < 0.05$). 87

Figure 3.27 Relative height growth at mid-cycle of the autumn season for broccoli under opaque panels (blue), semi-transparent panels (red), and open-field conditions (green). Bars express standard deviations. Letters indicate homogeneous groups obtained by the Tukey's test ($p < 0.05$). 88
Figure 3.28 Mean maximum diameter at the end of the summer cycle for Lettuce (cv. Francesca) under opaque panels (blue), semi-transparent panels (red), and open-field conditions (green). Bars express standard deviations. Letters indicate homogeneous groups obtained by the Tukey's test ($p < 0.05$). 89
Figure 3.29 Mean maximum diameter at the end of the autumn cycle for Lettuce (cv. Francesca) under opaque panels (blue), semi-transparent panels (red), and open-field conditions (green). Bars express standard deviations. Letters indicate homogeneous groups obtained by the Tukey's test ($p < 0.05$). 89
Figure 3.30 Mean minimum diameter at the end of the summer cycle for Lettuce (cv. Francesca) under opaque panels (blue), semi-transparent panels (red), and open-field conditions (green). Bars express standard deviations. Letters indicate homogeneous groups obtained by the Tukey's test ($p < 0.05$). 90
Figure 3.31 Mean minimum diameter at the end of the autumn cycle for Lettuce (cv. Francesca) under opaque panels (blue), semi-transparent panels (red), and open-field conditions (green). Bars express standard deviations. Letters indicate homogeneous groups obtained by the Tukey's test ($p < 0.05$). 91
Figure 3.32 Mean ratio between the maximum diameter and height at the end of the summer cycle for Lettuce (cv. Francesca) under opaque panels (blue), semi-transparent panels (red), and open-field conditions (green). Different letters indicate significant differences between sampling dates within the same treatment (Tukey's test, $p < 0.05$). 92
Figure 3.33 Mean ratio between the maximum diameter and height at the end of the autumn cycle for Lettuce (cv. Francesca) under opaque panels (blue), semi-transparent panels (red), and open-field conditions (green). Different letters indicate significant differences between sampling dates within the same treatment (Tukey's test, $p < 0.05$). 92
Figure 3.34 Mean maximum diameter at the end of the summer cycle for Lettuce (cv. Maravilla) under opaque panels (blue), semi-transparent panels (red), and open-field conditions (green). Bars express standard deviations. Letters indicate homogeneous groups obtained by the Tukey's test ($p < 0.05$). 94
Figure 3.35 Mean maximum diameter at the end of the autumn cycle for Lettuce (cv. Maravilla) under opaque panels (blue), semi-transparent panels (red), and open-field conditions (green). Bars express standard deviations. Letters indicate homogeneous groups obtained by the Tukey's test ($p < 0.05$). 95
Figure 3.36 Mean minimum diameter at the end of the summer cycle for Lettuce (cv. Maravilla) under opaque panels (blue), semi-transparent panels (red), and open-field conditions (green). Bars express standard deviations. Letters indicate homogeneous groups obtained by the Tukey's test ($p < 0.05$). 96
Figure 3.37 Mean minimum diameter at the end of the autumn cycle for Lettuce (cv. Maravilla) under opaque panels (blue), semi-transparent panels (red), and open-field conditions (green). Bars express standard deviations. Letters indicate homogeneous groups obtained by the Tukey's test ($p < 0.05$). 96
Figure 3.38 Mean ratio between the maximum diameter and height at the end of the autumn cycle for Lettuce (cv. Maravilla) under opaque panels (blue), semi-transparent panels (red), and open-field conditions (green). Bars express standard deviations. Letters indicate homogeneous groups obtained by the Tukey's test ($p < 0.05$). 97
Figure 3.39 Mean ratio between the maximum diameter and height at the end of the autumn cycle for Lettuce (cv. Maravilla) under opaque panels (blue), semi-transparent panels (red), and open-field conditions (green). Bars express standard deviations. Letters indicate homogeneous groups obtained by the Tukey's test ($p < 0.05$). 98
Figure 3.40 Mean maximum diameter at the end of the autumn cycle for broccoli under opaque panels (blue), semi-transparent panels (red), and open-field conditions (green). Bars express standard deviations. Letters indicate homogeneous groups obtained by the Tukey's test ($p < 0.05$). 99
Figure 3.41 Mean minimum diameter at the end of the autumn cycle for broccoli under opaque panels (blue), semi-transparent panels (red), and open-field conditions (green). Bars express standard deviations. Letters indicate homogeneous groups obtained by the Tukey's test ($p < 0.05$). 100

Figure 3.42 Mean ratio between the maximum diameter and height at the end of the autumn cycle in autumn cycle for broccoli under opaque panels (blue), semi-transparent panels (red), and open-field conditions (green). Bars express standard deviations. Letters indicate homogeneous groups obtained by the Tukey's test ($p < 0.05$)..... 101
Figure 3.43 Biomass at harvest of lettuce cultivars under the different radiation treatments evaluated during the summer cycle, shown separately for each treatment (i: opaque, ii: translucent, iii: open-field) for Maravilla (white) and Francesca (black). Values represent the mean biomass per group of ten lettuce plants. Bars express standard deviations. Letters indicate homogeneous groups obtained by the Tukey's test ($p < 0.05$)..... 102
Figure 3.44 Biomass at harvest of lettuce cultivars under the different radiation treatments evaluated during the autumn cycle, shown separately for each treatment (i: opaque, ii: translucent, iii: open-field) for Maravilla (white) and Francesca (black). Values represent the mean biomass per group of ten lettuce plants. Bars express standard deviations. Letters indicate homogeneous groups obtained by the Tukey's test ($p < 0.05$)..... 103
Figure 3.45 Fresh weight of lettuce cultivars under the different radiation treatments evaluated during the summer cycle, shown separately for each treatment (i: opaque, ii: translucent, iii: open-field) for Maravilla (white) and Francesca (black). Bars express standard deviations. Letters indicate homogeneous groups obtained by the Tukey's test ($p < 0.05$)..... 104
Figure 3.46 Fresh weight of lettuce cultivars under the different radiation treatments evaluated during the autumn cycle, shown separately for each treatment (i: opaque, ii: translucent, iii: open-field) for Maravilla (white) and Francesca (black). Bars express standard deviations. Letters indicate homogeneous groups obtained by the Tukey's test ($p < 0.05$)..... 105
Figure 3.47 Fresh weight of broccoli cultivars under the different control treatments evaluated during the autumn cycle (grey bars). Bars express standard deviations. Letters indicate homogeneous groups obtained by the Tukey's test ($p < 0.05$)..... 106
Figure 4.1 Lemon trees and lavender plants in the scalea demonstrator..... 111
Figure 4.2 Daily energy-production in the months October, November and December 2024..... 112
Figure 4.3 Power output from the inverters, battery charging behaviour and battery discharging behaviour onto the loads..... 113
Figure 4.4 PAR1 sensor installed close to trackers; Graph below - PAR2 Sensor in open field close to the demonstrator..... 114
Figure 4.5 Rainfall (blue lines) and moisture level at – 20 cm depth in the tracker based agri-PV demo (black line) and in the free filed area (purple line) (October – December 2024)..... 116
Figure 4.6 Rainfall (blue lines) and moisture level at – 20 cm depth in the tracker based agri-PV demo (black line) and in the free filed area (purple line) (7thto 14th December 2024)..... 117
Figure 5.1 Six control zones in the greenhouse.....120
Figure 5.2 Comparison between zone 1 and zone 2.....122
Figure 5.3 Comparison between zone 3 and 4.....123
Figure 5.4 Comparison between zone 5 and 6.....124

List of tables

Table 1.1. Abbreviation list 15
Table 2.1 Sensors installed on each station, used to characterise baseline microclimatic and soil conditions. 21
Table 2.2 Sensors dedicated to the monitoring of photovoltaic components and radiation balance within the agri-PV system. 21
Table 2.3 Sensors installed in the weather station (P0) providing site-level meteorological data. 21
Table 2.4 Sum of shoot grow at tree level (cm). Panel-row with low transparency (P5), panel-row with higher transparency (P40), inter-row with low transparency (I5), inter-row with higher transparency (I40), and a control treatment without photovoltaic panels (C). Different letters indicate significant differences among treatments (Tukey HSD, $p < 0.05$). 30
Table 2.5 Mean Specific Leaf Area (SLA) per treatment. Control (C), Inter-row (I), and Under-panel (P). Each sample represents 10 leaves. Different letters indicate significant differences among treatments (Tukey HSD, $p < 0.05$). 32
Table 2.6 For each treatment category (C, P, I), two rows (C1 and C2; P1 and P2; I1 and I2) were selected for analysis. From each row, two independent samples were collected, resulting in sample pairs such as C11 and C12 etc.). 35
Table 2.7 Mean starch index values and Tukey's HSD grouping. 37
Table 3.1 Chronology of experimental activities during the summer cycle 74
Table 3.2 Chronology of experimental activities during the autumn cycle. 74
Table 3.3 Mean crop compactness index of the Lettuce (cv. Francesca) cultivar by treatment and sampling time at the end of the summer cycle. 93
Table 3.4 Mean crop compactness index of the Lettuce (cv. Francesca) cultivar by treatment and sampling time at the end of the autumn cycle. 94
Table 3.5 Mean crop compactness index of the Lettuce (cv. Maravilla) cultivar by treatment and sampling time at the end of the summer cycle. 98
Table 3.6 Mean crop compactness index of the Lettuce (cv. Maravilla) cultivar by treatment and sampling time at the end of the autumn cycle. 99
Table 3.7 Mean crop compactness index of the broccoli cultivar by treatment and sampling time during the autumn cycle. 101
Table 3.8 Mean dry matter values of the lettuce cultivar by treatment and sampling time during the summer cycle. 106
Table 3.9 Mean dry matter values of the lettuce and broccoli cultivar by treatment and sampling time during the autumn cycle. 107
Table 4.1 Summary of the energy related quantities in SCALEA demonstrator. 109
Table 4.2 Electrical parameters acquired through the inverters. 109
Table 4.3 Agronomic sensor installed in the Scalea demonstrator. 111
Table 4.4 Envrionemntal parameters collected with the meteorological station in the Scalea demonstrator. 112

1. Introduction

1.1. Description of the Deliverable Contents

This deliverable (D5.5) presents the status of research activities conducted during the first year of operation of the Agri-PV demonstrators within the SYMBIOSYST project, as part of Work Package 5 (WP5). The main objective of WP5 is to demonstrate innovative agri-PV solutions developed by the project, with a particular focus on real-world implementation and performance assessment.

Previous deliverables (D5.1–D5.4) documented the progression from conceptual design to final project specifications (D5.1, D5.2), detailed the executive design (D5.3), and outlined the execution schedule for the demonstrators (D5.4). Building on these foundations, this deliverable focuses on the activities and results from the first year of demonstrator operation.

The report covers the implementation phase (2025) of the demonstrators located in Italy, the Netherlands, and Spain. Demonstrators in Italy and Spain were successfully installed and became fully operational, enabling the launch of research and monitoring activities.

For the Netherlands demonstrator, the structural and technical implementation was completed, and the demonstrator was the first equipped with operational sensor systems for light measurements and PV installation, actively generating data that has been made available for the project partners, without including preparations for cultivation of crops and crop performance data.

For the demonstrators in activity, a wide array of sensors and monitoring systems were deployed to monitor PV modules, electronic components, energy production and microclimatic conditions, facilitating comprehensive data collection and analysis throughout the first growing season. In parallel, detailed monitoring of environmental and physiological parameters related to the crops was carried out. The quality and quantity of agricultural yields were assessed and compared with control plots not covered by PV modules, in order to evaluate the impact of agri-PV systems on crop performance.

LAIMBURG evaluated for the Bolzano site the effects of PV panels on apple yield and quality, effects of PV panels on the microclimate within the apple orchard, the effects of PV panels on soil water content and the possibilities for combining PV modules with hail protection nets.

UPC implemented the Barcelona demonstrator, performing replicated crop trials and integrated agronomic–microclimatic monitoring to evaluate the impact of PV-mesh structures on crop growth, yield and physiological responses.

EF Solare operated and monitored the tracker-based agri-PV system in Scalea, analysing electrical performance together with PAR, microclimate, soil water dynamics, and crop physiological responses under off-grid conditions.

KUBO operated the greenhouse agri-PV demonstrator in Schipluiden, focusing on high-resolution PAR monitoring, analysis of PV-induced shading, and modelling of crop impacts and LED supplementation strategies.

The findings are organized into four dedicated chapters, each focusing on one demonstrator. These chapters provide an in-depth description of the experimental setup, monitoring strategies, and initial observations regarding crop development, yield quality and quantity, energy production and the influence of photovoltaic structures on the microclimate.

1.2. Abbreviation List

Table 1.1. Abbreviation list

Abbreviation	Meaning
ΔDLI	Deficit in Daily Light Integral
AC	Alternating Current
Agri-PV	Agriphotovoltaic system
ANCOVA	Analysis of Covariance
ANOVA	Analysis of Variance
BIPV	Building Integrated Photovoltaics
CI	Compactness Index
DLI	Daily Light Integral
EC	European Commission
EMMs	Estimated Marginal Means
ePAR	Extended Photosynthetically Active Radiation
EURAC	Eurac Research
FAO	Food and Agriculture Organization
GA	Grant Agreement
GHG	Greenhouse Gas
HSD	Honest Significant Difference
IEC	International Electrotechnical Commission
IES	Illuminating Engineering Society
IoT	Internet of Things
IPM	Integrated Pest Management
kPa	Kilopascal
kWp	Kilowatt peak
LED	Light Emitting Diode
LCA	Life Cycle Assessment
MPPT	Maximum Power Point Tracker
NIR	Near-Infrared
PAR	Photosynthetically Active Radiation
PAR_LED	Supplemental Photosynthetically Active Radiation provided by LEDs
PE	Polyethylene

POA	Plane of Array
PPFD	Photosynthetic Photon Flux Density
PT100	Platinum Resistance Temperature Sensor
PV	Photovoltaic
R&D	Research and Development
RH	Relative Humidity
SLA	Specific Leaf Area
SSC	Soluble Solids Content
TTN	The Things Network
UPC	Universitat Politècnica de Catalunya
VWC	Volumetric Water Content
WP	Work Package

2. Agri-PV demonstrator - Bolzano (IT)



Figure 2.1 Agri-PV demonstrator in Bolzano (IT).

2.1. Site description and experimental design

The agri-PV demonstrator in Ora (Bolzano) was successfully constructed during 2025, adhering to the planned characteristics specified in Deliverable 5.3. This open system is oriented north-south and consists of an elevated single axis Convert multifunctional trackers made of weathering steel, chosen for their durability and minimal visual impact (Figure 2.1). In the northern Italian climate, this type of single-axis solar tracking structure enhances energy production by 15-20 % compared to a fixed system with equivalent capacity. This improvement is achieved by optimizing the capture of direct solar irradiance on the PV module's surface throughout the day. **Each tracker is designed to accommodate 20 modules, organized into groups of 5 modules per span** (across 4 spans), and allows for a maximum rotation of ±55° for the PV modules. These 20 modules are arranged in 4 groups of 5 modules each, with each group separated by 0.15 meters. The rotation axis of the trackers is set at 4.78 meters, ensuring compatibility with agricultural machinery. With modules mounted in portrait orientation, the minimum clearance from the ground is approximately 3.8 meters, which has proven sufficient for standard orchard operations. No disruptions to agricultural practices were reported during the first year of activity. 200 PV modules from Aleo are installed in a 1P configuration. The nominal power of the plant is 74,6 kWp. The site covers an area of approximately 3,000 m² and is specifically designed to support the cultivation of the Ipador (Giga) apple variety grafted on dwarfing rootstocks (M9).

Agri-PV system layout and treatments

The Bolzano agri-photovoltaic demonstrator is divided into **four main sectors** as described below, each representing a distinct agronomic and structural configuration. Within the agri-PV areas, **two main treatment positions are defined:** under-panel (P), corresponding to tree rows located directly beneath the photovoltaic modules, and inter-row (I), corresponding to tree rows located between adjacent PV trackers and therefore subject to partial or indirect shading. These treatments allow for the evaluation of spatial variability in light availability and microclimatic conditions induced by the photovoltaic structures. The following four experimental sectors were defined:

Existing plant sector (spindle training system)

This area includes four rows of photovoltaic trackers, each equipped with 20 bifacial 120 HC PV modules with an estimated transparency of less than 10%, manufactured by Aleo. The trackers were installed above an **already established apple orchard planted in 2017 and trained according to the spindle system**. Tree rows located directly beneath the photovoltaic modules represent the under-panel (P) treatment, while tree rows positioned between adjacent trackers represent the inter-row (I) treatment. The spacing between the trackers is 6.4 m, matching the orchard spacing of 3.2 m, thus ensuring alignment between the photovoltaic infrastructure and the existing orchard layout. This sector allows the evaluation of agri-PV integration in a mature orchard under commercial production conditions.

New plant sector (multileader training system)

Prior to PV installation, a **new orchard section was planted in 2024 using the multileader (guyot) training system**, which promotes two-dimensional canopy development and reduces canopy width, making it particularly suitable for integration with photovoltaic structures. In this sector, the spacing between the trackers is 5 m, corresponding to an orchard spacing of 2.5 m, optimizing land use efficiency and light distribution *(Figure 2.2).*

The sector includes three rows of photovoltaic trackers, each equipped with 20 bifacial 120 HC PV modules. As in the existing plant sector, tree rows located directly beneath the trackers correspond to the under-panel (P) treatment, while tree rows located between trackers correspond to the inter-row (I) treatment. In addition, this sector includes 60 bifacial 80 HC semi-transparent PV modules with an estimated transparency of approximately 40 % by Aleo, allowing for a comparative assessment of different panel transparency levels and their effects on orchard performance (Figure 2.3).



Figure 2.2 New plant sector with multileader (guyot) training system.



Figure 2.3 Bifacial 80 HC PV modules semi-transparent modules by Aleo in the Bolzano's demonstrator.

Reference Areas (Control)

Adjacent to both agri-PV sectors, **reference areas without photovoltaic structures** were established and managed according to standard orchard practices. These plots represent the control treatment (C) and are

essential for comparing tree growth, yield, fruit quality, and microclimatic conditions under agri-PV systems with those of a conventional orchard (Figure 2.4).

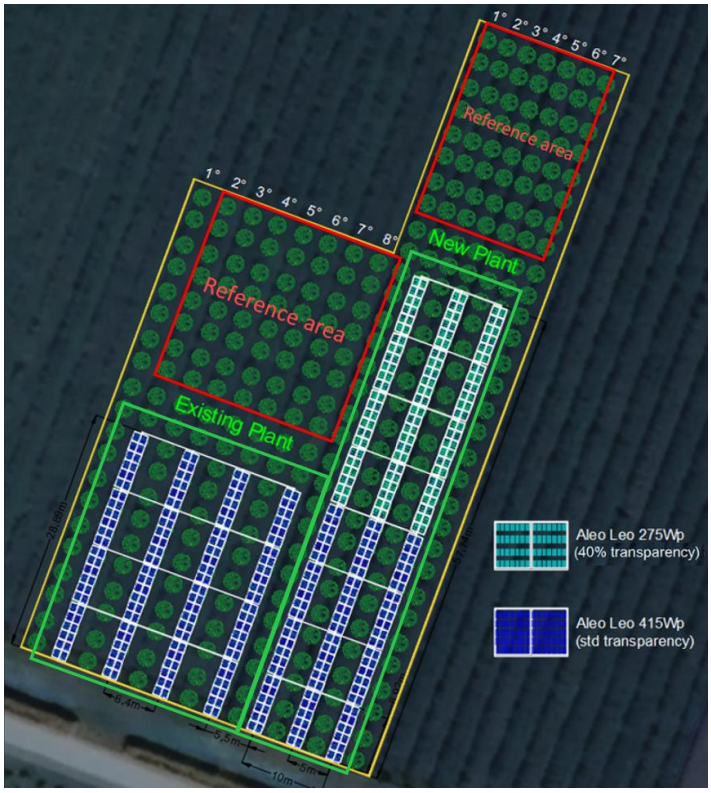

Figure 2.4 Schematic layout of the agri-PV demonstrator in Bolzano and its sectors.

Auxiliary systems and agronomic management and monitoring

Microclimatic monitoring (EURAC)

Microclimatic monitoring at the Bolzano agri-PV demonstrator was carried out by EURAC Research to characterize environmental conditions under varying shading configurations and to quantify the impact of photovoltaic structures on orchard microclimate and soil properties.
The monitoring system was designed to capture spatial variability across treatments and training systems and includes both reference stations located outside the PV-covered area and monitoring stations installed within the agri-PV structures.

Monitoring layout and station typology

The monitoring layout accounts for both the existing and the new orchard typologies present at the Bolzano site (Figure 2.5). Two reference stations (R1 and R2) are located in orchard areas not covered by PV modules, representing the control condition. In addition, three agri-PV monitoring stations (S1, S2 and S3) are installed within the tracker sections of the agri-PV system. **This configuration allows a direct comparison of microclimatic conditions between the treatments.**

Measured variables and sensors

The monitoring system covers **three main domains**: air, soil, and solar irradiance, with additional measurements related to the photovoltaic system. Sensors were selected to ensure accuracy, robustness, and compatibility with long-term field deployment. Sensors position in the field is represented in Figure 2.5.

Air and soil measurements (agricultural domain)

Air temperature, relative humidity, and dew point data were collected within the canopy zone to characterise plant-relevant microclimatic conditions. Soil temperature and volumetric water content were monitored to assess potential agronomic impacts of shading on soil thermal regime and water availability.
Photosynthetically active radiation (PAR) was measured using pyranometers positioned above and within the canopy to quantify light availability for photosynthesis under different treatments (Table 2.1).

Table 2.1 Sensors installed on each station, used to characterise baseline microclimatic and soil conditions.

Domain	Measured parameter	Sensor type	Accuracy
Air	Temperature	Polycarbonate probe with cable	±0.3 °C at 23 °C
Air	Relative humidity	Polycarbonate probe with cable	±2.5 % RH at 23 °C
Irradiance	PAR	Pyranometer	< 5 %
Soil	Temperature	NTC 10 kΩ @ 25 °C	±0.5 °C
Soil	Volumetric water content (VWC)	Capacitive sensor	±3 %

Photovoltaic-related measurements

In addition to agronomic variables, specific sensors were installed to monitor PV system performance and its interaction with the orchard microclimate (Table 2.2).

Table 2.2 Sensors dedicated to the monitoring of photovoltaic components and radiation balance within the agri-PV system.

Domain	Measured parameter	Sensor type
PV modules	Global irradiance on plane of array (G_POA)	Pyranometer (IEC 61724-1:2021, Class B)
PV modules	Albedo	Pyranometer (IEC 61724-1:2021, Class B)
PV modules	Module temperature	PT100 class B, 3/4-wire

Weather stations

A dedicated weather station (P0) complements the static monitoring network by providing general meteorological conditions for the site (Table 2.3).

Table 2.3 Sensors installed in the weather station (P0) providing site-level meteorological data.

Domain	Measured parameter	Sensor type	Accuracy
Air	Temperature	Thermometer	±0.3 °C at 23 °C
Air	Relative humidity	Hygrometer	±2.5 % RH at 23 °C

Air	Precipitation (type and quantity)	Radar-based sensor	–
Wind	Wind speed	Anemometer	>4 m s^{-1}; ±3 %

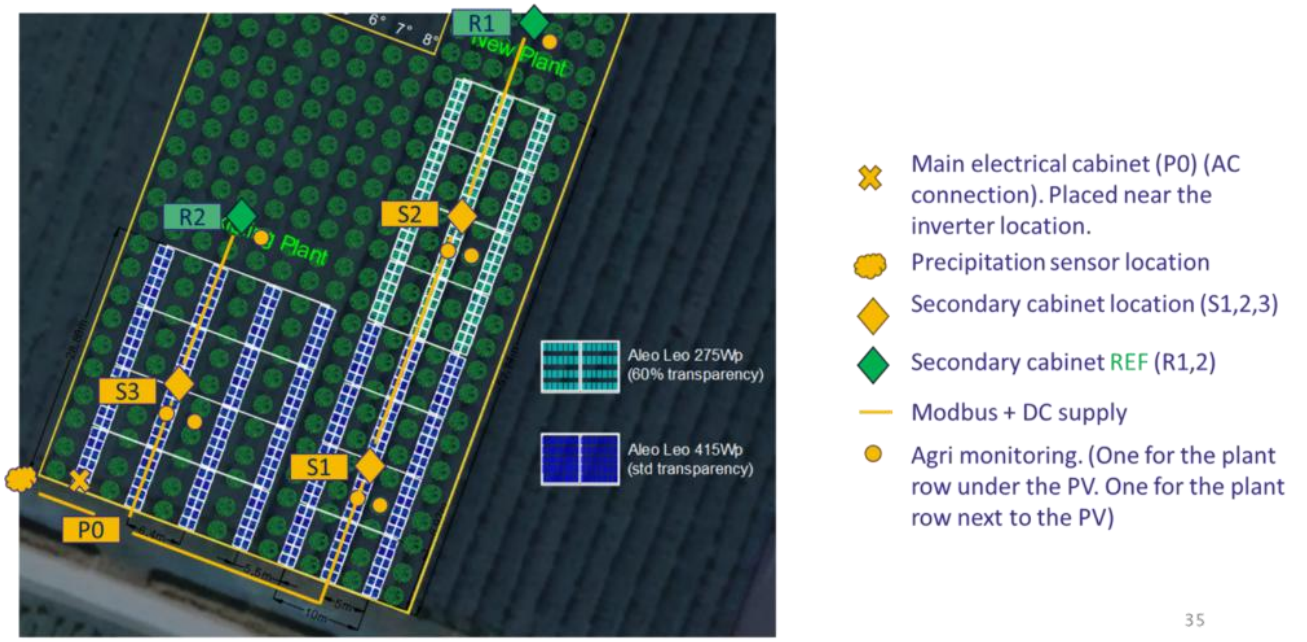

Figure 2.5 Spatial arrangement of reference and agri-PV monitoring stations at the Bolzano site, including sensor positions for agricultural and photovoltaic components.

Anti-frost system

The site of the demonstrator orchard is in a valley floor and therefore in an area prone to the risk of late spring frosts. Under such conditions the presence of an **anti-frost irrigation system is a prerequisite** for commercial apple production. Since the water delivered by the commonly used overhead sprinklers would be intercepted by the PV-modules, the demonstrator plots have been fitted with sprinklers characterized by a lower water trajectory and were installed in such a way that the water is emitted in the space between the treetops and the PV modules (Figure 2.7). The sprinkler used is the "Netafim Meganet 15D" (Figure 2.6), installed at a spacing of about 12 x 6 meters. Figure 2.8 shows the installation of the anti-frost system at the Bolzano demonstrator site.



Figure 2.6 Netafim MegaNet™ 15D

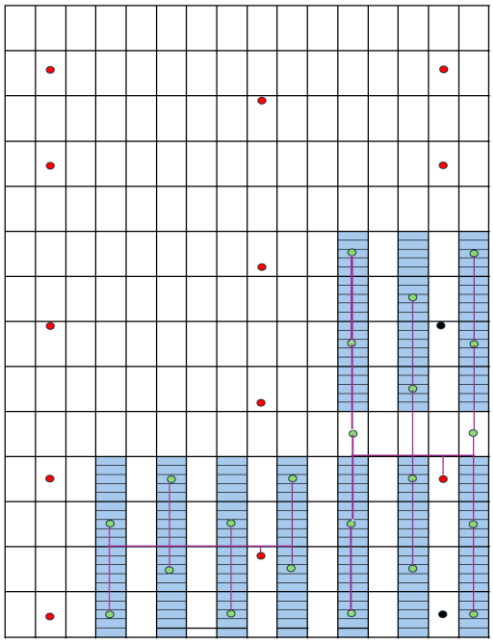

Figure 2.7 Schematic layout of the anti-frost irrigation system. Red dots denote the pre-existing sprinkler locations, whereas green dots identify the newly installed sprinklers.



Figure 2.8 Anti-frost system installed in the Bolzano demonstrator.

Hail-Net protection

In June 2025, **hail protection nets were installed** across all zones of the Bolzano agri-PV demonstrator (Figure 2.9). This integration was carried out without requiring any structural modifications to the existing photovoltaic system or its supporting infrastructure. The nets were mounted in a way that fully preserved the original design and functionality of the agri-PV installation. From a technical standpoint, the compatibility between the PV structures and the hail net system demonstrates the modularity and adaptability of the agri-PV design. The elevated tracker height (rotation axis at 4.78 m) and the spacing between rows allowed for the seamless installation of the nets without interfering with the movement of the panels or the passage of agricultural machinery.



Figure 2.9 Hail nets installed in the new plant orchard in Bolzano demo.

Irrigation and water managment

In June 2025, Laimburg, in collaboration with the local land authority (*Demanio*), designed and implemented the **irrigation system** for the Bolzano agri-PV demonstrator. This system addresses one of the key objectives of SYMBIOSYST: **evaluate potential water savings** in agri-PV systems compared to conventional orchards. The irrigation system has been divided into five independent zones (Figure 2.9), each representing a specific experimental condition:

- Zone 1: Newly planted orchard with PV modules (5 % transparency)
- Zone 2: Newly planted orchard with PV modules (40 % transparency)
- Zone 3: Newly planted orchard without PV modules (open-field control)
- Zone 4: Established orchard with PV modules (5 % transparency)
- Zone 5: Established orchard without PV modules (open-field control)

This zoning strategy enables comparative analysis of irrigation requirements and water-use efficiency under different shading conditions and plant development stages.

A 40 mm PE PN6 main distribution line runs along the entire field, positioned above the crop canopy and supported by the hail net structure (Figure 2.10). From this line, five 25 mm PE PN6 laterals branch off to supply each zone, crossing the field transversely and descending to ground level. Each lateral tube is equipped with an Irritec solenoid valve (Figure 2.11) (total number 5), controlled by a solar-powered Milesight UC511 IoT controller (total number 3), each one supporting up to two valves (Figure 2.11). From these laterals, 16 mm drip lines run along each crop row, ensuring localized water delivery, significantly reducing water loss due

to evaporation or runoff compared to traditional sprinkler systems. Drip irrigation is particularly well-suited for orchards, as it promotes efficient water use, minimizes weed growth, and reduces disease pressure by keeping foliage dry.

To monitor soil water status, two ELMED TNS tensiometers (Figure 2.11) were installed in each zone (total number 10): one under the PV panels and one in the inter-row without PV panels. These sensors measure soil suction tension, a direct indicator of water availability to roots. The TNS-03 model integrates a ceramic sensor tip, electronics, solar panel, and LoRa antenna. Data is transmitted periodically via LoRaWAN to the ELMED Cloud, accessible through a web dashboard and mobile app with graphical visualization tools. Unlike capacitive sensors, tensiometers require no calibration and are unaffected by soil composition, ensuring reliable long-term monitoring. The irrigation system operates dynamically based on soil moisture conditions. When suction tension exceeds approximately -300 mBar, the corresponding solenoid valve is activated for a predefined duration. Valve actuation is managed wirelessly via LoRaWAN protocol using The Things Network (TTN) infrastructure. Commands are sent as downlink messages from TTN to the Milesight controllers, enabling remote and automated irrigation scheduling without physical intervention. This architecture ensures low-power, long-range connectivity, ideal for agricultural environments with limited network coverage. These data are used to regulate irrigation cycles and quantify water consumption per sector throughout the growing season.

A custom dashboard developed by Laimburg integrates tensiometer data and valve control, allowing centralized management and real-time decision-making. This approach supports the evaluation of potential water savings under the agri-PV system compared to the open-field control, as well as the assessment of soil drying rates and water retention under both conditions. The objective is to determine whether the agri-PV configuration contributes to prolonged soil moisture persistence and improved water-use efficiency.

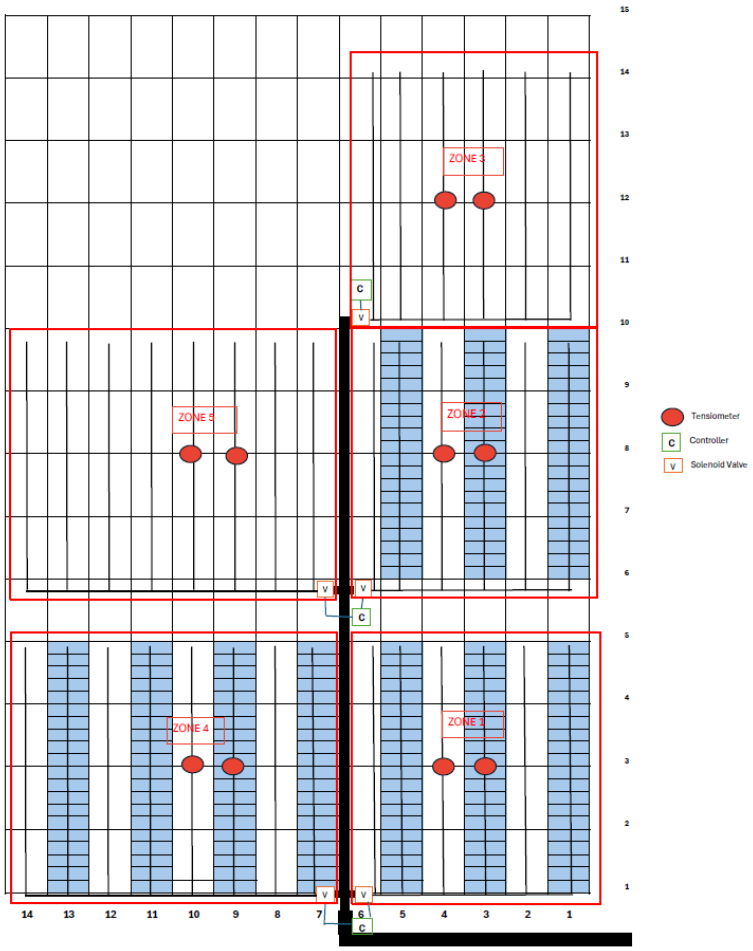

Figure 2.10 Layout of the irrigation system, showing the subdivision of the orchard into five irrigation zones.

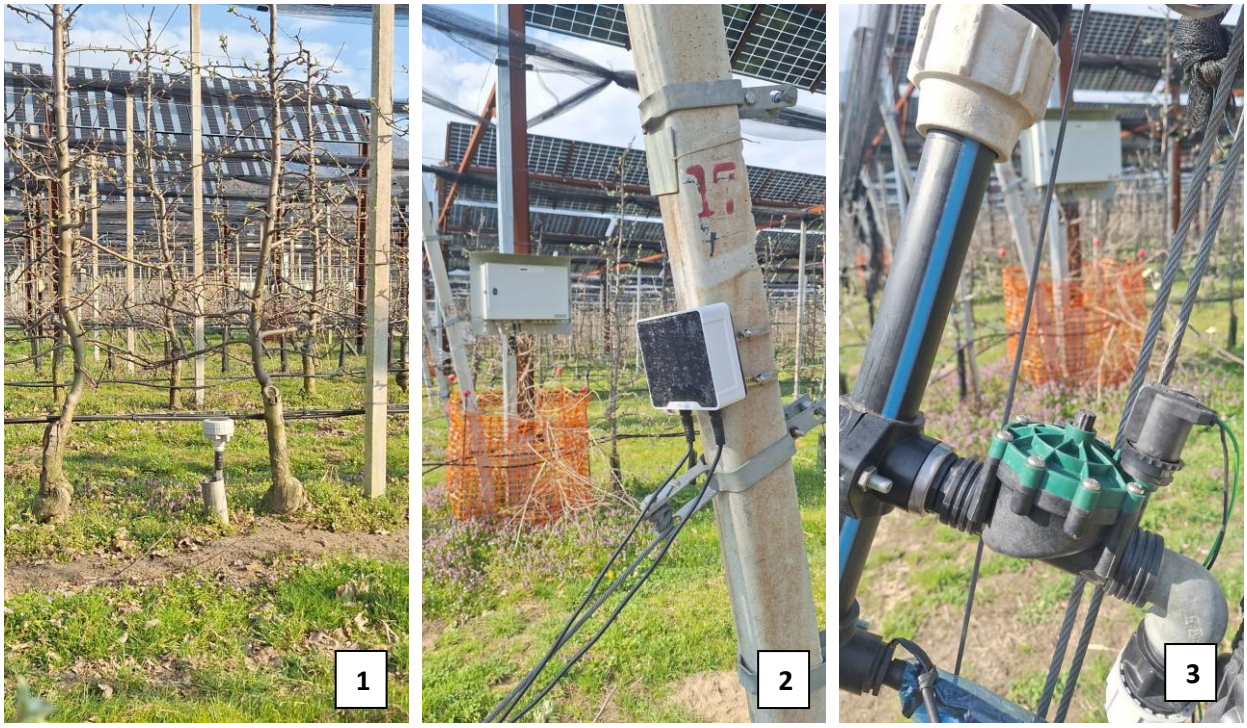

Figure 2.11 (1) ELMED TSN Tensiometer installed; (2) Milesight UC 511 controller; (3) Irritec solenoid valve installed in the Bolzano demonstrator.

2.2. Results of the first year of activity

Physiological traits

Shoot growth measurements in the new plant sector

Shoot growth was assessed in the new plant orchard composed of **young apple trees** trained in a multileader (guyot-type) system. The aim was to evaluate the effects of the agri-PV shading configurations on vegetative growth during the 2025 growing season. **Five treatments were compared**: panel-row with low transparency (P5), panel-row with higher transparency (P40), inter-row with low transparency (I5), inter-row with higher transparency (I40), and a control treatment without photovoltaic panels (C). Each new shoot of every tree was measured manually by the operator.

Statistical Analysis

Shoot growth was assessed at the individual tree level using **two complementary metrics**: mean shoot length per tree, reflecting the typical elongation of individual shoots, and total shoot length per tree (sum of all measured shoots), used as an indicator of overall vegetative vigour. Both variables were analyzed using a **one-way analysis of variance (ANOVA**), with treatment as a fixed factor. Although the number of trees differed slightly among treatments, this imbalance was considered acceptable given the similar variance structure and the robustness of ANOVA under moderately unbalanced designs. When significant treatment effects were detected, pairwise comparisons were performed using Tukey's honest significant difference (HSD) test (α =

0.05). Figures 1.5 and 1.6 illustrate the distribution of mean and total shoot length per tree across treatments, respectively.

Results

Mean shoot length

The analysis of variance **did not reveal a statistically significant effect of treatment on mean shoot length per tree** ($F_{4,40}$ = 1.19, p = 0.33), indicating that the elongation of individual shoots was broadly comparable among shading configurations and the control. Mean values ranged from 14.9 cm (I5) to 18.0 cm (I40), and post-hoc comparisons confirmed that all treatments belonged to the same homogeneous group (Table 2.4).

Total shoot length per tree

In contrast, treatment had a **highly significant effect on total shoot length per tree** ($F_{4,40}$ = 9.03, p < 0.001), indicating substantial differences in overall vegetative vigor among treatments (Figure 2.12 and Figure 2.13). The inter-row high-transparency treatment (I40) showed the greatest cumulative growth (mean: 1108.6 cm per tree), followed by the control (C: 941.1 cm) and the inter-row low-transparency treatment (I5: 769.8 cm). The lowest values were recorded for both panel-row treatments (P40: 628.5 cm; P5: 605.1 cm). Tukey's HSD test identified three partially overlapping homogeneous groups: I40 was assigned to group *a*, C and I5 to the intermediate group *ab*/*bc*, and P5 and P40 to group *c*, indicating that cumulative shoot growth was significantly reduced in trees positioned directly beneath the photovoltaic panels (Table 2.4).

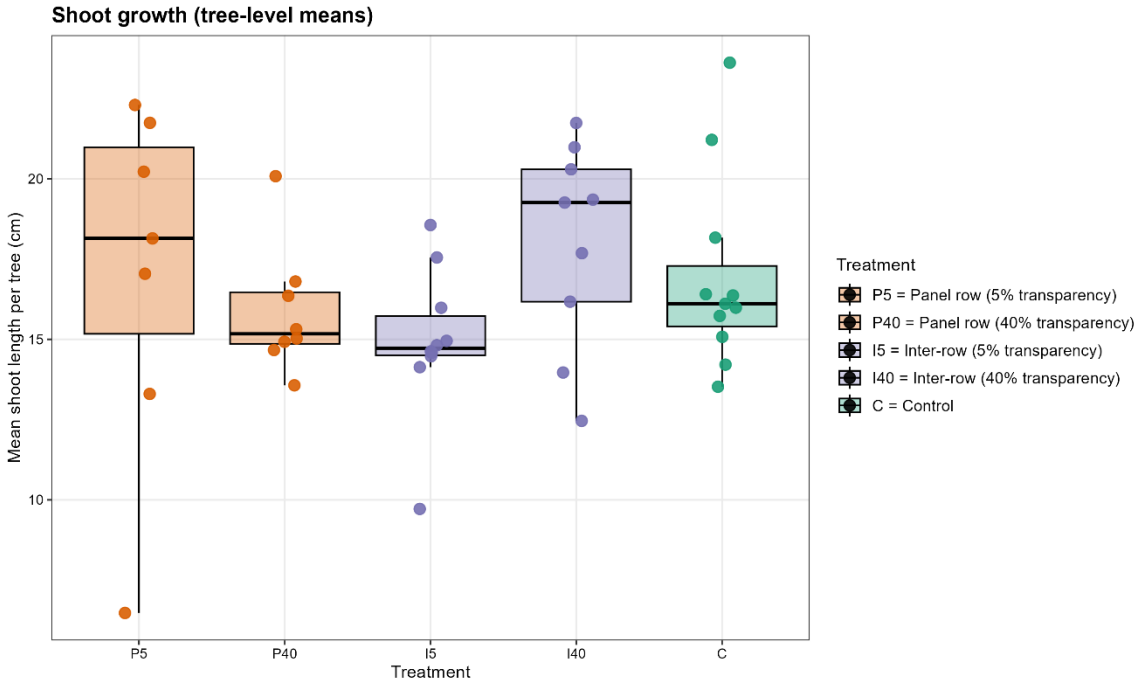

Figure 2.12 Illustrates the distribution of mean shoot length per tree across treatments. Each point represents the average shoot length of an individual tree, while boxplots summarise variability among trees within each treatment.

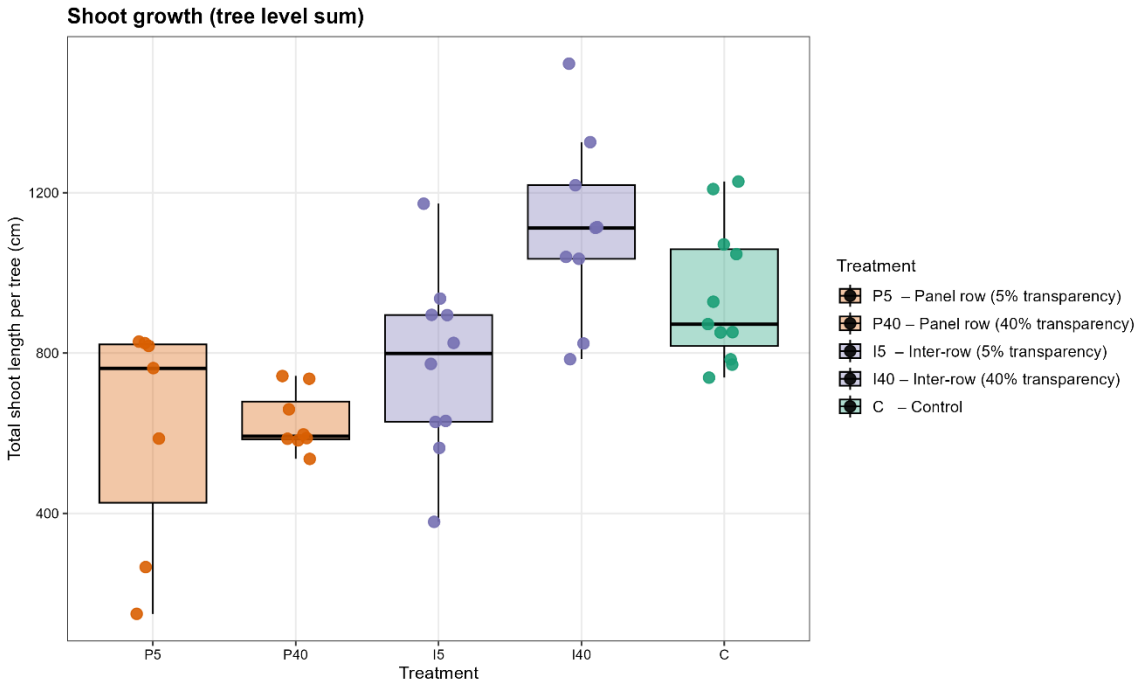

Figure 2.13 Illustrates the distribution of the sum of shoot length per tree across treatments. Each point represents the sum of the shoot length of an individual tree, while boxplots summarise variability among trees within each treatment.

Table 2.4 Sum of shoot grow at tree level (cm). Panel-row with low transparency (P5), panel-row with higher transparency (P40), inter-row with low transparency (I5), inter-row with higher transparency (I40), and a control treatment without photovoltaic panels (C). Different letters indicate significant differences among treatments (Tukey HSD, $p < 0.05$).

Treatment	Sum of shoot grow (cm) Mean ± SD	Tukey group
C	941.1 ± 173.0	ab
I5	769.8 ± 226.0	bc
I40	1108.6 ± 231.0	a
P5	605.1 ± 286.0	c
P40	628.5 ± 76.4	c

Specific Leaf Area (SLA)

Specific Leaf Area (SLA) was calculated as the ratio between total leaf area (cm^2) and leaf dry mass (g), and expressed as $cm^2\ g^{-1}$. Each sample consisted of 10 leaves, resulting in six independent samples per treatment (total n = 18 samples, 60 leaves x treatment, 180 leaves in total).

Leaf area was determined through **digital image analysis**. Leaves were scanned together with a reference scale (Figure 2.14). Images were processed using GIMP (GNU Image Manipulation Program). For each image, leaf surfaces were delineated and the corresponding number of pixels was quantified. Pixel counts were then converted into square centimeters using a pixel-to-length calibration derived from the reference scale included in each image. The total leaf area per sample was obtained by summing the area of the 10 leaves.

Leaf dry mass was measured in the laboratory after oven-drying the samples at 70 °C for 48 h, following standard protocols for leaf dry matter determination. After drying to constant weight, samples were weighed using a precision analytical balance, and dry mass values were recorded in grams.

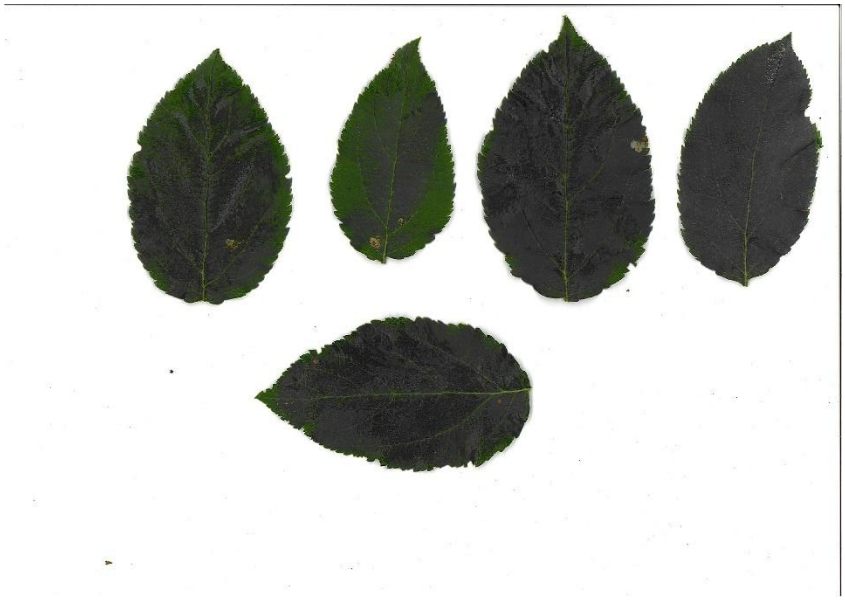

Figure 2.14 Representative scanned apple leaves used for the determination of leaf area. Leaves were arranged on a flat contrasting background and digitally acquired prior to image analysis.

SLA was calculated as:

$$SLA = \frac{\text{Leaf area (cm}^2\text{)}}{\text{Dry mass (g)}}$$

Statistical analysis

Statistical analysis was performed using a **one-way analysis of variance (ANOVA**), with treatment (C, I, P) included as a fixed factor. Model assumptions were verified prior to analysis. Residuals were normally distributed (Shapiro–Wilk test, $p = 0.719$), and homogeneity of variances was confirmed by Levene's test ($p = 0.869$), supporting the use of parametric analysis. Figure 2.15 illustrates the distribution of SLA across treatments using a boxplot graph.

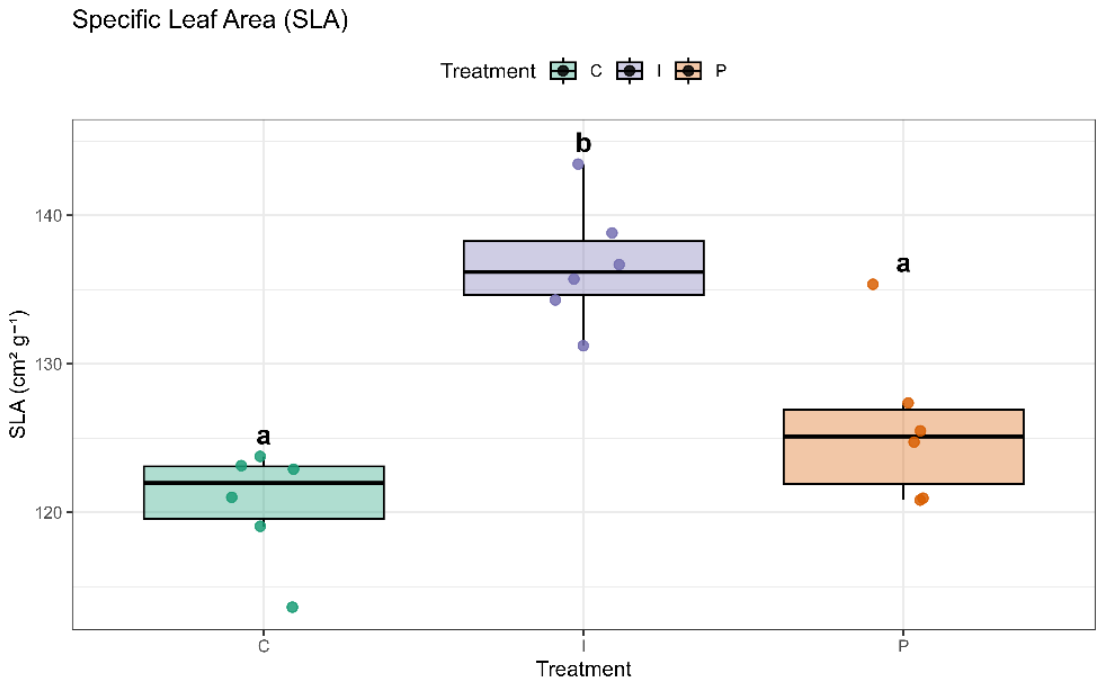

Figure 2.15 Specific Leaf Area (SLA, cm² g⁻¹) across treatments: Control (C), Inter-row (I), and Under-panel (P). Boxplots represent the interquartile range, the horizontal line indicates the median, and points represent individual composite samples (each sample consisting of 10 leaves). Different letters indicate statistically significant differences among treatments according to Tukey's post-hoc test ($p < 0.05$).

Results

A highly **significant effect of treatment on SLA was detected** ($F_{2,15} = 20.06$, $p < 0.001$; generalized $\eta^2 = 0.73$). Mean SLA values were highest in the inter-row treatment (I; 137 ± 4.2 cm² g⁻¹), intermediate under the photovoltaic panels (P; 126 ± 5.4 cm² g⁻¹), and lowest in the control (C; 121 ± 3.8 cm² g⁻¹).

Post-hoc comparisons using Tukey's adjustment showed that SLA in the inter-row treatment was significantly higher than both the control ($p < 0.001$) and the under-panel treatment ($p = 0.002$), whereas no significant difference was observed between control and under-panel conditions ($p = 0.145$) (Table 2.5).

Table 2.5 Mean Specific Leaf Area (SLA) per treatment. Control (C), Inter-row (I), and Under-panel (P). Each sample represents 10 leaves. Different letters indicate significant differences among treatments (Tukey HSD, $p < 0.05$).

Treatment	n (samples)	SLA (cm² g⁻¹) Mean ± SD	Tukey group
C	6	121.0 ± 3.8	a
I	6	137.1 ± 4.2	b
P	6	125.8 ± 5.3	a

Overall, these **results indicate that the agrivoltaic system influenced leaf morphological traits**. Higher SLA values observed in the inter-row position suggest thinner leaves with greater surface area per unit of dry mass, consistent with structural adaptation to modified light environments.

Apple Harvest and Quality Assessment

The apple harvest at the Bolzano Agri-PV demonstrator was conducted in two separate picking rounds, on October 14th and 22nd, 2025, following standard commercial orchard practices to optimize fruit quality. During the first round, only apples that had reached optimal color and size were harvested, while the remaining fruits were collected during the second round. This two-step strategy allowed for a more accurate assessment of ripening dynamics under different shading conditions.

Experimental Design and Sampling: the harvest focused exclusively on adult trees trained to the spindle system (Existing plant), as Guyot-trained trees (New planted trees in 2024) did not produce a sufficient number of fruits to ensure statistically valid analysis. Apples from each individual tree were collected into separate crates to enable tree-level yield tracking. To avoid border effects, only trees located within the central part of each row were included in the analysis, excluding those at the extremes of the PV tracker.

The experimental design included three treatments, each with two replicates of 10 trees (total: 60 trees):

- **Under-panel rows**: Trees located directly beneath PV modules (2 replicates × 10 trees)
- **Inter-row (within PV area)**: Trees in rows without panels but within the agri-PV section (2 replicates × 10 trees)
- **Control**: Trees in the conventional orchard without PV modules (2 replicates × 10 trees)

All fruits from each tree were harvested and weighed to determine tree-level yield. Immediately after harvesting, apples were stored in cold chambers at 2 °C to preserve post-harvest quality prior to further analysis.

Post-Harvest Sorting and Quality Parameters: sorting was performed using Laimburg's AWETA grading machine, which enabled the evaluation of key post-harvest parameters:

- Fruit width, weight, red color, intensity of the red **color**,
- Presence of physiological **disorders** (e.g., sunburn, russeting)
- Pathogen-related **damage**

For destructive quality analysis, two replicate samples of 15 apples per treatment (total: 90 apples) were collected and analyzed using the Pimprenelle system (Figure 2.16), which measures:

- **Soluble solids** content (°Brix)
- Titratable **acidity** (g of malic acid /L)
- Fruit **firmness** (kg /cm2)



Figure 2.16 Pimprenelle II machine for quality analysis.

AWETA Calistar with Ultravision and Inscan Pulse

The AWETA Calistar is a fruit grading and sorting machine designed for high-precision handling of fresh produce, particularly apples. This AWETA machine is integrated with advanced optical quality inspection technologies. Ultravision is an external vision system that captures detailed images of each fruit from multiple angles and evaluates external quality parameters such as surface defects, bruises, sunburn, shape, size, and color. Using configurable sorting criteria, Ultravision **allows producers to categorize products according to specific market quality standards, thereby enhancing product value and consistency**.

Complementing Ultravision, Inscan Pulse is an internal quality detection system based on near-infrared (NIR) spectroscopy. Unlike external vision alone, Inscan Pulse analyzes the internal characteristics of each individual fruit non-destructively. This allows the system to detect internal browning, internal decay, sugar content (Brix), maturity levels, and firmness—attributes that are crucial for ensuring taste quality, shelf life, and consumer satisfaction. By incorporating both internal and external quality data into the sorting process, the Calistar system equipped with Ultravision and Inscan Pulse dramatically improves the overall grading performance and reduces reliance on manual inspection. Together, these technologies help optimize quality control in high-throughput fruit sorting operations, supporting agribusinesses in achieving consistent product standards, reducing waste, and enhancing product marketability.

Lugol test for starch measurement

The Lugol test is a widely used method for assessing the **physiological maturity** of apples by determining the degree of starch degradation during ripening. Starch is a key carbohydrate stored in the fruit during its development, and as the apple matures, it is progressively converted into sugars. This process provides a reliable indicator of harvest readiness and ripening dynamics.

The test is based on the reaction between iodine and starch. When Lugol's solution (a mixture of iodine and potassium iodide) is applied to the cut surface of an apple, any starch present reacts with iodine to form a blue-black coloration. The intensity and distribution of this staining indicate the amount of starch remaining: a dark, uniform color corresponds to high starch content and immaturity, partial staining reflects intermediate maturity, and little or no staining indicates advanced ripening with most starch already degraded.

The Lugol test was performed on apples collected from the Bolzano Agri-PV demonstrator to compare ripening dynamics under different shading conditions. Representative apples were selected from three treatments: under-panel rows (2 replicas, P1, P2), inter-row within the PV area (2 replicas, I1, I2), and control rows without PV modules (2 replicas, C1, C2). Each treatment included two repetitions of 10 trees, and from each replicate, two groups of 10 apples were sampled for starch analysis. This resulted in a total of 120 apples tested (3 treatments × 2 replicates × 2 groups × 10 apples) (Figure 2.17)
To perform the test, apples were cut in half along the equatorial axis, and the exposed surface was sprayed with Lugol's solution. The staining pattern was visually evaluated and scored using a standardized starch index scale, where higher scores indicate greater starch presence and lower scores indicate advanced ripening. This method provided rapid and reliable information on physiological maturity, complementing other quality measurements such as soluble solids content, titratable acidity, and firmness obtained through destructive analysis. To complement these measurements, Lugol starch tests were performed on the same samples to assess physiological maturity. This allowed for a comparative evaluation of ripening dynamics between shaded (under PV panels, P), partially shaded (inter-row, I), and unshaded (control, C) conditions (Table 2.6).



Figure 2.17 Apple slices treated with Lugol for the starch test.

Table 2.6 For each treatment category (C, P, I), two rows (C1 and C2; P1 and P2; I1 and I2) were selected for analysis. From each row, two independent samples were collected, resulting in sample pairs such as C11 and C12 etc.).

Treatment											Mean
C1-1	3,2	2,7	2,3	3,3	3	3	2,1	2,8	4	2,7	2,91

C1-2	3,2	2,6	2,5	2,5	2,4	3,5	4,5	2,7	2,7	3,4	3
C2-1	2,4	3	2,2	3,3	2,8	1,8	2,6	2,3	2,4	2,8	2,56
C2-2	3,5	3,5	3	2,5	3	2,7	2,7	3,4	2,4	3,7	3,04
P1-1	2,8	2,7	2,8	2,1	3	2,8	3,5	2,8	1,8	2,8	2,71
P1-2	1,7	2,4	2,7	2,5	2,5	2,4	2,8	2,7	2,4	2,3	2,44
P2-1	2,6	1,8	2,6	2,1	2,1	3	3,2	1,7	2,8	3	2,49
P2-2	2,8	2,6	2,4	2,9	2,4	1,4	1,7	2,2	3,6	1,3	2,33
I1-1	1,9	2	2,3	3,4	2,6	2,5	2,8	2,9	3,4	2,8	2,66
I1-2	2,4	2,2	2,2	2,2	2,3	2,3	2,4	2,2	2,7	2,8	2,37
I2-1	2,3	3,2	2,2	2,3	4,5	3,2	2,2	2,7	4	3,2	2,98
I2-2	2,1	2,6	2,2	2,2	2,3	2,9	2,9	2,8	2,8	2	2,48

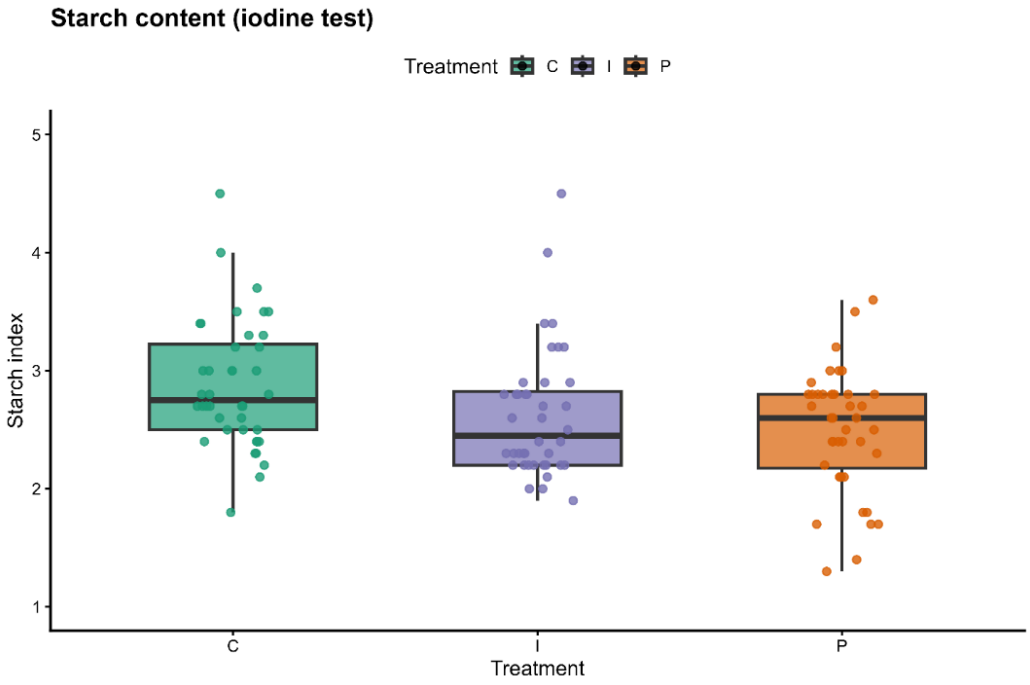

Figure 2.18 Boxplot of starch index across the treatments. Control (C), Inter-row (I), and Under-panel (P). Boxes represent the interquartile range, the horizontal line indicates the median, and points represent individual fruit measurements.

Statistical analysis

An **analysis of variance (ANOVA)** was performed to evaluate differences in starch index among the three treatments: under-panel rows (P), inter-row within the PV area (I), and control rows without PV modules (C). The analysis revealed a significant effect of treatment on starch index values ($F_{2,117} = 5.29$, $p = 0.006$), indicating that at least two groups differed statistically.

Assumption checks confirmed the validity of the analysis. The Shapiro–Wilk test indicated slight deviations from normality ($p = 0.013$); however, given the balanced experimental design, the ANOVA was considered robust. Homogeneity of variances was confirmed by Levene's test ($p = 0.983$), indicating comparable variance among treatments. Figure 2.18 illustrates the starch index across treatments using a boxplot graph.

Results

Post-hoc comparisons using Tukey's HSD test showed that apples from the under-panel rows (P) had significantly lower starch index values than those from the control rows (C) ($p = 0.005$), whereas no significant differences were observed between inter-row (I) and control (C) ($p = 0.091$) or between under-panel (P) and inter-row (I) ($p = 0.529$) (Table 2.7).
These results indicate that **PV shading is associated with a slower starch degradation compared to conventional orchard conditions, suggesting a delayed physiological maturity of fruit under the panels.** In contrast, trees located in inter-row positions within the PV area exhibited ripening dynamics comparable to those observed in the control treatment.

Table 2.7 Mean starch index values and Tukey's HSD grouping.

Treatment	Starch index (mean ± SD)	Tukey group
C	2.88 ± 0.54	a
I	2.63 ± 0.51	ab
P	2.49 ± 0.48	b

Pimprenelle analysis for internal quality analysis

Soluble Solids Content (SSC, °Brix)

Statistical analysis

Soluble solids content (SSC, °Brix) was analysed using a **linear mixed-effects model** in order to account for the hierarchical structure of the experimental design. Treatment (C, I, P) was included as a fixed effect, while replica and sample nested within replica were included as random effects. Model assumptions were evaluated by visual inspection of residual plots and Q–Q plots, and by performing a Shapiro–Wilk test on model residuals. The effect of treatment was tested using a Type II Wald χ^2 test. When a significant treatment effect was detected, post-hoc pairwise comparisons were performed using Tukey's adjustment based on estimated marginal means (emmeans). Figure 2.19 illustrates the distribution of SSC values across treatments using a boxplot graph.

Results

A **significant effect** of treatment on SSC was observed:

$\chi^2(2) = 105.3$, $p < 0.001$

Mean SSC values differed clearly among treatments (Table 2.8). Fruits from the control treatment (C) showed the highest SSC values, followed by the inter-row treatment (I), while the under-panel treatment (P) exhibited the lowest SSC.

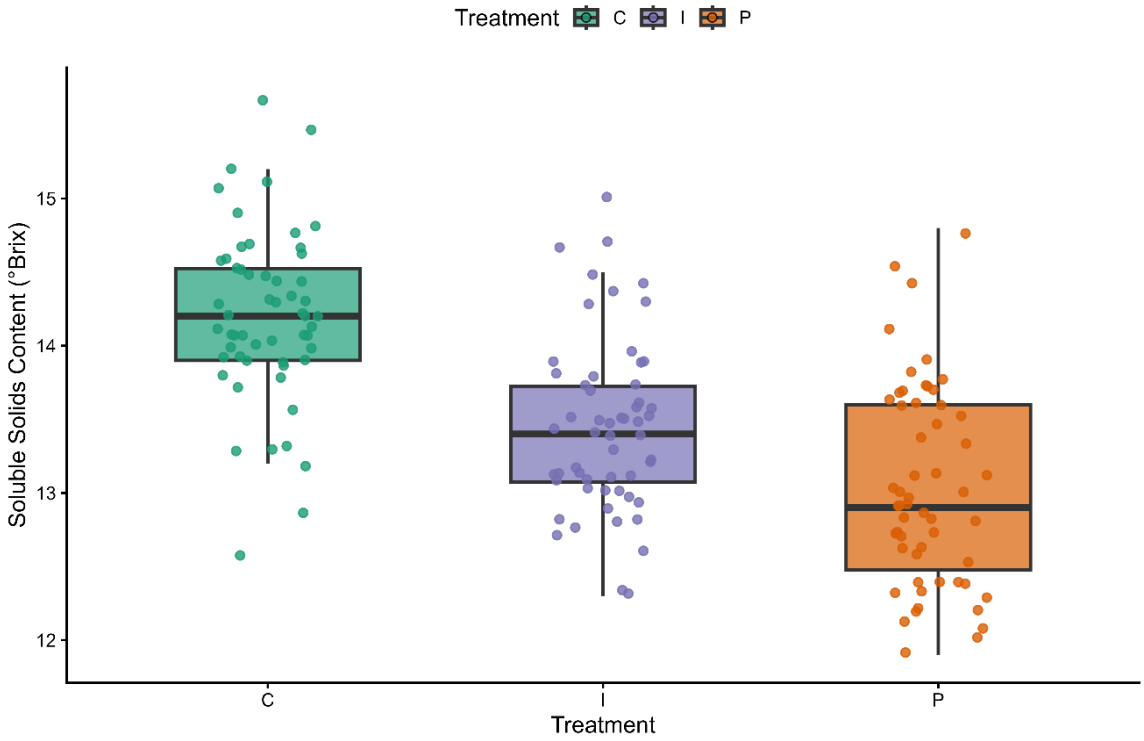

Figure 2.19 The distribution of SSC values across treatments. Control (C), Inter-row (I), and Under-panel (P). Boxes represent the interquartile range, the horizontal line indicates the median, and points represent individual fruit measurements.

Post-hoc comparisons confirmed that all treatments differed significantly from each other (Tukey's test, $p < 0.05$).

Accordingly, treatments were ranked as C > I > P with respect to SSC (Table 2.8).

Table 2.8 Mean soluble solids content (SSC, °Brix ± SD) by treatment. Different letters indicate significant differences among treatments according to Tukey's post-hoc test ($p < 0.05$).

Treatment	n	Mean	SD	Group
C	60	14.21	41.6	a
I	60	13.45	40.1	b
P	60	13.03	40.7	c

Fruit Firmness (kg cm^{-2})

Statistical analysis

Fruit firmness was analyzed using a **linear mixed-effects model**. Treatment (C, I, P) was included as a fixed effect, while replica was included as a random effect. The inclusion of sample as an additional random factor was not supported due to model singularity; therefore, a more parsimonious random-effects structure was

adopted. Model assumptions were checked by inspection of residual diagnostics. The effect of treatment was tested using a Type II Wald χ^2 test. Estimated marginal means were calculated to explore differences among treatments. Figure 2.20 illustrates the distribution of fruit firmness values across treatments using a boxplot graph.

Results

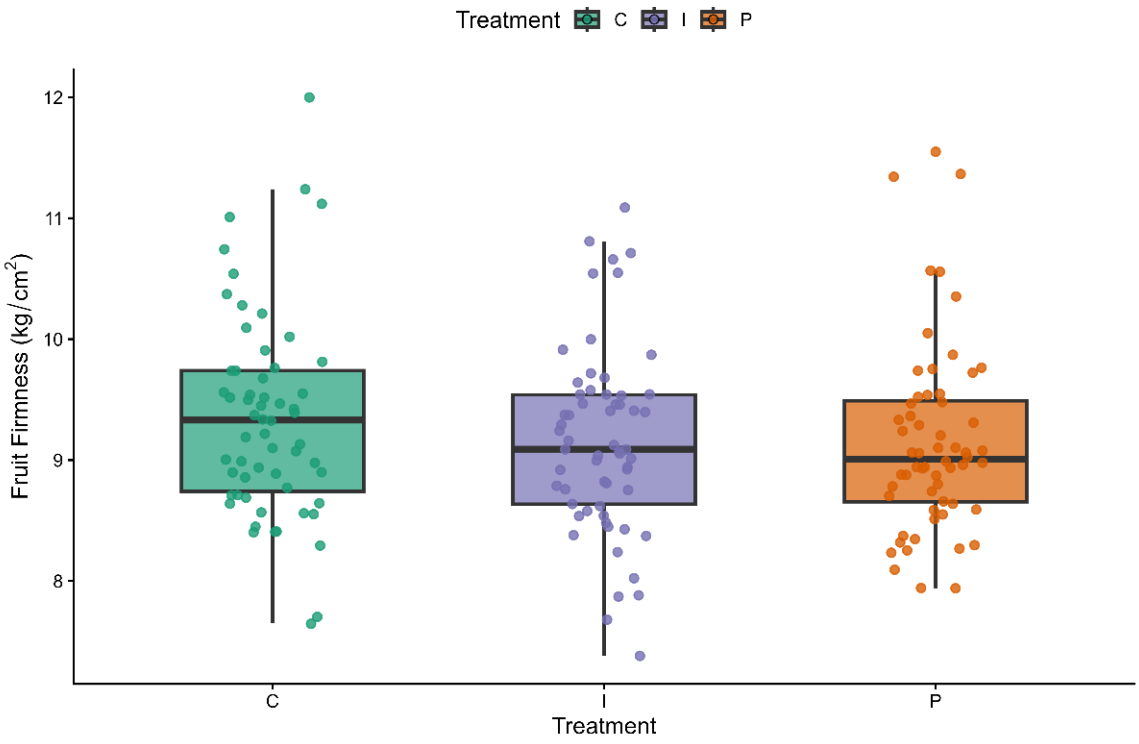

Figure 2.20 The distribution of fruit firmness values across treatments. Control (C), Inter-row (I), and Under-panel (P). Boxes represent the interquartile range, the horizontal line indicates the median, and points represent individual fruit measurements.

No significant effect of treatment on fruit firmness was detected.

$\chi^2(2) = 2.60$, $p = 0.273$

Mean firmness values were similar across treatments, and post-hoc comparisons did not reveal any statistically significant differences. All treatments shared the same significance group, **indicating comparable firmness levels under control conditions, in the inter-row area, and beneath the photovoltaic panels** (Table 2.9).

Table 2.9 Mean fruit firmness (kg cm^{-2} ± SD) by treatment. No significant differences were detected among treatments (Type II Wald χ^2 test, $p > 0.05$).

Treatment	n	Mean	SD	Group
C	60	9.3	0.8	a
I	60	9.2	0.8	a

P	60	9.2	0.8	a

Acidity (malic acid g/L)

Titratable acidity was measured on composite fruit samples obtained from each experimental unit (i.e., group of 15 apples per treatment/replicate), following standard procedures of the **Pimprenelle fruit quality assessment system** (Figure 2.21). In this method, the acidity value is derived from a single analysis on the entire sample, rather than on individual fruits. As such, the acidity measurement represents the average fruit response within that sample, and not independent observations at the fruit level. Total observations 12.

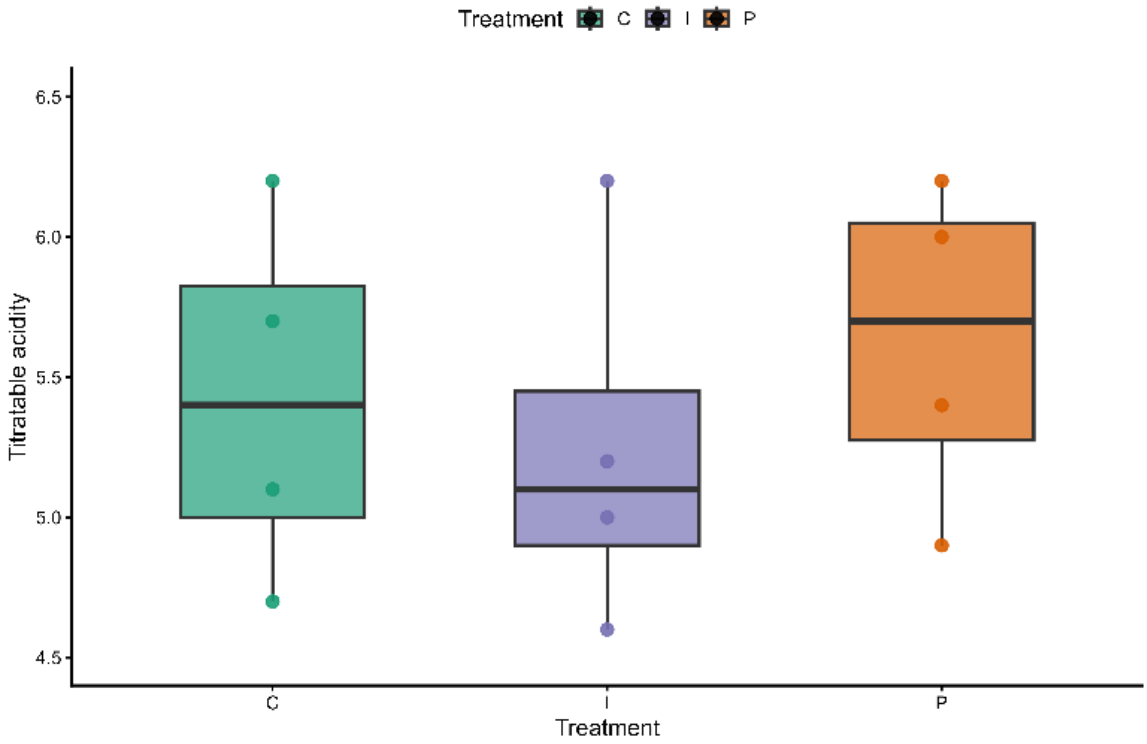

Figure 2.21 The distribution of acidity values (malic acid g/L) across treatments. Control (C), Inter-row (I), and Under-panel (P). Boxes represent the interquartile range, the horizontal line indicates the median, and each point corresponds to one sample mean (n = 4 per treatment).

Statistical analysis

Titratable acidity was analyzed using a **linear mixed-effects model**. Treatment (C, I, P) was included as a fixed effect, while replica was included as a random effect $(1 \mid Replica)$, in order to account for variability among experimental replicates.

Model assumptions were assessed by inspection of residual diagnostics. The effect of treatment on titratable acidity was tested using a Type II Wald χ^2 test. When a significant treatment effect was detected, post-hoc comparisons were performed using Tukey's adjustment based on estimated marginal means (emmeans).

Results

A **significant effect of treatment** on titratable acidity was detected:

$\chi^2(2) = 13.54$, $p = 0.001$

Mean titratable acidity values differed among treatments (Table 2.10). The **under-panel treatment (P) showed the highest acidity values, while the inter-row treatment (I) exhibited the lowest values.** The control treatment (C) displayed intermediate acidity levels.
Post-hoc comparisons indicated that titratable acidity was significantly higher in P than in I (Tukey's test, $p < 0.05$). The control treatment did not differ significantly from either P or I.

Table 2.10 Mean titratable acidity (± SD) by treatment. Different letters indicate significant differences among treatments according to Tukey's post-hoc test ($p < 0.05$).

Treatment	n	Mean	SD	Group
C	4	5.4	0.6	a
I	4	5.2	0.6	ab
P	4	5.6	0.5	b

AWETA optical fruit grader for apple fruit quality

Laimburg has evaluated the effect of agri-PV on the apple fruit quality, focusing on **size- and colour-related traits** measured with an AWETA optical fruit grader. Only the old-plants with spindle training system have been evaluated because the young plants did not have enough fruit to have a reliable statistic in the first season. Three treatments were compared: control trees in a conventional orchard without panels (C), trees grown within the agri-PV system in the inter-row position (I), and trees located directly under photovoltaic panels (P). The experimental design included two replicates for each treatment.

The following AWETA-derived traits were analysed at tree levels using analysis of covariance (ANCOVA), with fruit number per tree (n) included as a covariate to account for crop load effects:

- **Yield (kg/treatment)**: yield per tree and total yield per treatment
- **Width (mm):** fruit diameter
- **BlushArea (%):** percentage of fruit surface with red overcolour
- **Blush color:** red colour intensity descriptor

Results indicated that the agri-PV treatments had strong impacts on red coloration traits, with control trees producing significantly higher blush area and colour intensity than agri-PV treatments. Fruit diameter and weight did not differ significantly among treatments after covariate adjustment, although trends were

observed. These findings suggest that **shading conditions within the agri-PV system may reduce colour development and slightly affect physical quality traits.**

Yield

Fruit number per tree (n)

Fruit number per tree was determined at harvest **by collecting fruits from each individual tree** (sample size 20 trees per treatment) into separate boxes, with tree identity and treatment clearly recorded. This procedure ensured full traceability of fruits at the tree level throughout post-harvest handling and quality assessment.
The number of fruits per tree was subsequently quantified using the AWETA, which automatically counted all fruits processed from each box. This approach provided an accurate and objective measurement of crop load for each tree.

ANOVA Results

Fruit number per tree differed significantly among treatments ($F_{2,54} = 13.66$, $p < 0.001$), with control trees (C) carrying on average approximately 31 more fruits per tree than trees under the agri-PV system (C: 135 ± 21.8; I: 104 ± 22.1; P: 104 ± 23.3) (Figure 2.22). Inter-row (I) and under-panel (P) trees did not differ significantly from each other.
The limited sample size of 10 trees per treatment per replicate reflects a deliberate constraint of the experimental design. The agri-PV installation covers a relatively small area, and only central trees within central rows were included in the analysis in order to avoid edge effects, as border trees are exposed to substantially higher lateral light infiltration compared to trees in central positions. At harvest, trees were selected based on a standardised crop load criterion, excluding visually overbearing and underbearing individuals, in order to reduce between-tree variability and improve the comparability of fruit quality measurements across treatments.
Both chemical and manual thinning operations were carried out following standard orchard management practices, with no differential intervention among treatments. Furthermore, the agri-PV structure was installed in 2025, meaning that flower induction for the 2025 growing season occurred in 2024, prior to panel installation. Differences in initial flowering intensity among treatments can therefore be excluded as a contributing factor to the observed variation in fruit number.
The most plausible biological explanation for the lower fruit number observed under the agri-PV system is an increase in physiological fruit drop during the 2025 growing season, potentially driven by reduced photosynthetically active radiation under the panels during the critical period of early fruit development. Reduced light availability is known to impair carbohydrate supply to developing fruitlets, thereby promoting abscission.

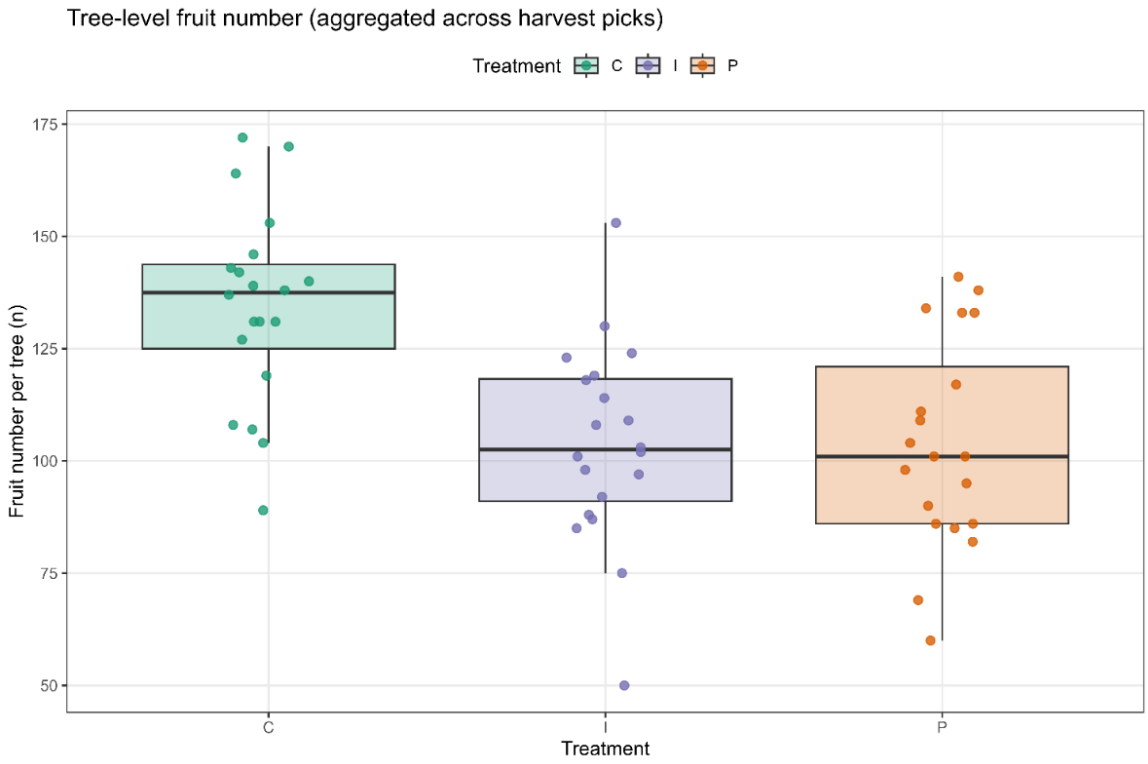

Figure 2.22 Boxplot of fruit number (n) at tree level. Control (C), Inter-row (I), and Under-panel (P). Boxes represent the interquartile range, the horizontal line indicates the median, and points represent tree-level mean values.

Fruit weight (g)

Individual fruit weight was measured using the **AWETA optical fruit grading** system during post-harvest processing. Fruit weight data were used to calculate tree-level yield (Figure 2.23).

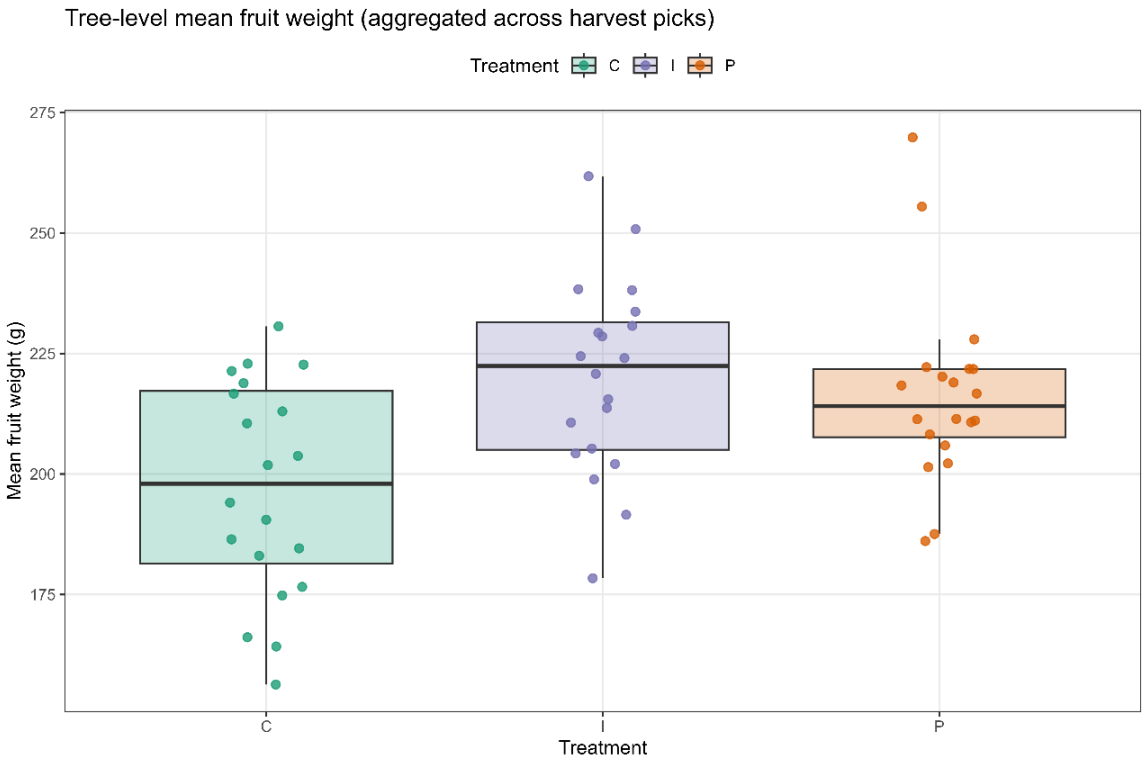

Figure 2.23 Boxplot of the mean fruit weight (g). Boxes represent the interquartile range, the horizontal line indicates the median, and points represent tree-level mean values. Control (C), Inter-row (I), and Under-panel (P)

Verification of model assumptions

Mean fruit weight per tree was analysed using a **two-way analysis of variance (ANOVA**), with treatment and replicate included as fixed factors. Residuals were normally distributed (Shapiro–Wilk test, W = 0.992, p = 0.957), variances were homogeneous across groups (Levene's test, p = 0.539), and the treatment × replicate interaction was not significant (p = 0.943), indicating a consistent treatment response across experimental replicates.

ANOVA results

A significant effect of treatment on mean fruit weight was detected ($F_{2,54}$ = 6.87, p = 0.002). Trees under the agri-PV system produced heavier fruits than control trees (I: 220.0 ± 20.2 g; P: 216.5 ± 19.3 g; C: 197.0 ± 22.4 g). Post-hoc comparisons using Tukey's HSD test indicated that both inter-row (I) and under-panel (P) treatments belonged to the same homogeneous group (group a), which differed significantly from the control (group b). No significant difference was detected between inter-row and under-panel trees.

This result is consistent with the classical source–sink dynamic in apple production: **control trees carried substantially more fruits per tree than agri-PV trees** (C: 135 ± 21.8; I: 104 ± 22.1; P: 104 ± 23.3), resulting in greater competition for photosynthetic assimilates and consequently reduced individual fruit weight.

Exploratory mediation analysis

In order to explore the extent to which the observed differences in fruit weight are attributable to the reduction in fruit number per tree — as opposed to a direct effect of panel shading on fruit development — a mediation analysis was conducted. Fruit number per tree was treated as a potential mediator of the treatment effect on mean fruit weight, with replicate included as a control variable. Bootstrap confidence intervals were based on 1000 simulations. It should be noted that this analysis rests on the assumption that fruit number is causally influenced by the agri-PV treatment.

For the C vs. I contrast, the total effect was significant (Total effect = +23.1 g, $p < 0.001$), with approximately 38% attributable to the indirect pathway via fruit number (ACME = 8.9 g, $p = 0.142$) and the remaining 62% to the direct effect (ADE = 14.2 g, $p = 0.152$). Neither component reached individual significance, suggesting that both pathways contribute to the observed difference but that the available sample size was insufficient to isolate them statistically.

For the C vs. P contrast, the total effect was similarly significant (Total effect = +19.5 g, $p < 0.001$), with only 15% attributable to the indirect pathway (ACME = 3.0 g, $p = 0.724$) and a borderline direct effect (ADE = 16.5 g, $p = 0.070$). This pattern suggests that for under-panel trees, the improvement in fruit weight relative to the control is driven predominantly by a direct effect — most likely the reduction in fruit number per tree, rather than by shading per se acting directly on fruit growth.

No significant difference in fruit weight was detected between inter-row and under-panel trees in either the ANOVA or the mediation analysis (Total effect = −3.6 g, $p = 0.556$), indicating comparable fruit weight performance between the two agri-PV positions."

Figure 2.24 illustrates the relationship between fruit load and mean fruit weight at the tree level across the three treatments. In the inter-row treatment (I), a negative relationship between fruit number and mean fruit weight was observed, consistent with the classical source–sink dynamic in apple production, whereby increasing fruit load results in reduced mean fruit size. Panel-row trees (P) showed a comparably narrow range of fruit numbers, concentrated at lower values, with a nearly flat regression line, suggesting that shading by the photovoltaic panels constrained fruit set without substantially affecting mean fruit weight. Control trees (C) exhibited the widest range of fruit load but no apparent relationship between fruit number and mean weight

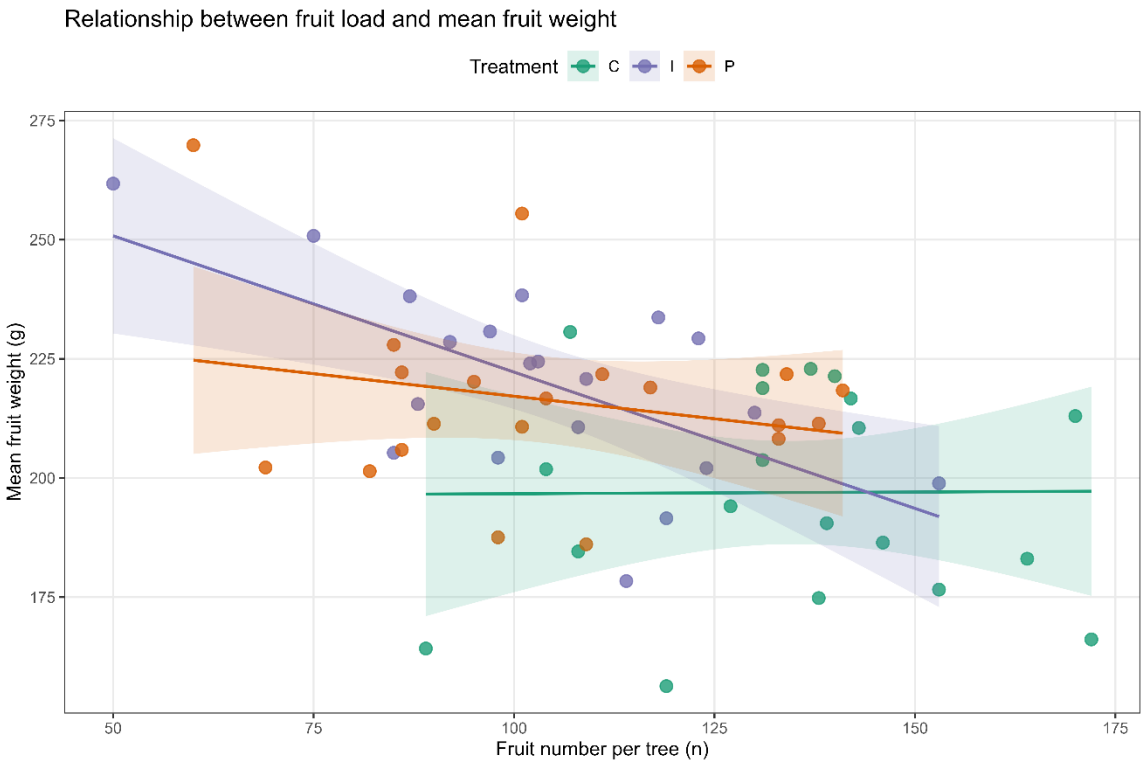

Figure 2.24 Scatter plot showing the relationship between fruit number per tree and mean fruit weight (g) for each treatment (C = control, I = inter-row, P = panel-row). Lines represent linear regression fits with 95% confidence intervals.

Fruit diameter (mm)

Fruit diameter (width), measured using an AWETA optical fruit grader, was analysed using **analysis of covariance (ANCOVA).** The number of fruits analysed per batch (n) was included as a continuous covariate in order to account for potential effects of sample size on the estimation of mean fruit diameter. Treatment and replicate were considered as fixed factors (Figure 2.25).

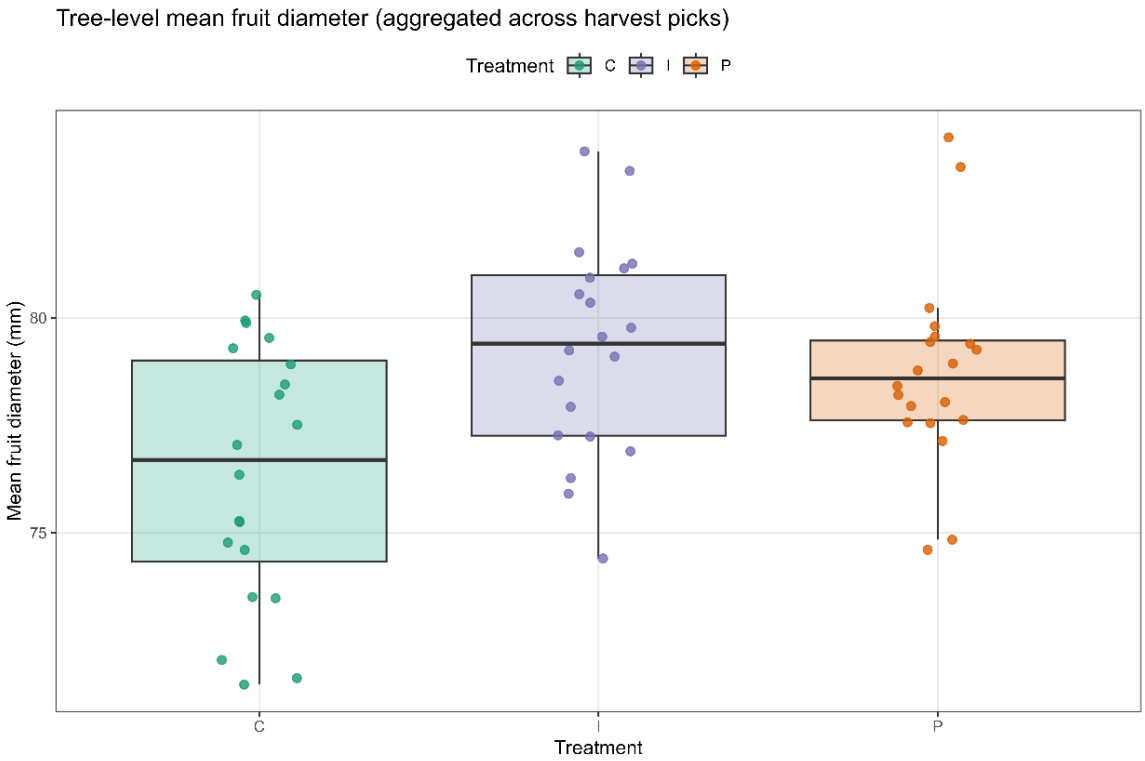

Figure 2.25 Boxplot of the mean fruit diameter (mm). Boxes represent the interquartile range, the horizontal line indicates the median, and points represent tree-level mean values. Control (C), Inter-row (I), and Under-panel (P).

Verification of model assumptions

Prior to the ANCOVA, the main model assumptions were evaluated. Visual inspection of the data indicated an approximately linear relationship between the covariate *n* and mean fruit diameter across all treatments.

Homogeneity of regression slopes was assessed by testing interactions between the covariate and the experimental factors. The interaction between *n* and treatment was not significant (p = 0.182), nor was the three-way interaction (*n × treatment × replicate*, *p* = 0.599), indicating that the effect of the covariate on fruit diameter was comparable among treatments. A significant interaction between *n* and replicate was detected (*p* = 0.014), suggesting a different relationship between sample size and mean fruit diameter between the two replicates; however, as this effect did not involve the treatment factor, it does not compromise the comparison among agri-PV treatments.

Normality of model residuals was confirmed by the Shapiro–Wilk test (*p* = 0.639), and homogeneity of variances was supported by Levene's test (*p* = 0.345). No influential outliers were identified (|standardized residual| > 3).

ANCOVA results

The analysis of covariance **did not reveal statistically significant differences in mean fruit diameter** among treatments after accounting for the effect of the covariate *n* ($F_{2,53}$ = 2.17, *p* = 0.125). The main effect of replicate was also not significant (*p* = 0.994), and no significant interaction between treatment and replicate

was observed (p = 0.953), indicating a consistent fruit diameter response across the two experimental replicates.

The covariate *n* showed a marginal effect on mean fruit diameter ($F_{1,53}$ = 3.37, p = 0.072), although this effect did not reach conventional levels of statistical significance.

Despite the lack of statistically significant treatment effects, the effect size associated with treatment (generalized η^2 = 0.076) indicates a small-to-moderate magnitude of effect, which may be biologically or agronomically relevant.

Total yield (kg)

Total yield per tree was obtained by **summing the weights of all fruits belonging to the same tree** and expressed as kilograms per tree (Figure 2.26). Yield was calculated by summing the yields of all individual trees within each treatment. This comparison provides an integrated overview of overall productivity under the different agri-PV conditions. The control treatment (C) showed the highest total yield (530.0 kg), followed by the inter-row treatment (I, 451.5 kg) and the under-panel treatment (P, 446.8 kg) (Table 2.11).

Table 2.11 Total fruit yield (kg) per treatment, calculated as the sum of yields from all sampled trees and relative change (%) compared to the control (C). Values represent cumulative production for the control (C), inter-row (I), and under-panel (P) treatments.

Treatment	Total yield (kg)	Change vs C (%)
C	**530,00**	**-**
I	**451,50**	**-15,8**
P	**446,78**	**-15,7**

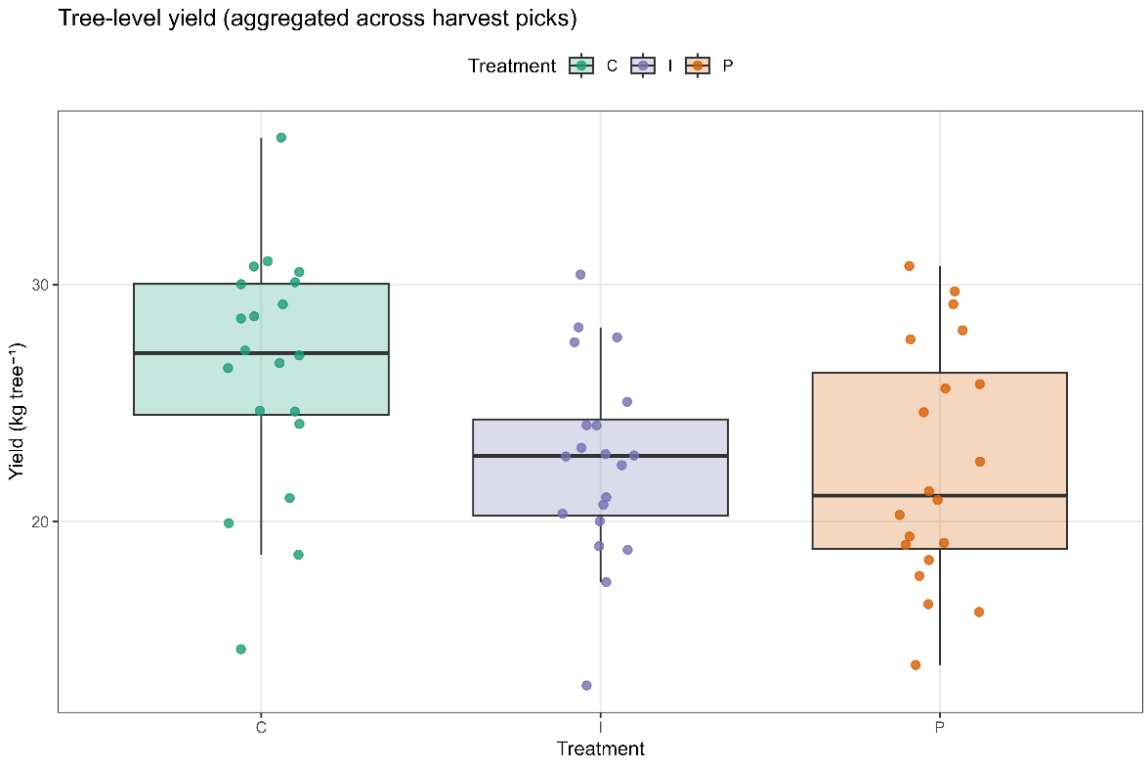

Figure 2.26 Boxplot of the tree-level yield (kg/tree). Boxes represent the interquartile range, the horizontal line indicates the median, and points represent tree-level mean values. Control (C), Inter-row (I), and Under-panel (P).

Verification of model assumptions

Fruit yield was analyzed at the tree level in order to allow a statistically valid comparison among treatments. Statistical analyses were performed using a two-way analysis of variance (ANOVA), with treatment (C, I, P) and replicate included as fixed factors. Model assumptions were verified by inspection of residual diagnostics. Residuals were normally distributed (Shapiro–Wilk test, p = 0.516), variances were homogeneous across groups (Levene's test, p = 0.733), and no influential outliers were detected.

Results

A **significant effect of treatment on tree-level yield was observed** ($F_{2,54}$ = 5.13, p = 0.009), whereas the effect of replicate (p = 0.133) and the treatment × replicate interaction (p = 0.179) were not significant, indicating a consistent treatment response across experimental replicates. Estimated marginal means showed that trees in the control treatment (C) had the highest yield per tree, while both agri-PV treatments (P and I) exhibited lower yields. Post-hoc comparisons using Tukey's adjustment confirmed that yield in the control was significantly higher than in both the inter-row (I) and under-panel (P) treatments (p < 0.05), whereas no significant difference was detected between I and P (Table 2.12). Overall, these results indicate a reduction in tree-level yield under agri-PV conditions, with comparable yield performance between inter-row and under-panel positions.

Table 2.12 Yield (kg/tree) + SD per tree per treatment. Different letters indicate significant differences among treatments according to Tukey's post-hoc test ($p < 0.05$).

Treatment	n (trees)	Yield (kg tree^{-1} ± SD)	Group
C	20	26.5 ± 5.0	b
I	20	22.6 ± 4.1	a
P	20	22.3 ± 5.0	a

The higher tree-level yield observed in the control (C) appears primarily driven by a greater number of fruits per tree.

Blush area (% of fruit surface showing red coloration)

The **percentage of fruit surface showing red coloration** (Blush area), measured using an AWETA optical fruit grader, was analysed to assess the effect of the agri-PV system on apple fruit coloration (Figure 2.27).

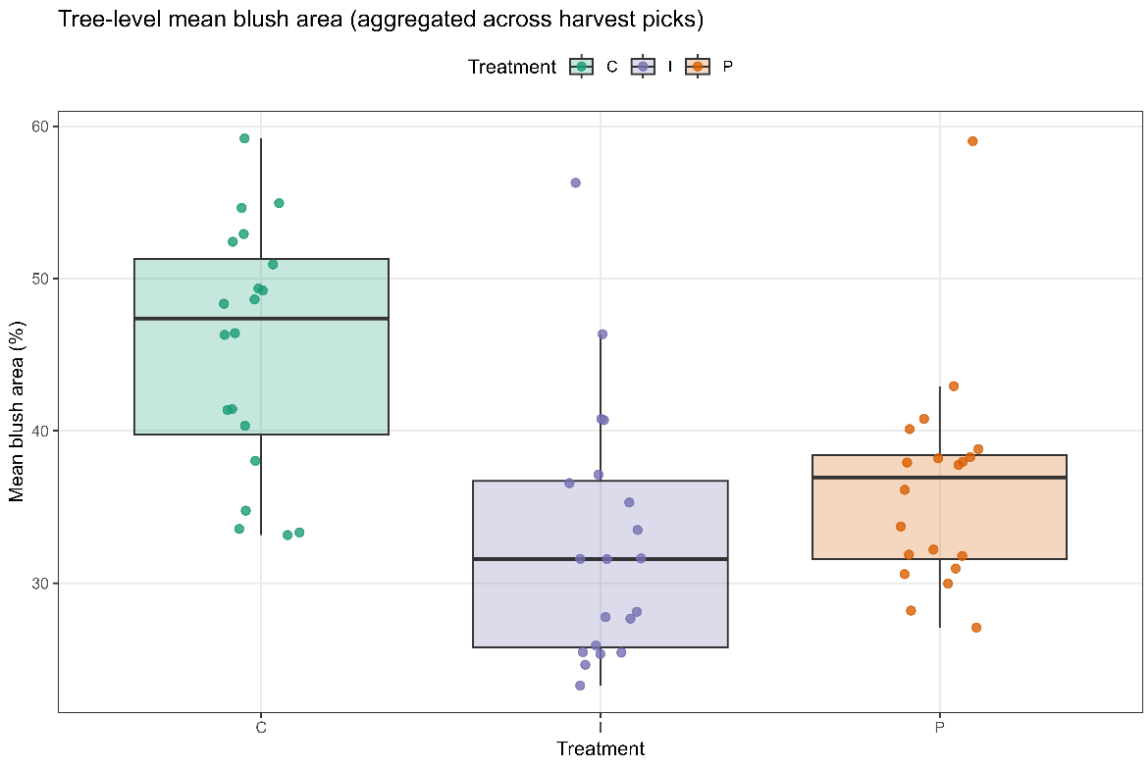

Figure 2.27 Boxplot of the tree-level mean blush area (% of fruit surface red coloured area). Boxes represent the interquartile range, the horizontal line indicates the median, and points represent tree-level mean values. Control (C), Inter-row (I), and Under-panel (P).

Verification of model assumptions

Visual inspection of the data indicated an approximately linear relationship between the covariate *n* and the percentage of blush area across treatments and replicates.

Homogeneity of regression slopes was assessed by testing interactions between the covariate and the experimental factors. The interaction between *n* and treatment was not significant ($p = 0.380$), nor was the three-way interaction (*n × treatment × replicate*, $p = 0.755$), indicating that the effect of the covariate on blush area was comparable among treatments. A significant interaction between *n* and replicate was detected ($p = 0.003$), suggesting a different relationship between crop load and fruit coloration between the two experimental replicates. A significant treatment × replicate interaction was also observed in the preliminary model ($p = 0.027$), indicating some variability in treatment responses between replicates.

Normality of residuals was confirmed by the Shapiro–Wilk test ($p = 0.802$), and homogeneity of variances was supported by Levene's test ($p = 0.718$). One outlier (|standardized residual| > 3) was identified; however, as it was not considered influential and did not materially affect model outcomes, it was retained in the analysis.

ANCOVA results

The analysis of covariance revealed a **strong and statistically significant effect** of the covariate *n* on the percentage of fruit blush area ($F_{1,53} = 19.65$, $p < 0.001$), indicating a pronounced influence of crop load on fruit coloration.

Highly significant differences among treatments were detected for blush area after adjusting for the covariate ($F_{2,53} = 26.52$, $p < 0.001$; generalized $\eta^2 = 0.50$). Post-hoc pairwise comparisons based on estimated marginal means (EMMs), using Tukey's adjustment for multiple testing, showed that fruits from control trees (C) exhibited a significantly higher percentage of blush area compared with both trees located under photovoltaic panels (P) and those in the inter-row position (I) ($p < 0.001$ in both cases). In contrast, no statistically significant difference was observed between the P and I treatments ($p = 0.265$) (Table 2.13).

Table 2.13 Estimated differences are based on estimated marginal means adjusted for the covariate (number of fruits per tree) and averaged across replicates. P-values were adjusted using Tukey's method.

Contrast	Estimated difference (percentage points)	p-value	Interpretation
C – I	+18.64	< 0.0001	Significant
C – P	+15.21	< 0.0001	Significant
I – P	−3.43	0.265	Not significant

Blush color (blush color intensity)

Fruit **blush color intensity** (Blush color), measured using an AWETA optical fruit grader, was analysed to assess the effect of the agri-PV system on the chromatic quality of apple fruits (Figure 2.28).

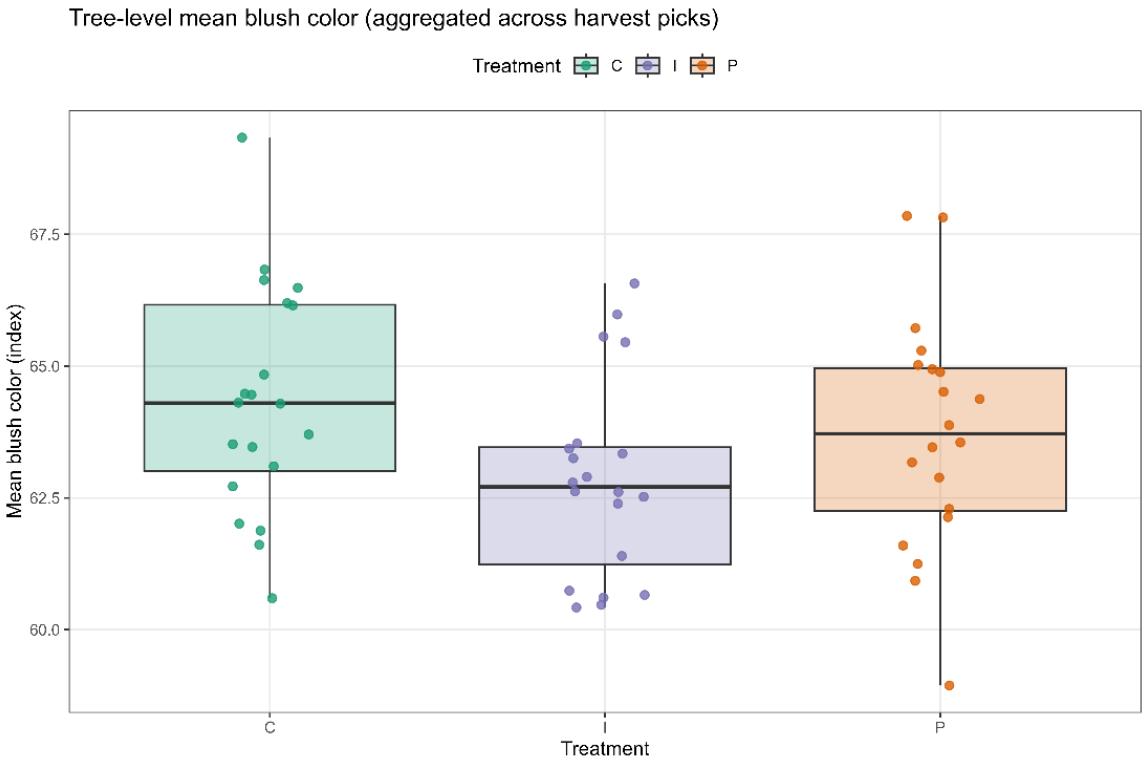

Figure 2.28 Boxplot of the tree-level mean blush color (index indicating the intensity of the red color). Boxes represent the interquartile range, the horizontal line indicates the median, and points represent tree-level mean values. Control (C), Inter-row (I), and Under-panel (P).

Verification of model assumptions

Homogeneity of regression slopes was confirmed by the **absence of significant interactions** between the covariate and the experimental factors (*n × treatment*, $p = 0.697$; *n × treatment × replicate*, $p = 0.869$). A significant interaction between *n* and replicate was detected ($p = 0.031$), suggesting a different relationship between crop load and blush color intensity between experimental replicates; however, this effect did not involve the treatment factor.

Normality of residuals was confirmed by the Shapiro–Wilk test ($p = 0.963$), and homogeneity of variances was supported by Levene's test ($p = 0.734$). No influential outliers were detected.

ANCOVA results

The analysis of covariance did not reveal statistically significant effects on mean blush color intensity. Specifically, neither the covariate *n* ($F_{1,53} = 0.96$, $p = 0.332$) nor treatment ($F_{2,53} = 2.98$, $p = 0.059$) had a significant effect on fruit blush color. The main effect of replicate ($p = 0.690$) and the treatment × replicate interaction ($p = 0.854$) were also not significant.

Although the treatment effect **did not reach statistical significance**, the observed effect size (generalized $\eta^2 = 0.10$) suggests a potential trend that may become evident with increased statistical power.

Fruit density

Fruit density (Density), measured using an **AWETA optical fruit grader**, was analysed to assess the effect of the agri-PV system on the physical properties of apple fruits (Figure 2.29).

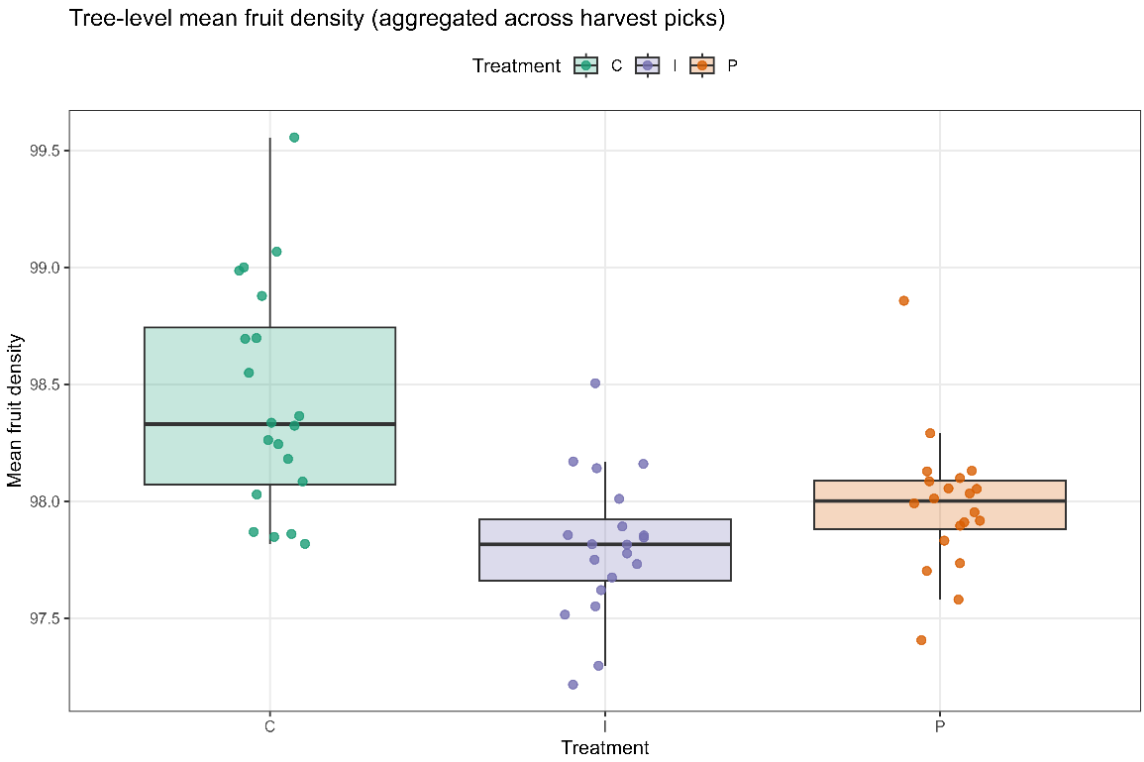

Figure 2.29 Boxplot of the tree-level mean fruit density. Boxes represent the interquartile range, the horizontal line indicates the median, and points represent tree-level mean values. Control (C), Inter-row (I), and Under-panel (P).

Verification of model assumptions

Visual inspection of the data indicated an approximately linear relationship between the covariate *n* and mean fruit density across treatments and replicates.

Homogeneity of regression slopes was confirmed by the **absence of significant interactions** between the covariate and the experimental factors (*n × treatment*, $p = 0.154$; *n × treatment × replicate*, $p = 0.895$). Normality of residuals was confirmed by the Shapiro–Wilk test ($p = 0.148$), and homogeneity of variances was supported by Levene's test ($p = 0.131$).

One outlier (|standardized residual| > 3) was identified; however, as it was not influential and did not materially affect the model outcomes, it was retained in the analysis.

ANCOVA results

The analysis of covariance did **not reveal a significant effect of the covariate *n* on fruit density** ($F_{1,53} = 0.24$, $p = 0.626$), indicating that crop load did not influence this parameter.

In contrast, a highly significant effect of treatment on fruit density was detected ($F_{2,53} = 10.63$, $p < 0.001$), with a large effect size (generalized $\eta^2 = 0.29$). Post-hoc pairwise comparisons based on estimated marginal means (EMMs), using Tukey's adjustment for multiple testing, showed that fruits from control trees (C) exhibited significantly higher density than those from both trees located under photovoltaic panels (P) and those in the inter-row position (I) ($p = 0.003$ and p = 0.0001, respectively). In contrast, no statistically significant difference was observed between the P and I treatments ($p = 0.321$).

Neither the main effect of replicate ($p = 0.621$) nor the treatment × replicate interaction ($p = 0.464$) were significant, indicating a consistent density response across experimental replicates (Table 2.14).

Table 2.14 Pairwise comparisons among treatments based on estimated marginal means. Estimated differences, p-values, and statistical significance are reported. Significant differences were identified using Tukey's post-hoc test (p < 0.05).

Comparison	Estimated difference	p-value	Interpretation
C – I	+0.659	0.0001	Significant
C – P	+0.485	0.0030	Significant
I – P	−0.174	0.3205	Not significant

Meteorological data-analysis

Seasonal temperature analysis

Experimental setup and temperature monitoring

Continuous air temperature monitoring was carried out at each treatment position within both the Multileader and Spindle agrivoltaic systems. **Temperature sensors** were installed and maintained by EURAC Research (Bolzano, Italy) as part of the SYMBIOSIST project instrumentation. Each sensor recorded air temperature at sub-hourly resolution throughout the monitoring period.

For the purpose of this analysis, the monitoring period was restricted to the apple tree growing season, defined here as April–October, encompassing the phenological stages from budbreak to harvest. This period represents the agronomically relevant window during which microclimatic conditions are most likely to influence tree physiology, fruit development, and crop water demand.

From the daily time series, the following thermal indicators were derived for each treatment: daily mean temperature (Tmean), daily maximum temperature (Tmax), daily minimum temperature (Tmin), and the diurnal temperature range (DTR = Tmax − Tmin). Daily temperature anomalies (ΔT) relative to the respective control station (R1 for the Multileader system; R2 for the Spindle system) were computed for each treatment day to isolate the agrivoltaic microclimate effect from background meteorological variability.

Multileader system

Seasonal overview

The seasonal temperature throughout the growing season summary for the Multileader system is presented in Figure 2.30 (seasonal dot plot) and Figure 2.31 (daily ΔTmean time series). Over the monitoring period (July–October, n = 122 days per treatment), all treatments recorded broadly similar absolute seasonal temperatures:

mean Tmax ranged from approximately 25.3°C (I40) to 25.7°C (Control); mean Tmean ranged from approximately 19.1°C (I40) to 19.5°C (P5); and mean Tmin ranged from approximately 14.7°C (I40) to 15.7°C (P5). While these absolute values appear close, the paired delta analysis reveals highly structured and statistically significant treatment effects, as described below.

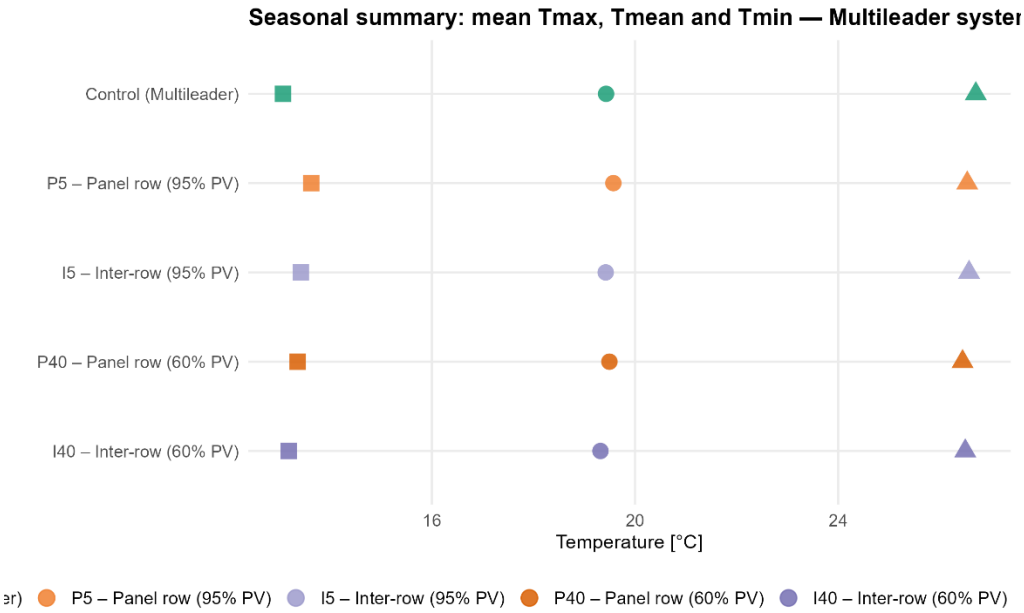

Figure 2.30 Seasonal temperature throughout the growing season summary in the multileader (newerplant) section. C = control, P5 = plant under the panels with 5% transparency, I5= plants in the inter-row between panels with 5% transparency, P40 = plants under the panels with 40% transparency, I40= plants in the inter-row between panels with 40% transparency).

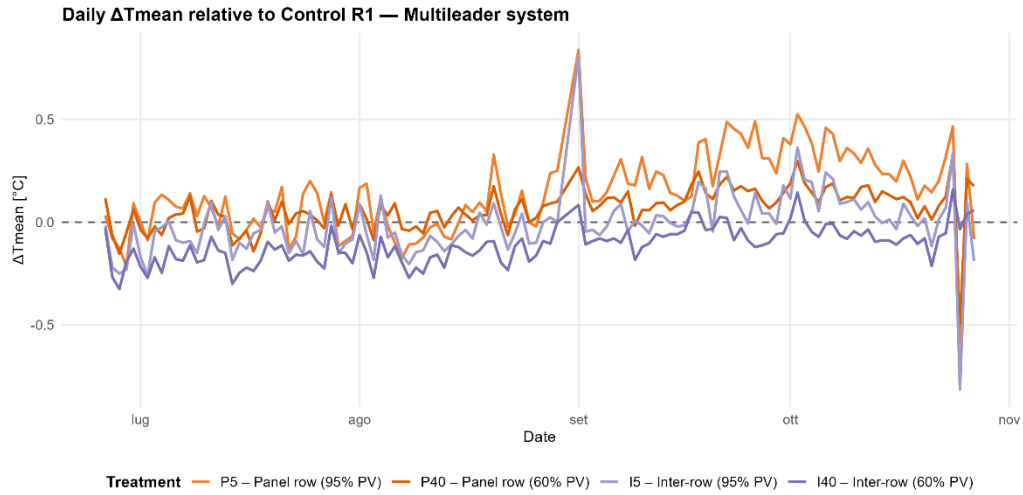

Figure 2.31 Daily ΔTmean time series in the multileader (newerplant) section. C = control, P5 = plant under the panels with 5% transparency, I5= plants in the inter-row between panels with 5% transparency, P40 = plants under the panels with 40% transparency, I40= plants in the inter-row between panels with 40% transparency).

To isolate the agrivoltaic effect from background meteorological variability, daily temperature anomalies (ΔT) relative to the Control were computed and compared across treatments using the Kruskal-Wallis test followed

by Dunn's post-hoc test with Bonferroni correction. This paired approach removes the confounding influence of seasonal temperature variation and directly quantifies the microclimatic effect of the PV panels (Figure 2.32).

ΔTmean showed highly significant differences among treatments (Kruskal-Wallis $p = 1.9\times10^{-40}$). Post-hoc analysis revealed two distinct groups: Panel-row treatments (P5 and P40, letters "c") consistently recorded warmer daily mean temperatures than the Control (+0.1 to +0.2°C), while Inter-row treatments (I5, I40) recorded cooler temperatures, with I40 showing the strongest cooling effect (letter "a", $p < 0.001$ vs all other treatments). P5 and P40 were not significantly different from each other (ns), nor were I5 and I40, suggesting that PV cell density (95% vs 60%) had a limited effect on Tmean (Figure 2.32).

ΔTmax showed significant but weaker differentiation among treatments ($p = 2.6\times10^{-2}$). All treatments recorded lower daily maximum temperatures than the Control (negative ΔTmax), consistent with shading from PV panels. Only the I5 vs P40 comparison reached significance ($p = 0.016$), while most other pairwise comparisons were non-significant, suggesting that shading effects on Tmax are relatively uniform across positions (Figure 2.32).

ΔTmin showed the strongest and most structured differentiation ($p = 3.6\times10^{-49}$). P5 recorded the highest positive ΔTmin (letter "c", i.e. warmest nights), followed by P40 (letter "b") and I5 (letter "b"), while I40 showed near-zero or slightly negative ΔTmin (letter "a"). This pattern suggests that the panel structure retains heat more effectively in the panel-row positions, particularly under higher PV density (Figure 2.32).

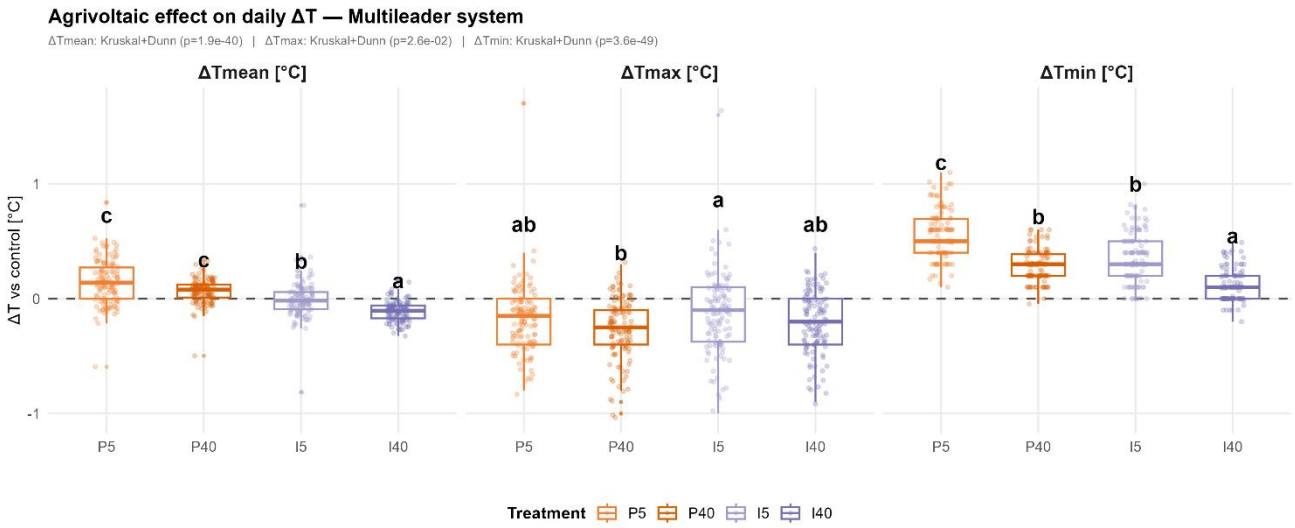

Figure 2.32 Daily temperature anomalies (ΔT) relative to the Control R1 were computed and compared across treatments using the Kruskal-Wallis test followed by Dunn's post-hoc test with Bonferroni correction.

Spindle system

Seasonal overview

In the Spindle system, both Panel-row (P) and Inter-row (I) treatments showed consistently negative ΔTmean throughout the monitoring period (July–October, n = 115 days per treatment), ranging approximately between −0.2 and −0.7°C relative to Control R2 (Figure 2.33). This persistent cooling pattern indicates that the older Spindle structure, characterised by a single PV panel density (95% cell opacity), induces a generalised reduction in mean air temperature across all positions within the agrivoltaic canopy.

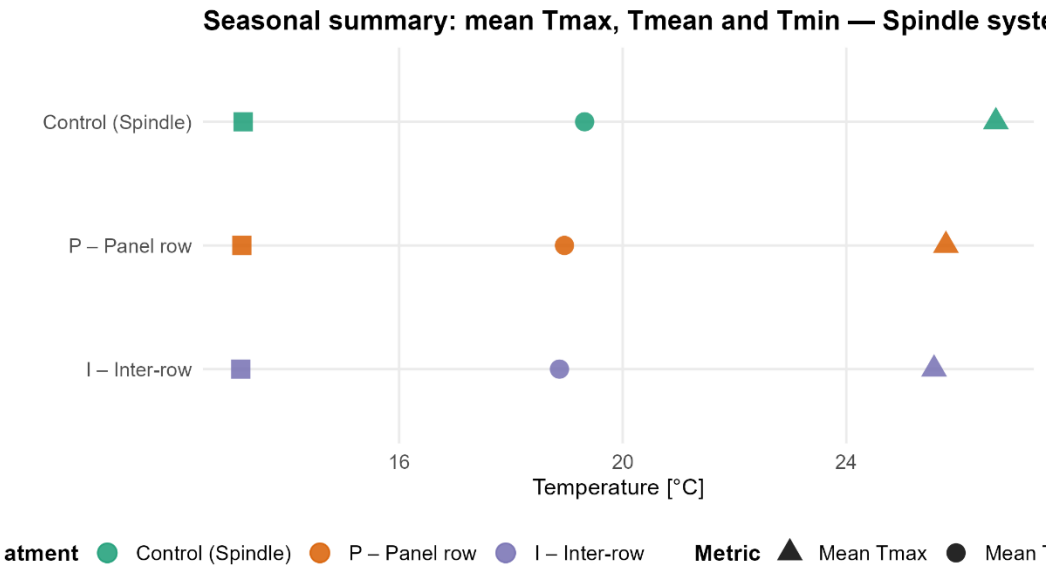

Figure 2.33 Seasonal temperature throughout the growing season summary in the spindle (olderplant) section. C = control, P = plant under the panels, I= plants in the inter-row between panels.

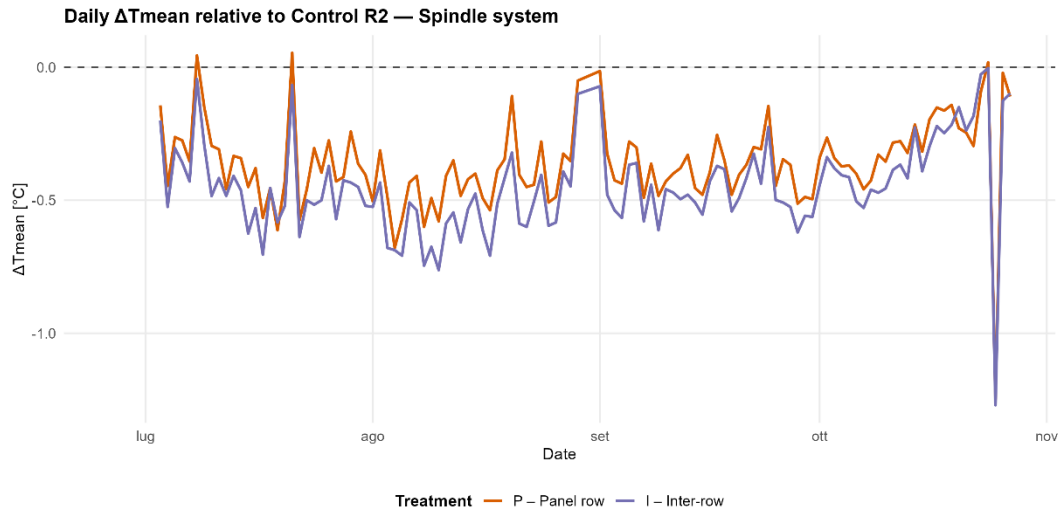

Figure 2.34 Daily ΔTmean time series in the Spindle (olderplant) section. C = control, P = plant under the panels, I= plants in the inter-row between panels.

The Kruskal-Wallis test confirmed significant differences between P and I for both ΔTmean ($p = 7.9\times10^{-7}$) and ΔTmax ($p = 1.4\times10^{-3}$), while ΔTmin did not differ significantly between the two treatments (p = 0.50) (Figure 2.34).

For **ΔTmean**, the Inter-row position (I) showed a stronger cooling effect than Panel-row (P) (letter "a" vs "b"), indicating that temperatures between panel rows were more effectively buffered. For **ΔTmax**, a similar pattern was observed (P letter "b" > I letter "a"), with the Inter-row recording lower daily maxima. The absence of significant differences in **ΔTmin** suggests that both positions experience similar nocturnal thermal conditions under the Spindle canopy structure (Figure 2.35)

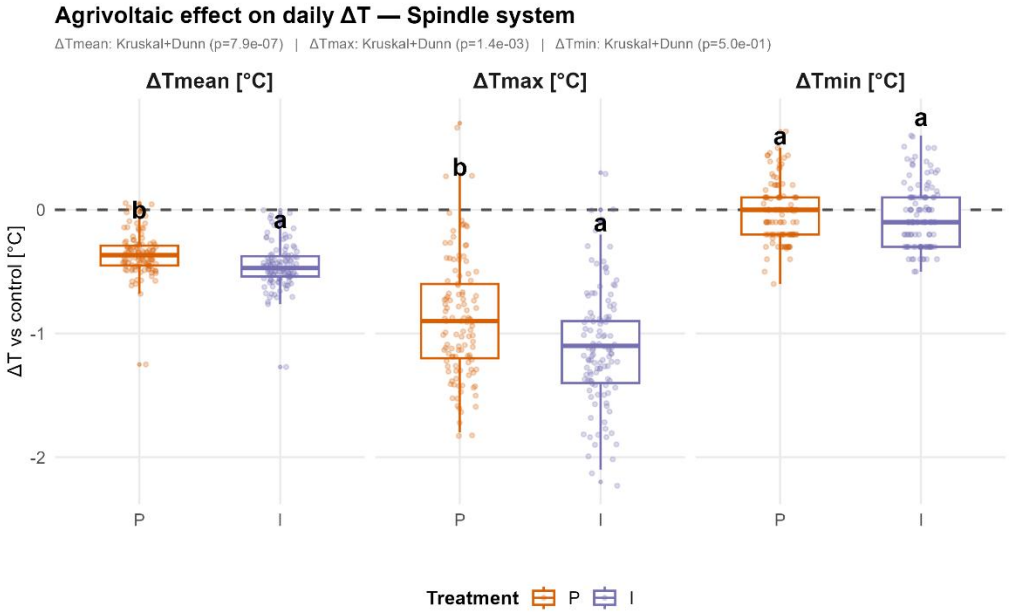

Figure 2.35 Daily temperature anomalies (ΔT) relative to the Control R1 were computed and compared across treatments using the Kruskal-Wallis test followed by Dunn's post-hoc test with Bonferroni correction.

Summary and agronomic implications

Across both systems, the **agriPV structure consistently modified the microclimate relative to the open field control**. In the Multileader system, panel-row positions (P5, P40) experienced warmer nights and cooler daytime maxima Tmax compared to the Control, while inter-row positions (particularly I40) showed cooler nights and a moderate Tmax reduction. The net effect on Tmean was a slight warming under panels and slight cooling in inter-rows. The PV cell density (95% vs 60%) had a limited influence on Tmean and Tmax but influenced Tmin more markedly.

In the Spindle system, both positions experienced a generalised cooling effect on Tmean and Tmax, with the inter-row position showing consistently lower temperatures than the panel row. Nocturnal temperatures were unaffected by treatment position in this system.

These results suggest that the spatial arrangement and coverage fraction of PV panels are key determinants of agrivoltaic microclimate effects, and that position-specific temperature buffering may have implications

for crop heat stress mitigation during extreme thermal events — a hypothesis explored further in the following section.

Soil water status and irrigation efficiency assessment

Monitoring approach

Soil water status was monitored using **tensiometers** installed in the apple orchards within the Bolzano agri-PV demonstrator (methodology and layouts explained in chapter 2.2.3). Tensiometers continuously recorded soil water tension (expressed in mbar, negative values), providing high-resolution temporal data on soil moisture dynamics during the irrigation season.

The following analysis focused on the period between 30 July and 14 August 2025, which included a clearly identifiable irrigation event on 2 August 2025 at 10:00. This irrigation cycle was selected as a representative example for evaluating soil drying dynamics and irrigation efficiency under different agri-PV treatments. A soil water tension threshold of −300 mbar was adopted to indicate conditions of relevant soil water depletion, in line with common irrigation management practices for apple orchards.

Soil water tension dynamics after irrigation

Raw soil water tension curves showed distinct post-irrigation responses among treatments (Figure 2.36). Following the irrigation event, all treatments exhibited a rapid decrease in soil water tension (less negative values), indicating soil rewetting. However, both the magnitude of the rewetting peak and the subsequent drying dynamics differed between treatments. The control (C) showed a strong initial rewetting but also a rapid decline in soil water status in the following days. The inter-row treatment (I) exhibited a more moderate rewetting peak and a slower, more gradual drying pattern. The panel row treatment (P) showed intermediate behavior, with pronounced short-term fluctuations superimposed on a gradual drying trend.

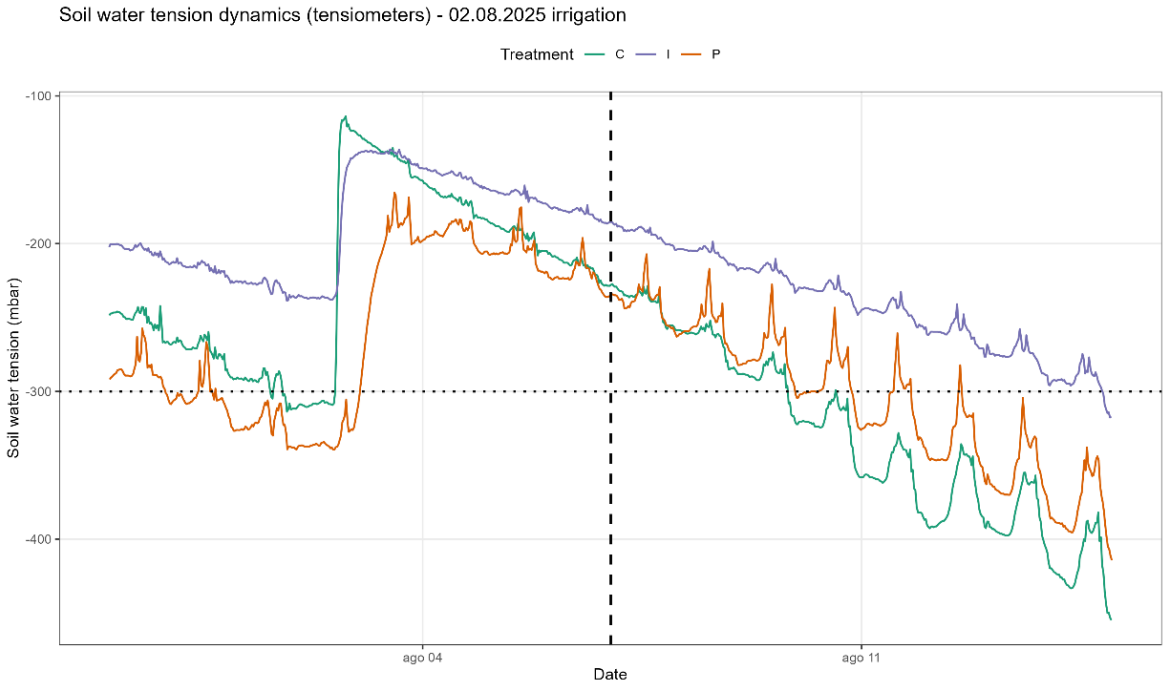

Figure 2.36 Soil water tension dynamics (mbar) for the control (C), inter-row (I), and under-panel (P) treatments.

Irrigation efficiency indicators

Time to reach dry soil conditions

The time required to reach the −300 mbar threshold after irrigation differed markedly among treatments. The control and panel row treatments reached the threshold after 6 days, while the inter-row treatment maintained soil water availability for a substantially longer period of 10 days (Table 2.15).

Table 2.15 Time to dry (hours from peak) of the soil tensiometers after the normalization.

Treatment	Time to dry (hours from peak)
C	170 h
I	273 h
P	154 h

Soil drying rate

Drying rates were estimated as the slope of soil water tension decline from the post-irrigation peak to the dry threshold (Figure 2.37). This indicator is **independent from the soil water tension** of the treatment at the moment of the irrigation, so is better describing the acidity of the soil. The control treatment showed the steepest drying slope, indicating the fastest water loss. The inter-row treatment exhibited the slowest drying rate, while the panel row treatment showed intermediate values (Table 2.16).

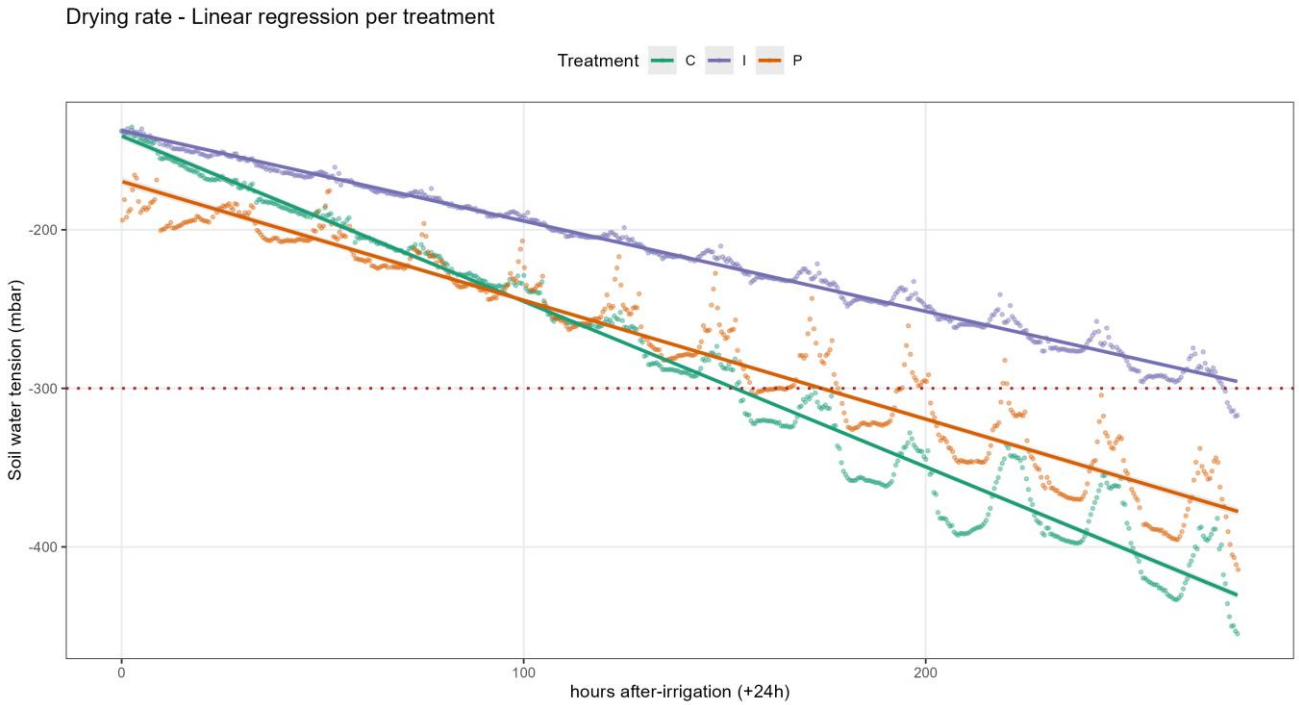

Figure 2.37 Linear regression per treatment of the drying rate of the soil in the three treatments (C control, P panels, I inter-row).

Table 2.16 Soil drying rate estimated as the slope of soil water tension decline from the post-irrigation peak to the −300 mbar threshold for each treatment.

Treatment	Drying rate (mbar h^{-1})
C	−1.01
I	−0.57
P	−0.65

Together, these indicators consistently suggest that the presence of photovoltaic structures, contributed to a reduction in soil water depletion rates, likely due to partial shading and reduced evaporative demand.

Implications

Although the irrigation system **did not always operate optimally during the season**, and the growing season was characterized by frequent rainfall events, making irrigation effects difficult to isolate, the tensiometer-based analysis provided clear insights into soil water dynamics under different agri-PV configurations. The results indicate that agri-PV systems can significantly influence soil water retention and drying behavior, with potential implications for irrigation scheduling and water use efficiency. This approach demonstrates the value of continuous soil water monitoring combined with post-irrigation normalization techniques to assess irrigation efficiency under complex field conditions such as agri-PV systems.

2.3. Conclusion and Perspectives

The first year of activity of the Bolzano Agri-PV demonstrator provided a comprehensive overview of the agronomic and physiological responses of an apple orchard integrated with PV structures. Overall, the results indicate that the agri-PV system significantly modified the orchard microclimate, with clear effects on soil water dynamics and fruit quality, while having a more limited impact on vegetative growth. Soil monitoring revealed slower drying rates and prolonged water availability under and between PV panels, suggesting a potential improvement in water-use efficiency compared to the open-field control, even though the interpretation of irrigation effects was partly constrained by a rainy growing season. From a production perspective, tree-level yield was significantly lower (-15 %) under agri-PV conditions than in the control, mainly driven by a reduced number of fruits per tree rather than by differences in individual fruit size. Fruit quality analyses consistently showed reduced red coloration, lower soluble solids content (SSC), higher acidity, and lower starch degradation under PV panels, while fruit firmness was not significantly affected. Taken together, these results suggest that shading primarily influences fruit maturation and ripening dynamics, potentially inducing a delay in physiological maturity.

Future activities will focus on strengthening and extending these findings. The experimental trials will be repeated during the 2026 growing season using the same experimental design, allowing the assessment of inter-annual variability and improving the robustness of the conclusions. In addition, the scope of measurements will be expanded to include detailed phenological observations, such as flower bud number, flowering intensity, and flowering dynamics. These measurements were not included in the first year because floral induction occurred in the previous season (2024), before the installation of the PV structures. Integrating phenological data will be essential to disentangle whether the observed differences in fruit coloration, sugar accumulation, and acidity are mainly the result of a delayed phenological development or whether agri-PV shading directly limits fruit maturation processes. This extended approach will support a more mechanistic understanding of plant responses to agri-PV systems and contribute to defining agronomic strategies that optimize both energy production and fruit quality under agri-PV conditions.

3. Agri-PV demonstrator – Barcelona (SP)

3.1. Site description and experimental design

Location of the experiment

Pilot plant plot

The field experimental activities for this study were conducted at Agropolis (Figure 3.1), a dedicated agri-food innovation and research living lab, managed by the Barcelona School of Agri-Food and Biosystems Engineering (EEABB) of the Universitat Politècnica de Catalunya (UPC), and located at approximately 2.0 m above sea level (41°17’ N, 2°03’ E). This is an open-air experimental research facility dedicated to applied agricultural innovation and the development of sustainable production systems. It occupies approximately 9.14 Ha. The facilities offer open-air field plots, irrigated cultivation areas, greenhouses (glass and plastic), mechanization facilities, laboratories and services for research, innovation and technology transfer. It is part of the CER research center Agrotech-UPC ecosystem of living labs that fosters collaboration between academia, producers and industry for sustainable agricultural development.



Figure 3.1 Aerial view of Agropolis (left) and facilities (right).

Within this experimental facility, a permanent agrivoltaic structure was installed on one cultivation plot (Agrivoltopolis), consisting of ten sets of photovoltaic modules mounted on ground support poles (Figure 3.2). This infrastructure forms the basis of comparative agronomic trials, enabling replicated crop cultivation under modified radiation conditions imposed by the PV-mesh system, alongside matched full-sun control plots. **The experiment was conducted over two cropping cycles (summer and autumn**), during which different crop varieties were cultivated. The experimental plot maintained the same overall block layout and general dimensions throughout both cycles. The total dimensions of the pilot plant plot are 66 × 18 m^2.



Figure 3.2 Agrivoltaic pilot plant at Agropolis.

Laboratories

At the Agropolis facilities (Figure 3.3a), laboratory spaces were available for handling harvested plant material, including equipment for measuring plant size and fresh weight, as well as appropriate material for sample handling and temporary storage after harvest. These laboratories are equipped and routinely used for measurements related to vegetable crop production and characterization. In Castelldefels (Barcelona), **analyses related to plant biomass** were carried out at the labs of EEABB. This engineering school is located at the Baix Llobregat Campus (CBL) and brings together several scientific UPC groups working in the fields of agronomy, biosystems engineering and agri-food sciences. The vegetable production laboratories available at these facilities are equipped with drying ovens for sample dehydration and subsequent determination of dry weight (Figure 3.3b). These laboratory spaces are designed both for experimental work and teaching activities and are conditioned for standard agronomic and biochemical analyses.



Figure 3.3 Laboratory facilities at Agropolis (a) and EEABB–UPC (b)

Description of the photovoltaic panels

The pilot plant consists of **150 photovoltaic panels (Aleo Solar GmbH, Prenzlau, Germany) with a total installed capacity of 50.25 kW**. They are able to generate approximately 400 kWh per day. The installation occupies a total surface area of 9,000 m² and includes a reference crop area used as an open-field control, located to the east. The panels are fitted with anti-reflective coating to minimize glare due to the proximity to Barcelona Airport. All panels are mounted on solar trackers, mechanical devices that adjust their east-west position to maximize solar energy capture. Panel movement is controlled through mathematical models accounting for meteorological conditions and plant light requirements ensuring crop development while maintaining energy production.

The panels are arranged in ten sets mounted on steel posts and organized into two blocks **with different transparency levels**. Each set is supported by four steel posts, with five photovoltaic panels installed between two adjacent posts. The modules are mounted on a galvanized steel supporting structure designed for outdoor operation and dynamic loading associated with solar tracking. One block presents five rows of panels with 5 % light transmittance, while the second block includes five rows of panels with 40 % transmittance (Figure 3.4). In addition, a third control block without photovoltaic structures is established under full-sun conditions.

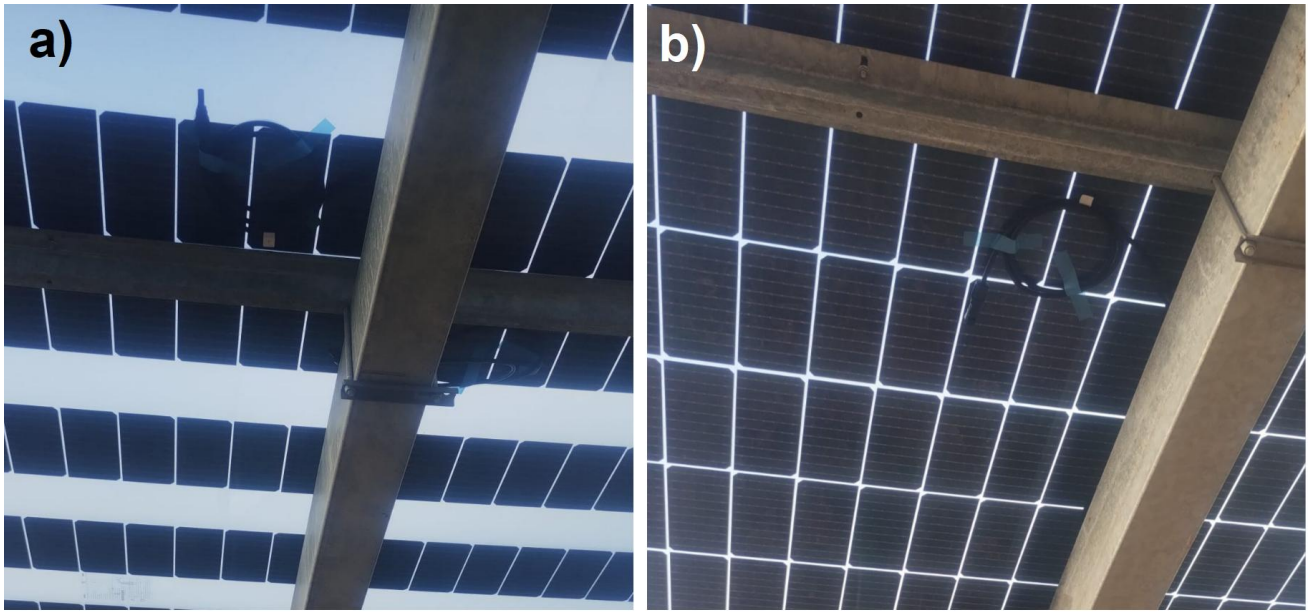

Figure 3.4 Photovoltaic panel arrangements with different transparency levels: (a) 40 % transmittance and (b) 5 % transmittance.

For the 40 % transparency configuration, light transmittance is achieved through regular spacing between photovoltaic cells rather than through translucent encapsulation. This design approach is typical of agri-PV systems, as it allows partial transmission of solar radiation to the underlying crop while maintaining energy generation. Regarding cell technology, the modules are composed of rectangular, dark-colored cells with visible busbars, consistent with crystalline silicon photovoltaic technology. From an optical standpoint, light transmission beneath the modules is not homogeneous but spatially modulated, with shaded areas directly below the cells and zones of direct radiation through the inter-cell gaps.

Microclimate monitoring

A field-based microclimate monitoring system is deployed across the experimental plots to continuously record key environmental variables under contrasting radiation regimes (Figure 3.5). For each block, the same set of sensors is replicated. The cropping area combines aerial and soil sensors. These sensors are characterizing the interaction between photovoltaic structures, microclimatic modification, and horticultural crop performance. All sensors are connected to on-site electrical control boxes and data logging units installed directly in the field. This configuration allows continuous and synchronized monitoring of environmental variables across the three experimental zones.



Figure 3.5 Environmental sensing in the agrivoltaic plots: (a) PAR radiation measurement; (b) soil monitoring at crop level.

Air conditions at crop height are monitored using a total of three air temperature-relative humidity probes (Epluse HTP201 model; E+E Elektronik Ges.m.b.H., Engerwitzdorf, Austria) installed inside three radiation shields to reduce measurement bias from direct solar exposure. Soil conditions in the root zone are monitored using eight combined soil moisture and temperature sensors (HD3910.1.10 model; DeltaOhm, Caselle di Selvazzano, Italy) installed close to the crop rows to track belowground dynamics throughout the cropping cycle. Soil sensors are installed close to the root zone to continuously register soil temperature and volumetric water content

In parallel, the modification of the crop light environment induced by the agrivoltaic structures is quantified using five ePAR sensors (SQ-618-SS model; Apogee Instruments, Inc., Logan, Utah, USA), supporting comparisons of radiation availability across treatments and its temporal variability over the cropping cycle. The system incorporates sensors specifically aimed at quantifying the modification of the light environment induced by the agrivoltaic structures. PAR radiation sensors are installed below the photovoltaic modules to measure the spatial and temporal distribution of photosynthetically active radiation reaching the crop canopy. These measurements are carried out under the two panel configurations as well as under open-field control conditions, enabling direct comparison of radiation availability and its variability across treatments. The resulting radiation datasets are used to analyze the incidence of shading on crop development and to support the interpretation of agronomic responses under contrasting light environments. Furthermore**, four broadband pyranometers** (SR05-D2A2 model; Hukx Sensor Technology, Delft, Netherlands) are installed at reference positions on the agrivoltaic structure to **measure incoming global solar radiation**. These measurements provide an external radiation baseline, allowing the characterization of overall atmospheric conditions and supporting the interpretation of PAR transmission and microclimatic modification induced by the photovoltaic system.

In parallel with the fixed monitoring system, crop development is monitored using a ground-based mobile robot operating within the experimental plots (Figure 3.6). The robotic platform complements the data obtained from the fixed sensor network by providing additional information on crop condition and spatial

variability. The robot is equipped with an RGB camera (RealSense D457 model; Intel, Mountain View, California, USA) and an active radiometric sensor (Crop Circle ACS-211 model; Holland Scientific, Lincoln, Nebraska, USA), which captures spectral information related to plant vigor. In addition, a thermal camera (Optris Xi 400 model; Optris GmbH, Berlin, Germany) is used to measure foliar temperature, enabling the assessment of plant thermal status and the detection of potential heat stress.

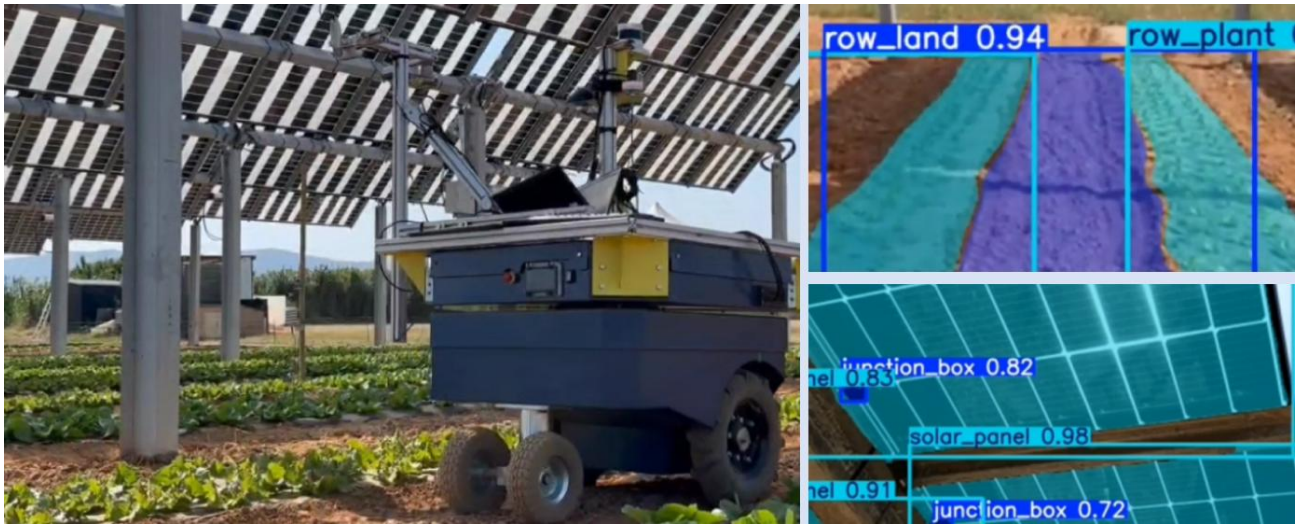

Figure 3.6 Mobile robot operating under the agrivoltaic structure (left); RGB-based scene analysis of crop rows (right).

Plant material

For the implementation of the experiment, *Lactuca sativa* L. cultivar Maravilla, *Lactuca sativa* L. cultivar Romana, and *Brassica oleracea* var. *italica* were used as plant material (Figure 3.7). During the summer cropping cycle, the two lettuce cultivars were combined, whereas during the autumn cycle all three crop types were included. A total of 15 trays containing 200 seedlings per cultivar were acquired for the summer cycle, and 10 trays containing 200 seedlings per cultivar for the autumn cycle. According to the distribution of sections and repetitions defined in the experimental design, 5,376 seedlings were initially transplanted during the summer cycle and 3,900 during the autumn cycle.



Figure 3.7 Crop cultivation at Agropolis to evaluate the performance of two lettuce varieties and one broccoli variety within an agrivoltaic system: a) Randomized experimental plots; b) close-up of the Maravilla lettuce variety; c) close-up of the broccoli crop.

Experimental layout

Structure of the subplots

The experiment is conducted in three main subplots designed to **evaluate the effects of different levels of photovoltaic coverage.** These subplots correspond to opaque panels with 5 % transmittance (denoted such as 'section 1'), semi-transparent panels with 40 % transmittance ('section 2'), and an open-field control area ('section 3'). The experiment takes place over **two cropping cycles, summer and autumn**, allowing the assessment of crop responses at different growth periods. All subplots were organized into 28 crop rows hosting the experimental replicates according to the cropping cycle and are oriented north-south, to account for radiation gradients generated by the photovoltaic panels and to ensure a balanced distribution of replicates across zones with different light exposure (Figure 3.8).

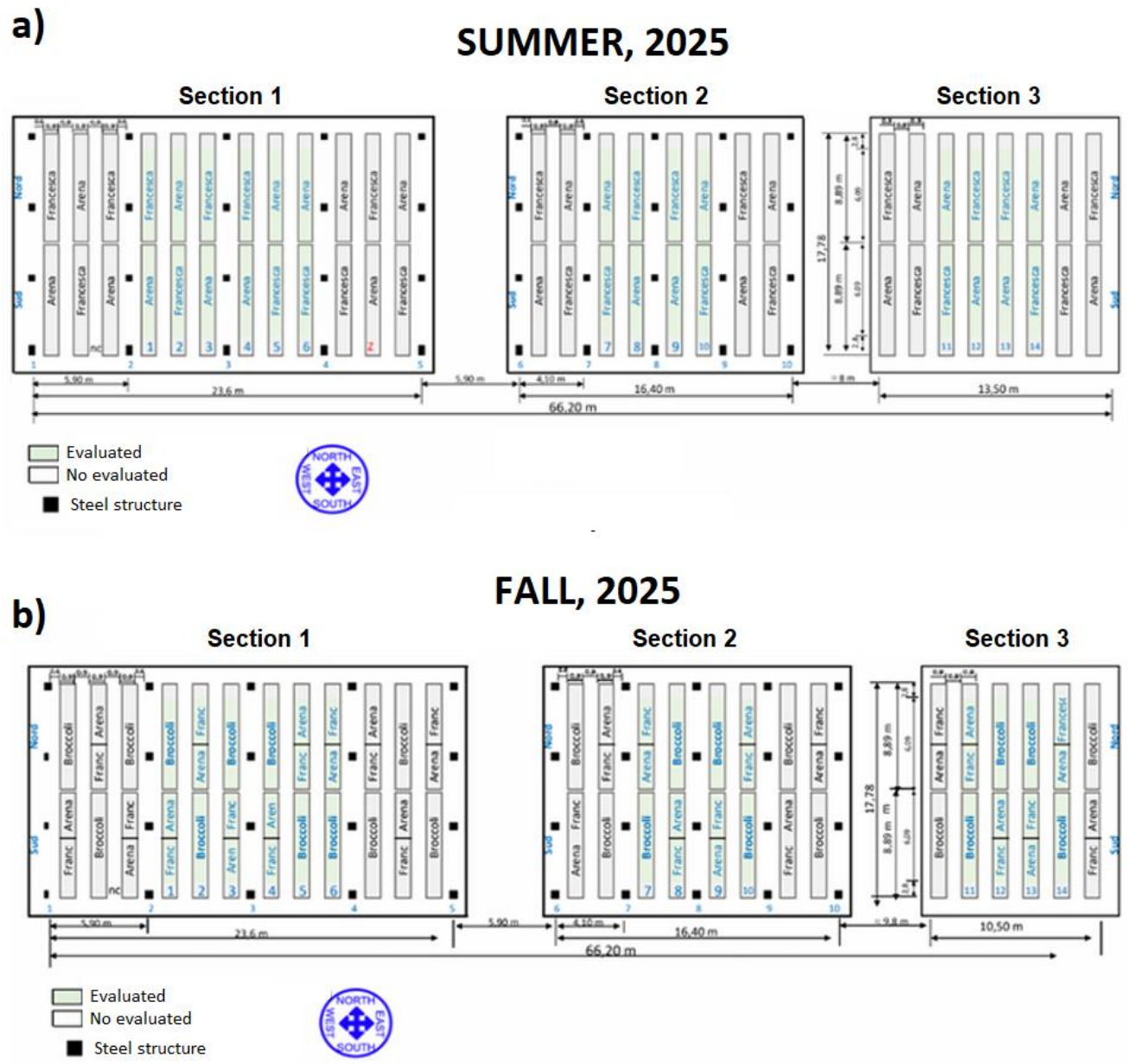

Figure 3.8 Experimental layout of crop rows across agrivoltaic sections and open-field control for the summer (a) and autumn (b) 2025 cropping cycles, showing the spatial distribution of evaluated and non-evaluated crop rows, crop species and cultivars, and the relative position of the photovoltaic structures within each section.

Each experimental section was subdivided into a fixed number of crop rows that constitute the experimental units. During both cycles, agrivoltaic section 1 (opaque panels, west) contained twelve crop rows, agrivoltaic section 2 had eight rows, and the open-field control section encompassed eight plant rows (east). The spacing between rows of standard module trackers was 5.9 m, allowing three crop rows with ground cover, whereas the spacing between rows of semi-transparent module trackers was 4.1 m, allowing two crop rows.

Subplot dimensions and distances between sections varied slightly between cycles. During the summer cycle, the opaque subplot covers an area of 23.60×17.78 m, the semi-transparent subplot extends 16.40 × 17.78 m, and the control subplot occupies 13.50×17.78 m. The distance between the opaque and semi-

transparent sections is 5.9 m, whereas the distance between the semi-transparent and control sections is approximately 8.0 m.

In agrivoltaic section 1 (opaque panels), six out of twelve rows were selected for evaluation, whereas in agrivoltaic section 2 (translucen modules), four out of eight rows were evaluated. In the open-field control section, four out of eight rows were checked. The remaining rows acted as buffer rows. This selection was applied to minimize border effects within each section and to ensure that the evaluated rows were representative of the radiation and microclimatic conditions generated by each treatment. This approach was carried out to ensure that crop performance was assessed under stable conditions by minimizing border effects and improving comparability across treatments.

With respect to planting density, during the summer cycle the opaque module section contained 2,304 seedlings, whereas translucent section and control subplots each included 1,536 seedlings. On the other hand, for the autumn cycle, the opaque section included 1,800 seedlings, the semi-transparent incorporated 1,200, and the control subplot of section 3 was 900.

Arrangement of beds and replication blocks

Each crop row corresponded to an individual bed, which was considered the basic experimental unit for crop management and data collection. **The arrangement of beds and replicate blocks was designed to ensure maximum representativeness and repeatability of the experimental factors**.

As it was mentioned in the previous section, the opaque and semi-transparent subplots comprised twelve and eight beds, respectively, while the control subplot included eight beds. For the summer period, each bed was divided into two halves corresponding to the two lettuce varieties, with each half considered an experimental block. This structure allowed replicates to be distributed in a balanced manner between the north and south zones, ensuring that all exposure combinations were represented. In total, the opaque subplot included twenty-four blocks, while the semi-transparent and control subplots each included sixteen blocks (Figure 3.8).

Besides this, following the incorporation of broccoli, the internal subdivision of each bed was adapted to accommodate the three studied crops in the autumn cycle. Each bed was divided into three differentiated sections. One half was entirely allocated to broccoli, while the remaining half was subdivided into two sections of different sizes to host the two lettuce varieties, with one section being approximately twice the size of the other. The position of the larger section alternated between the north and south sides, as did the distribution of the lettuce sections, with the aim of ensuring that all possible combinations of the studied factors were represented. In this cycle, the opaque subplot maintained the same number of beds, the semi-transparent subplot comprised eight beds, and the control subplot comprised six beds (Figure 3.8).

Regarding the internal organization of crop rows, during the summer cycle each half-bed included four lettuce rows with twenty-four plants per row, resulting in a total of ninety-six plants per bed. During the autumn cycle, the enlarged section allocated to broccoli included two rows with fifteen plants each, while the section assigned to lettuce was subdivided into two parts, consisting of four rows with ten plants in the smaller section and four rows with twenty plants in the larger section. Figure 3.9 shows a detailed schematic of the internal plant arrangement for both cropping cycles.

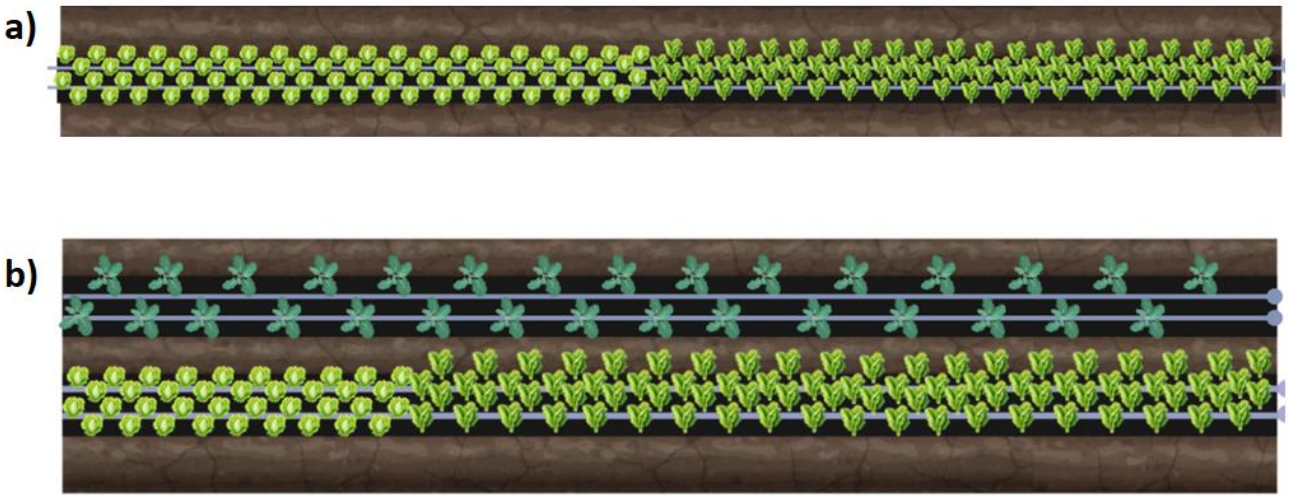

Figure 3.9 Organization of crop rows for the two single blocks of the summer cycle (a) and one representative block of the autumn cycle (b).

Experiment management

The experiment management was structured into **two main phases for both cropping cycles**. First, all activities required for the installation of the agrivoltaic structures, field preparation, initial crop establishment, and plant growth monitoring were carried out, including regular field inspections and routine crop management operations. After the completion of each experimental cycle, post-harvest tasks were performed, including laboratory analyses and the determination of the parameters defined for each cycle.

Plot and facility preparation

Before planting, bed preparation was performed using **standard mechanized tillage** (Figure 3.10a). The clearance under the agrivoltaic structure allowed normal tractor operation between rows, without constraining soil management practices. The external and internal boundaries were also delimited, and black mulching plastic was installed (Figure 3.10b). This material helped reduce weed growth, improve soil moisture conservation, and limit access to wildlife to the crop area. Drip irrigation was installed across the entire experimental area, with two drip lines per bed laid in parallel, equipped with emitters spaced every 40 cm and arranged in a staggered (triangular) configuration to ensure homogeneous water distribution.



Figure 3.10 Plot preparation under the agrivoltaic structure: (a) mechanized soil tillage and bed formation using conventional tractor operations; (b) final arrangement of prepared beds with mulching installed beneath the photovoltaic structure

In parallel, the photovoltaic modules corresponding to each treatment were installed, and several protective elements adapted to the local environmental conditions were implemented. Given that the Agropolis site is located within a Special Protection Area for Birds (ZEPA), specific measures were applied to **minimize damage caused by wildlife**, particularly birds and rabbits. These actions included the installation of a perimeter electric fence to prevent rabbit intrusion, the deployment of protective netting against birds over the most exposed crop areas, and the use of acoustic deterrent systems, such as scare devices and a gas-powered bird scarer.

The installation of the perimeter protection systems, including fencing and wildlife deterrent elements, was also performed entirely by hand (Figure 3.11).



Figure 3.11 Installation of perimeter fencing for crop protection around the agrivoltaic structure.

Planting and management of plant material

The transplanting was carried out on previously formed raised beds covered with plastic mulch, with seedlings manually placed through pre-cut holes to ensure uniform spacing and alignment along each crop row (Figure 3.12). Plant spacing and row geometry were defined using guide strings and visual markers, allowing consistent plant distribution and facilitating subsequent agronomic operations and monitoring activities. Immediately after transplanting, seedlings were manually pressed into the soil to improve root-soil contact and reduce transplant shock. Planting operations were carried out under stable soil moisture conditions to promote rapid establishment and reduce early-stage water stress. The layout of the plantation allowed a clear space between the rows for manual operations and field assessments to be carried out throughout the growing cycle.

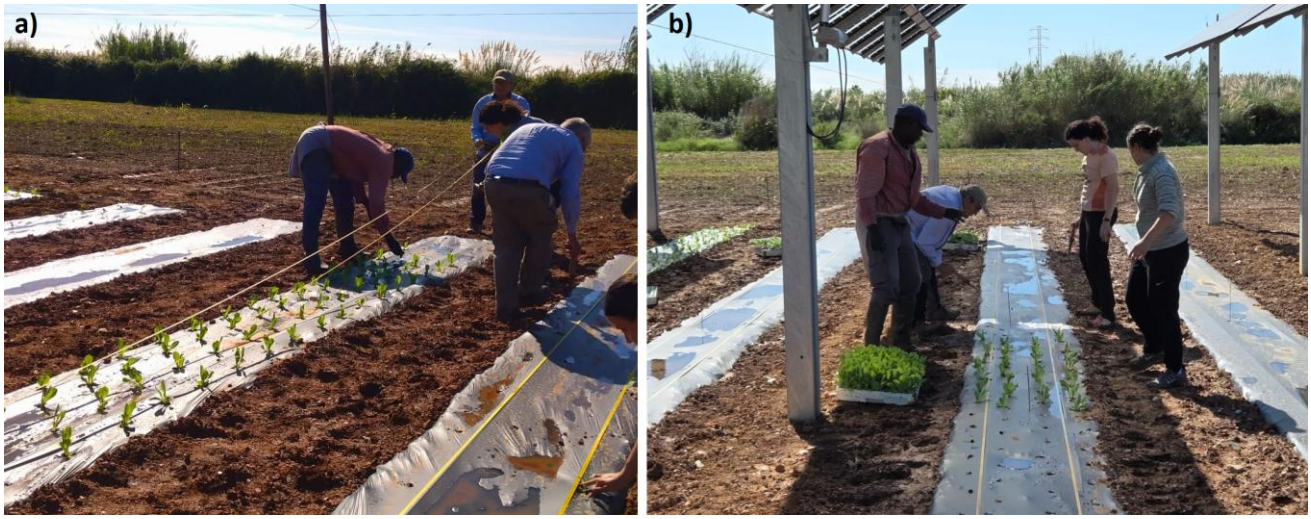

Figure 3.12 Transplanting work: a) alignment and spacing of seedlings along mulched crop rows and b) placement of seedlings within the prepared beds.

Due to the large number of plants and the staggered availability of seedlings from the nursery, transplanting was carried out over several consecutive days, as detailed in Tables 3.1 and 3.2 for summer and autumn cycle, respectively. Seedlings showing evident biometric anomalies, such as abnormal root development or extreme differences in aboveground height, were discarded and were not included in the experiment.

Table 3.1 Chronology of experimental activities during the summer cycle

Date	*Activity*
01/06/2025	Preliminary plot preparation (soil tillage and organic matter incorporation)
22/06/2025	Final plot conditioning and lettuce transplanting
26/06/2025	Crop monitoring 1 (phenotypic measurements)
03/07/2025	Crop monitoring 2
10/07/2025	Crop monitoring 3
16/07/2025	Crop monitoring 4
17/07/2025	Lettuce harvest and sample drying

Table 3.2 Chronology of experimental activities during the autumn cycle

Date	**Activity**
02/09/2025	Final plot conditioning and transplanting of romaine lettuce and broccoli
06/10/2025	Crop monitoring 1 (romaine lettuce and broccoli)
08/10/2025	Transplanting of ‘Maravilla’ lettuce
15/10/2025	Crop monitoring 2 (broccoli and romaine lettuce)
27/10/2025	Crop monitoring 3 (broccoli and lettuces)
29/10/2025	Harvest material preparation
30/10/2025	Harvest of romaine lettuce (rows 1 and 2)
31/10/2025	Harvest of romaine lettuce (rows 1 and 2)
03/11/2025	First dry biomass weighing

04/11/2025	Harvest of romaine lettuce (rows 3 and 4)
05/11/2025	Harvest of romaine lettuce (rows 3 and 4) and crop monitoring 4 (broccoli and 'Maravilla' lettuce)
10/11/2025	Second dry biomass weighing
12/11/2025	Third dry biomass weighing
17/11/2025	Crop monitoring 5 (broccoli and 'Maravilla' lettuce)
27/11/2025	Crop monitoring 6 (broccoli and 'Maravilla' lettuce)
11/12/2025	Crop monitoring 7 (broccoli and 'Maravilla' lettuce)
17/12/2025	Harvest of lettuce ('Maravilla')
18/12/2025	Harvest of broccoli

During the first week after transplanting, replanting was performed for seedlings that failed to establish, following standard agricultural practice in commercial fields. This operation aimed to maintain homogeneous plant density across subplots while minimizing plant losses, with only a minimal time difference relative to the initial planting date.

Crop management practices, including irrigation, manual weed control, and pest management, were applied uniformly across all subplots using the same decision criteria and schedules. Fungal disease control was carried out when required using a backpack sprayer and copper oxychloride as the active ingredient. This approach allowed the effects of the photovoltaic treatments to be isolated from those of routine agronomic management. Morphological and phenological variables were recorded during each monitoring session on the same set of plants to ensure traceability throughout the growing cycle. Harvesting was carried out when each crop reached its optimal commercial stage, following prior assessment of maturity parameters.

Growth evolution and monitoring

Following the experimental calendar (Tables 3.1 and 3.2), once planting was completed and after the initial replanting period to correct early losses**, periodic crop monitoring activities were conducted to assess plant growth and development under each photovoltaic treatment**. In this way, a methodological consistency across all subplots and detecting any deviations in growth dynamics during the cropping cycle could be guaranteed. The size of the plants was checked by means of the length of the longest leaf, and the maximum and minimum diameters generated by the set of external leaves of each plant. Given the high number of plants and in order to minimize edge effects, both monitoring and harvest activities were restricted to the internal beds (beds 1 to 14), allocated across the three experimental sections (Figure 3.9). Within each selected bed, measurements were conducted on the two inner crop rows in the case of lettuce, and on the two available rows in the case of broccoli. To further reduce border effects and avoid sampling all plants within each bed, measurements were initiated from the midpoint of the bed (Figure 3.13), moving towards the side closest to the center of the experimental block in beds that were not symmetrically arranged. In large lettuce blocks, ten consecutive plants were measured starting from this reference point. In smaller lettuce blocks, consisting of only ten plants, all individuals were measured. For broccoli, measurements also started from the midpoint of the bed, beginning with the third plant and recording data from ten consecutive plants.

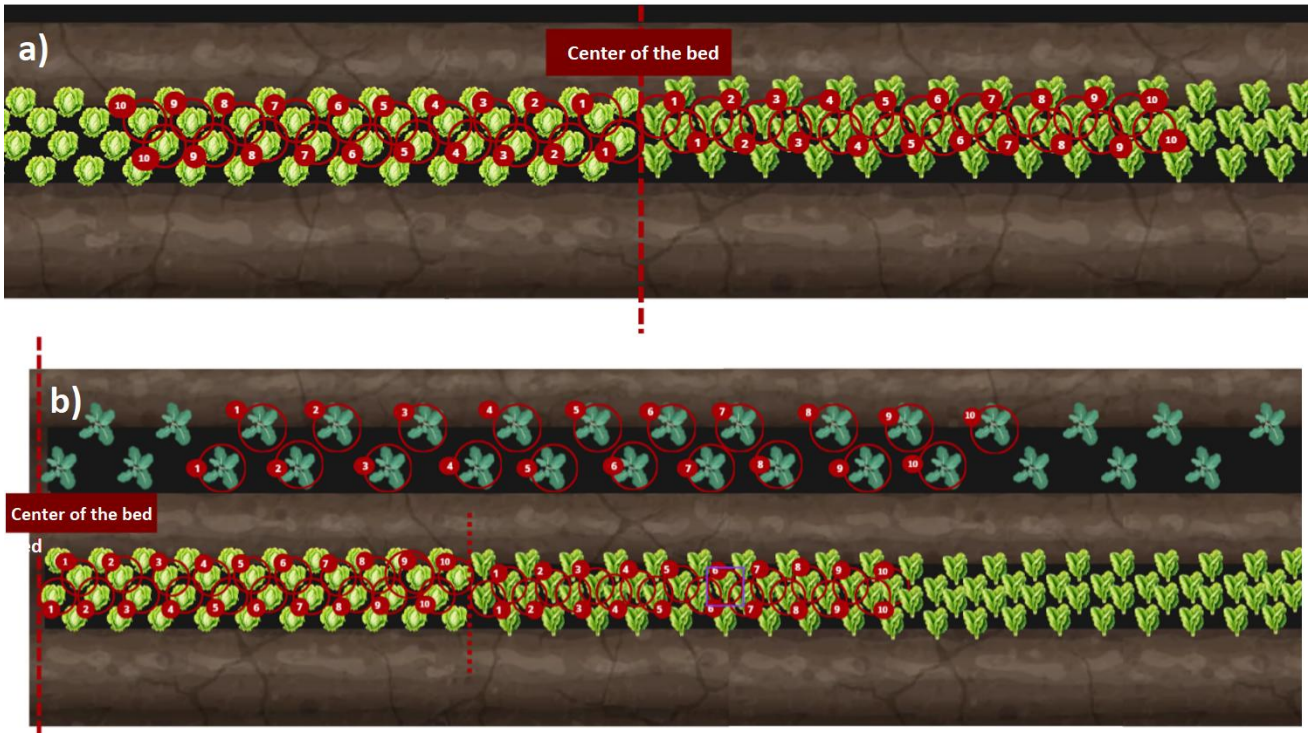

Figure 3.13 Sampling organization according to cropping cycles, for the two available block types in the summer cycle (a) and one representative block of the autumn cycle (b).

Figure 3.13 illustrates the sampling structure applied according to the block type and cropping cycle. For the summer cycle, the figure presents the two available section configurations, and the plants selected for monitoring within each one. For the autumn cycle, three sampling schemes are shown, indicating the starting point of sampling and the specific plants included in each case. Despite the initial replanting efforts, broccoli plots experienced a relatively high number of plant losses throughout the cycle. When a missing or visibly unhealthy plant was detected during monitoring, this was recorded and the next plant in sequence was measured in order to maintain a consistent sample size of ten plants per monitoring session.

The length of the longest leaf, located at the outer perimeter of the plant, was estimated using a measuring tape with a resolution of 1 mm and an accuracy of ±0.1 cm. Values were taken from the soil surface to the tip of the leaf (Figure 3.14). In addition, two plant diameters were determined: the major diameter, defined as the distance between the two most distant external leaves along one axis, and the minor diameter, measured perpendicular to the major diameter. Data was performed by selecting the outermost leaves to ensure coherence across sampling events.



Figure 3.14 Field measurements during a crop monitoring session.

Biomass measurements

Fresh weight

To obtain block-level aggregate measurements, an additional set of 10 plants per block was first collected from rows 1 and 4, which were not included in the main monitoring scheme. In the case of broccoli, sampling was limited to rows 1 and 2, as these were the only crop rows present for this species (Figure 3.15). This complementary sampling was intended to provide an estimation of the average fresh biomass produced per analyzed bed section, allowing a representative approximation of harvest yield at block level.



Figure 3.15 On-site fresh weight determination of harvested lettuce.

Individual fresh weight determination was carried out using the same 10 plants per block selected for the periodic monitoring described in the previous section. Fresh weight was quantified at harvest time in one of the auxiliary laboratories at Agropolis, to reduce water loss, which is particularly critical for leafy vegetables such as lettuce. Prior to weighing, all plants were individually identified and placed into labelled boxes following the organization scheme exposed in Figure 3.16.

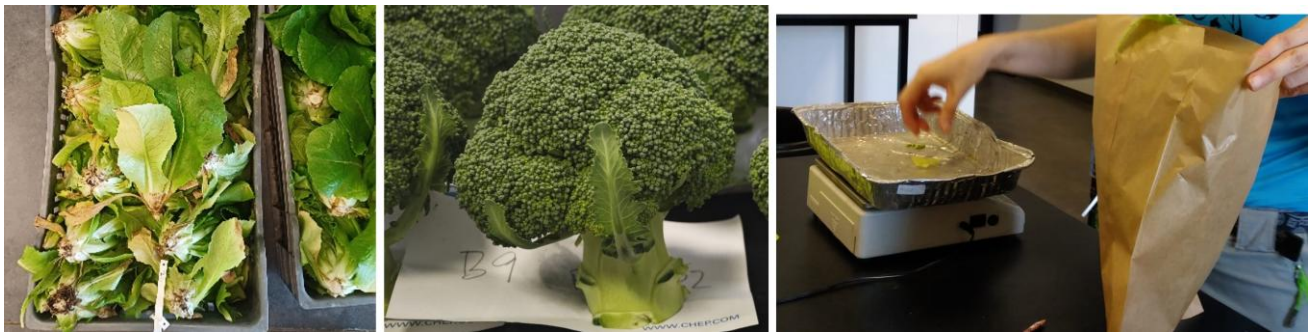

Figure 3.16 Post-harvest handling and sample preparation of lettuce and broccoli for laboratory analysis.

Dry weight

Fresh and dry weight were determined following a consistent sampling protocol for all crops considered, including both lettuce and broccoli. At harvest, each plant was cut into four approximately equal parts in order to obtain a representative subsample of the total biomass. One of these quarters was immediately weighed to determine fresh weight.

The same subsample was then placed in a labelled paper envelope to ensure correct identification and traceability. **Dry weight was determined from this material after drying in a forced-air oven** (DRY-BIG model; JP Selecta, Abrera, Spain) located at the laboratories of the EEABB, at 80 °C. Samples were kept in the oven for a minimum drying period of 24 hours. Subsequently, their drying state was checked at regular intervals of approximately 8 to 12 hours. When no further changes in sample weight or physical appearance were observed between consecutive checks, the material was considered to have reached constant weight. Once stabilized, dry weight was measured using a precision analytical balance (BP 310 S model; Sartorius AG, Göttingen, Germany) with a resolution of 0.001 g, also at the same facilities (Figure 3.17).



Figure 3.17 Equipment used for weight determination: a) precision balance for weight measurements and b) forced-air drying oven with labelled samples.

Derived agronomic indicators

Once absolute plant height was analyzed, relative growth was evaluated as an indicator of the vertical development dynamics of the crop. Relative height growth was **calculated as the percentage of the height reached at each monitoring time with respect to the height measured at harvest,** which was taken as the reference value. This analysis was only performed for crops in which plant height was measured at harvest. Relative growth was evaluated at the first monitoring date and at an intermediate control corresponding approximately to 50 % of the crop cycle. All values were expressed as percentages relative to the final height at harvest (100 %). Relative height growth was calculated according to Equation (3.1):

$$RG = \frac{H_t}{H_h} \times 100 \qquad (3.1)$$

where *RG* is the relative growth of plant height (%), H_t is the plant height at monitoring time t(cm), H_h is the plant height measured at harvest (cm). It is used to evaluate and compare the vertical growth dynamics of the crop between treatments, isolating the effect of the development rate with respect to the final size reached.

To characterize the global plant structure, both vertical and transversal growth dimensions were jointly considered. This approach allows the description of plant architecture beyond individual size measurements and enables the evaluation of whether crop development over time or the applied treatments influence the overall spatial arrangement of the canopy. Plant structural compactness was quantified using the ratio between the minimum and maximum transversal diameters of the canopy, calculated according to Equation (3.2):

$$CI = \frac{D_{min}}{D_{max}} \times 100 \qquad (3.2)$$

where CI represents plant structural compactness (%), *Dmin* is the minimum transversal diameter of the plant canopy (cm), and *Dmax* is the maximum transversal diameter of the plant canopy (cm). Higher values indicate a more uniform and compact canopy structure, while lower values are associated with more elongated or irregular plant architectures.

Water content was determined for each plant by relating fresh and dry mass values obtained from the same representative subsample. Absolute water content was calculated as the difference between fresh and dry mass, while relative water content was expressed as a percentage according to Equation (3.3):

$$WC = \frac{m_f - m_d}{m_f} \times 100 \qquad (3.3)$$

where *WC* is the water content of the plant subsample (%), m_f is the fresh mass of the subsample (g), and m_d is the dry mass of the subsample (g). This determination allowed the quantification of the water retention capacity of the plants under each of the environmental sections.

Statistical analysis

Prior to inferential analysis, data were evaluated to verify compliance with the assumptions of normality and homogeneity of variances. These assumptions were checked using **standard diagnostic tests** and were found to be satisfied, allowing the use of parametric statistical methods. Subsequently, post-hoc comparisons were performed using Tukey's test to identify statistically significant differences between controls and environmental sections for the different variables analysed. The significance level adopted for all tests was 5 % (α = 0.05). Statistical processing was performed using Minitab® 22 code (Minitab Inc., State College, PA, USA).

3.2. Results of the first year of activity

This section presents the data used to describe the development and growth patterns of each variety under the different treatments applied. Measurements were collected at several stages throughout the crop cycle, with the number of assessment dates and the set of variables adjusted according to crop type and cultivation length. For the analysis of temporal trends, harvest was taken as a reference point to describe the overall

development trajectory whenever morphological variables were available. Using harvest as a common reference facilitated the comparison of development dynamics among treatments and environmental sections.

Vertical crop development

Lettuce (cv. Francesca)

Height at harvest

During the **summer** cycle (Figure 3.18), plant height at harvest **showed very similar values across all radiation treatments**. Plants grown under opaque panels, semi-transparent panels, and open-field conditions reached similar final heights, with no clear differences among treatments. The slightly higher values observed under semi-transparent panels and open-field conditions remained small and did not translate into distinct growth patterns. Final plant height appeared to be consistent regardless of the radiation condition, suggesting that, under summer conditions, vertical growth was not substantially affected by the presence of agrivoltaic shading. From a physiological perspective, this behavior could be related to the capacity of lettuce to maintain vertical growth under a range of light conditions, possibly through adjustments in leaf expansion and light-use efficiency. Under reduced radiation, plants can compensate through morphological plasticity, allowing them to reach comparable final heights despite differences in light availability during intermediate stages.

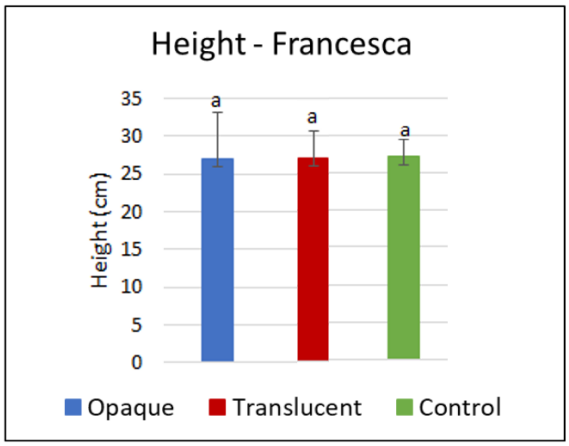

Figure 3.18 Mean plant height at the end of the summer cycle for Lettuce (cv. Francesca) under opaque panels (blue), semi-transparent panels (red), and open-field conditions (green). Different letters indicate significant differences between sampling dates within the same treatment (Tukey's test, $p < 0.05$).

In the **autumn** cycle (Figure 3.19), plant height at harvest **showed no significant differences among treatments**. Lettuce grown under opaque and semi-transparent panels reached height values comparable to those observed in the open-field control. This convergence at the end of the cycle suggested that vertical growth was not markedly affected by the type of panel coverage under the studied conditions. From the beginning to the end of the cycle, plant height tended to converge across treatments, pointing out that autumn vertical growth dynamics could be primarily governed by crop phenology rather than by the type of panel coverage.

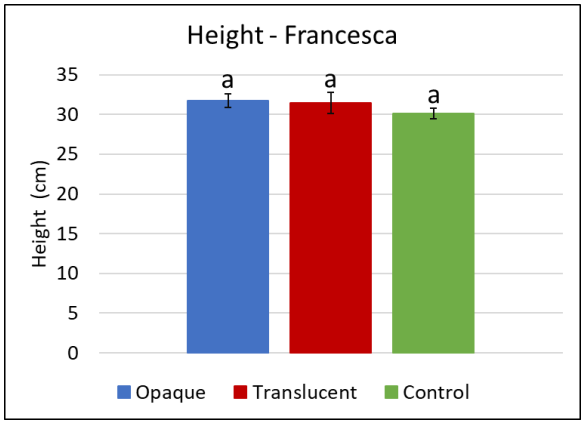

Figure 3.19 Mean plant height at the end of the autumn cycle for lettuce (cv. Francesca) under opaque panels (blue), semi-transparent panels (red), and open-field conditions (green). Bars express standard deviations. Letters indicate homogeneous groups obtained by the Tukey's test ($p < 0.05$).

Relative growth

During the **summer** cycle (Figure 3.20), relative growth at mid-cycle showed **higher values under opaque and semi-transparent panels** compared to open-field conditions. Plants grown under opaque and semi-transparent treatments were grouped within the same significance class, while those under open-field conditions showed significantly lower relative growth. These results indicate that, at this stage of the crop cycle, plants under agrivoltaic conditions maintained higher relative growth levels than those grown in open-field conditions. It could be associated with a more moderated light environment under panel coverage, potentially reducing stress conditions and allowing a more efficient allocation of resources to growth during this phase. However, these interpretations should be considered with caution and would benefit from further validation under different environmental conditions.

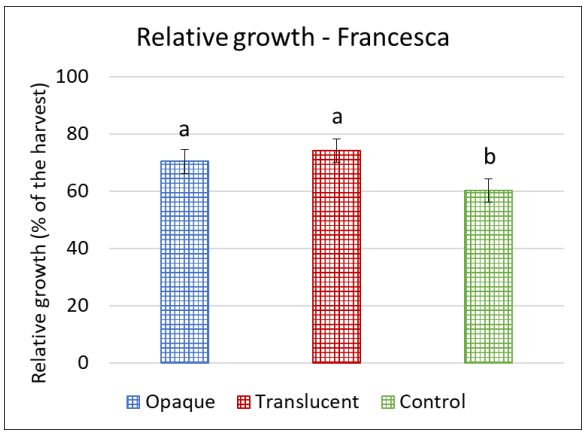

Figure 3.20 Mean relative height growth at mid-cycle of the summer season for Lettuce (cv. Francesca) under opaque panels (blue), semi-transparent panels (red), and open-field conditions (green). Bars express standard deviations. Letters indicate homogeneous groups obtained by the Tukey's test ($p < 0.05$).

On the other hand, at the end of the **autumn** season (Figure 3.21), relative height growth at **harvest did not differ significantly among treatments**. Lettuce grown under opaque and semi-transparent panels displayed

values comparable to those observed in the open-field control. These results indicated that, despite potential differences in growth dynamics during the cycle, the distribution of vertical growth at harvest was similar among different panel conditions. Since final plant heights were comparable among treatments, these results suggested a redistribution of vertical growth over time rather than an increase in total progression. This effect could be related to differences in microclimatic conditions under the panels. By providing warmer and more stable conditions during the early stages of development, panel-covered treatments could be allowed for plants to accumulate growth earlier in the cycle, even if final vegetal stature remains comparable across blocks.

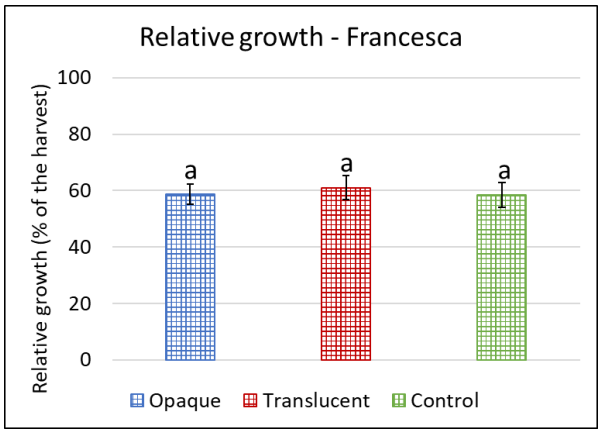

Figure 3.21 Mean relative height growth at mid-cycle of the autumn season for Lettuce (cv. Francesca) under opaque panels (blue), semi-transparent panels (red), and open-field conditions (green). Bars express standard deviations. Letters indicate homogeneous groups obtained by the Tukey's test ($p < 0.05$).

Lettuce (cv. Maravilla)

Height at harvest

Maravilla lettuce showed a c**onsistent increase in plant height throughout the cultivation period across the three growing conditions** (Figure 3.22). Although differences in height may have occurred during intermediate stages of the cycle, these did not persist until harvest. At the final sampling, plants grown under opaque panels, semi-transparent panels, and open-field conditions reached comparable heights, with no statistically significant differences among treatments.

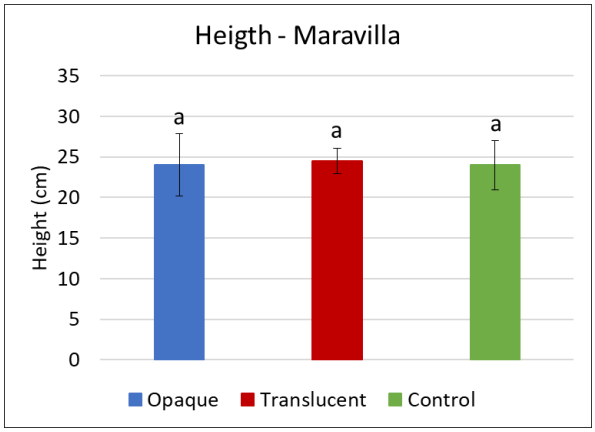

Figure 3.22 Mean plant height at the end of the autumn cycle for lettuce (cv. Maravilla) under opaque panels (blue), semi-transparent panels (red), and open-field conditions (green). Bars express standard deviations. Letters indicate homogeneous groups obtained by the Tukey's test ($p < 0.05$).

Despite the presence of different light environments, the final plant height at harvest was similar across opaque panels, semi-transparent panels, and open-field control. This convergence suggests that, under summer conditions, vertical development in Maravilla lettuce was primarily governed by intrinsic growth patterns rather than by the microclimatic differences associated with panel coverage. Any potential differences during earlier stages of the cycle were not maintained at harvest, indicating a convergence in plant stature as the crop reached maturity. It this could indicate that stem elongation and leaf expansion were not strongly limited by light availability within the range of radiation conditions evaluated, possibly due to compensatory responses such as increased light-use efficiency or morphological acclimation (e.g., adjustments in leaf angle or expansion).

Observing the **autumn** cycle (Figure 3.23), plant height at harvest **remained similar across all treatments**, with no significant differences observed between radiation conditions. Lettuce grown under opaque and semi-transparent panels reached final heights comparable to those recorded in the open-field control. This pattern is comparable with the behavior observed for cv. Francesca (Figure 3.19), where treatment effects on final plant height were also minimal. The temporal evolution of plant height reflected a progressive increase throughout the crop period in all blocks, with values rising consistently to harvest. For all the crops, height values tended to stabilize, indicating a relative plateau in vertical development as the crop approached maturity. Taken together, the autumn results reported that vertical development could be affected by the advancement of the crop cycle itself, while the influence of panel type on plant height remained limited, leading to comparable structural outcomes across all growing configurations.

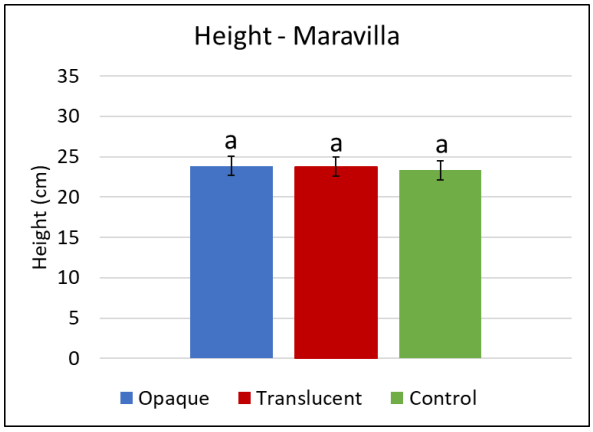

Figure 3.23 Mean plant height at the end of the autumn cycle for lettuce (cv. Maravilla) under opaque panels (blue), semi-transparent panels (red), and open-field conditions (green). Bars express standard deviations. Letters indicate homogeneous groups obtained by the Tukey's test ($p < 0.05$).

Relative growth

Relative vertical growth of Maravilla lettuce during the **summer** cycle **showed differences among radiation treatments at mid-cycle** (Figure 3.24). At this stage, plants under semi-transparent panels and open-field conditions were grouped within the same statistical class and exhibited higher relative growth values, whereas plants under opaque panels showed significantly lower values. This indicates that light attenuation under opaque panels may have temporarily reduced the rate of vertical development during this phase of the cycle. However, these mid-cycle differences did not persist until harvest. As observed in Figure 3.23, final plant

height was similar across all treatments, suggesting that plants grown under opaque panels were able to compensate for the initially lower relative growth rates. This convergence points to a recovery of growth dynamics over time, likely driven by the intrinsic developmental program of the crop, resulting in comparable final plant stature regardless of radiation conditions.

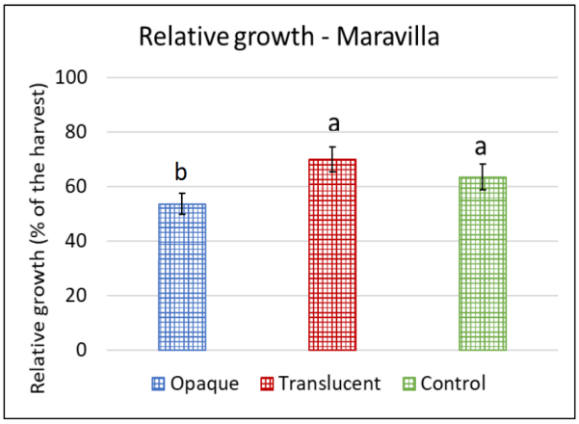

Figure 3.24 Relative height growth at mid-cycle of the autumn season for lettuce (cv. Maravilla) under opaque panels (blue), semi-transparent panels (red), and open-field conditions (green). Bars express standard deviations. Letters indicate homogeneous groups obtained by the Tukey's test ($p < 0.05$).

Relative vertical growth of Maravilla lettuce, during the **autumn** cycle (Figure 3.25), **relative height growth at harvest was similar across all treatments,** with no significant differences detected between treatments. Plants under opaque and semi-transparent panels reached comparable proportions of their final height to those grown in open-field conditions. This behavior aligns with the pattern observed for cv. Francesca (Figure 3.21), where relative growth at harvest also exposed a homogeneous response among crops. The evolution of relative height followed a similar trajectory in all growing conditions, with no clear divergence in the pace of vertical development among blocks. This homogeneous response suggested that, during the autumn cycle, vertical growth was conditioned by the advancement of the crop itself rather than by differences in the light environment associated with panel coverage. As observed in the summer cycle and in previous results obtained for the Francesca variety, plants grown under all conditions ultimately reached very similar to final heights at harvest.

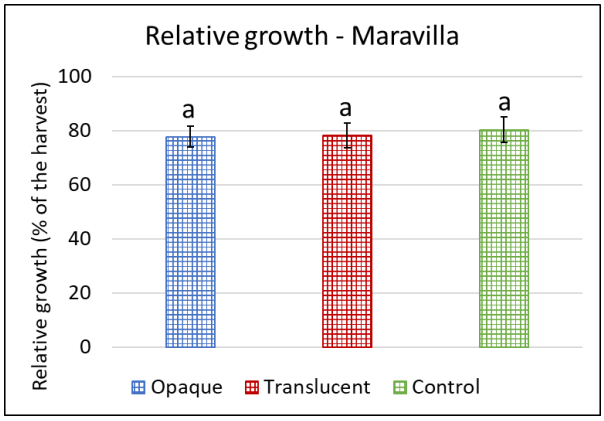

Figure 3.25 Relative height growth at mid-cycle of the autumn season for lettuce (cv. Maravilla) under opaque panels (blue), semi-transparent panels (red), and open-field conditions (green). Bars express standard deviations. Letters indicate homogeneous groups obtained by the Tukey's test ($p < 0.05$).

Broccoli

Height at harvest

The temporal evolution of broccoli plant height is shown in Figure 3.26. As broccoli harvest corresponds to the collection of the inflorescence rather than the whole plant, no morphological measurements of plant height were available at harvest. For this reason, **the analysis of vegetative height development was conducted up to the last monitoring date, which represents the final stage of crop development assessed in the field.** Across all growing conditions, plant heights again exhibited a progressive increase throughout the crop cycle. Under opaque panels, the first controls showed very similar height values, indicating a limited vertical expansion during the initial phase. Then, plant height augmented to get a stabilization of vertical growth during the final stage of the cycle. A similar temporal pattern was observed under semitransparent panels. In the open-field control, height progression was even more gradual and continuous, with successive increases observed across most monitoring dates before reaching a stabilization phase towards the end of the cycle. At the final monitoring date, clear differences in plant height were still observed among growing conditions. Broccoli plants grown in the open-field control reached greater heights than those cultivated under panel coverage, while plants under semitransparent panels showed slightly lower values than those under opaque panels. This pattern could be motivated by the panel-induced microclimatic conditions, influencing the rate of vertical development during the latter stages of the cycle. In particular, the reduced height observed under panel coverage at the final control indicates that vertical growth could have been delayed rather than suppressed. From an agronomic perspective, the data could be saying that, under panel systems, a longer growing period could be required for broccoli plants to reach a structural development comparable to that observed in open-field conditions, pointing to a potential shift in the optimal harvest timing when crops are cultivated beneath photovoltaic modules.

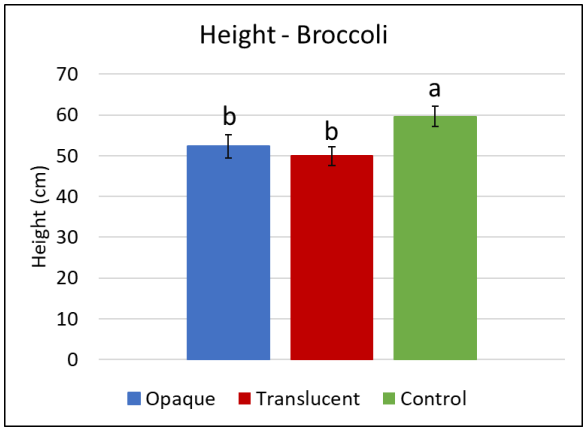

Figure 3.26 Mean plant height at the end of the autumn cycle for broccoli under opaque panels (blue), semi-transparent panels (red), and open-field conditions (green). Bars express standard deviations. Bars express standard deviations. Letters indicate homogeneous groups obtained by the Tukey's test ($p < 0.05$).

The lower plant height observed under semitransparent panels compared to opaque panels at the last control could be associated with a faster phenological advancement under higher light availability, which limits further vegetative growth at the final stages. In contrast, under opaque panels, reduced effective radiation could have delayed this progression, allowing vertical growth to be prolonged, although without reaching the values observed in the open-field crop. In addition, plants grown in the open field were exposed to higher total radiation and greater thermal accumulation, which favored both biomass accumulation and the extension of vegetative growth. Under panel coverage, even when crop development was adequate, partial limitations in light and energy availability tended to slow down the final increase in plant height.

Relative growth

Relative vertical growth of broccoli during the **autumn** cycle (Figure 3.27) **showed similar values across treatments at harvest, with no statistically significant differences between radiation conditions**. Despite the differences observed in plant height at the final monitoring stage (Figure 3.26), where open-field conditions led to higher values, these differences were not reflected in relative growth. This indicates that, although plants under panel coverage could have experienced a slight delay in vertical development, they achieved a comparable proportion of their final height by the end of the cycle. Therefore, the distribution of growth over time appears to have been adjusted among treatments, resulting in a homogeneous relative growth at harvest. This behavior expressed that panel-induced microclimatic effects could be affecting the timing of growth rather than its overall completion.

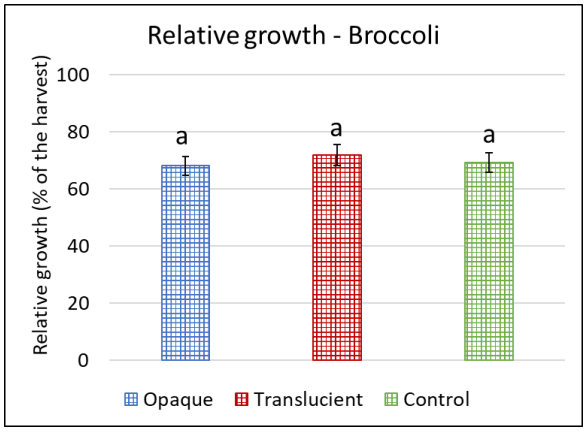

Figure 3.27 Relative height growth at mid-cycle of the autumn season for broccoli under opaque panels (blue), semi-transparent panels (red), and open-field conditions (green). Bars express standard deviations. Letters indicate homogeneous groups obtained by the Tukey's test ($p < 0.05$).

At mid-cycle, the relative height values were similar across all growing conditions, reflecting that subsequent vertical development progressed at a comparable pace, and that early differences in relative growth were progressively compensated. When considered alongside the analysis of absolute plant height, this pattern is consistent with the observation that broccoli grown in the open-field control ultimately reached greater final height (Figure 3.26). While opaque panels could stimulate faster early elongation, the higher total radiation and thermal accumulation experienced in open-field conditions likely support continued growth during later stages, resulting in taller plants at the end of the monitoring period compared with those developments under panel coverage.

Diameters and plant architecture

Lettuce (cv. Francesca)

Maximum diameter

At harvest in summer, **maximum plant diameter did not show statistically significant differences among radiation treatments** (Figure 3.28). Plants grown under opaque panels, semi-transparent panels, and open-field conditions reached comparable final values, indicating that lateral development was not affected by the different light environments. From a physiological perspective, this suggests that leaf expansion and canopy radial growth were maintained across treatments, likely due to a sufficient level of incident radiation even under panel-covered conditions. In this context, lettuce can have equilibred for reduced light availability through morphological and physiological adjustments, such as optimizing leaf area development or maintaining photosynthetic activity within non-limiting ranges. As a result, no differences in final plant diameter were observed among treatments. Future analyses will contrast these observations with the microclimatic data recorded by the sensor network to better understand the relationship between radiation conditions and crop development.

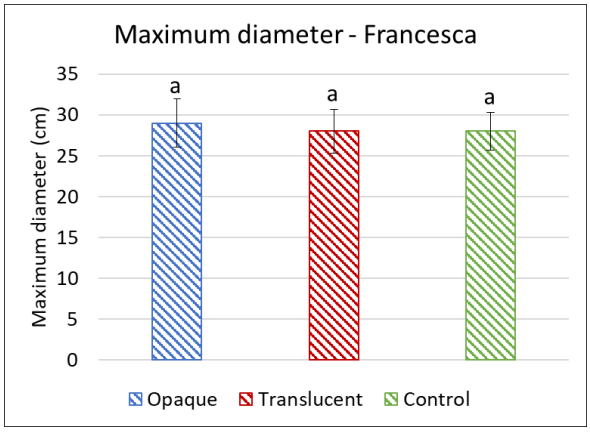

Figure 3.28 Mean maximum diameter at the end of the summer cycle for Lettuce (cv. Francesca) under opaque panels (blue), semi-transparent panels (red), and open-field conditions (green). Bars express standard deviations. Letters indicate homogeneous groups obtained by the Tukey's test ($p < 0.05$).

During the **autumn** cycle (Figure 3.29), **maximum plant diameter at harvest showed similar values across treatments**, with no statistically significant differences detected among radiation conditions. Earlier in the cycle, plant diameter increased progressively across sampling dates under all treatments, reflecting a consistent temporal expansion of plant size. At harvest, lettuce grown under opaque and semi-transparent panels reached comparable final diameters to those observed in the open-field control, indicating that panel coverage did not substantially affect the final lateral development of the crop. Taken together, these results suggest that, although panel-induced modifications may influence the rate of expansion during specific phases of the cycle, plants tended to converge towards similar structural outcomes by harvest, resulting in a homogeneous final canopy size across radiation conditions.

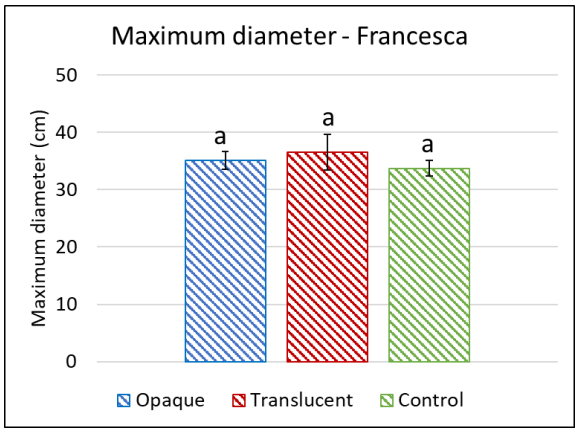

Figure 3.29 Mean maximum diameter at the end of the autumn cycle for Lettuce (cv. Francesca) under opaque panels (blue), semi-transparent panels (red), and open-field conditions (green). Bars express standard deviations. Letters indicate homogeneous groups obtained by the Tukey's test ($p < 0.05$).

Minimum diameter

At harvest in **summer**, **minimum plant diameter did not show statistically significant differences among radiation treatments** (Figure 3.30). Plants grown under opaque panels, semi-transparent panels, and open-field conditions reached comparable values, indicating that plant development along the minor axis was not affected by the different light environments. This behavior is consistent with the results observed for maximum diameter (Figure 3.28), where no significant differences among treatments were also detected. Together, these findings suggest that overall plant architecture, in terms of both major and minor axes, was maintained across radiation conditions. It could mean that canopy expansion and structural balance were preserved, likely because radiation levels remained within a non-limiting range for leaf development. As a result, even under modified light environments, it seemed that plants were able to sustain a uniform canopy structure without alterations in compactness or symmetry.

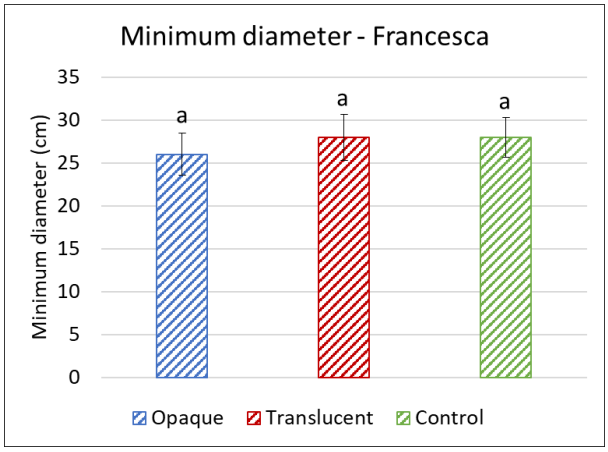

Figure 3.30 Mean minimum diameter at the end of the summer cycle for Lettuce (cv. Francesca) under opaque panels (blue), semi-transparent panels (red), and open-field conditions (green). Bars express standard deviations. Letters indicate homogeneous groups obtained by the Tukey's test ($p < 0.05$).

During the **autumn** cycle, earlier in the **season minimum diameter increased progressively across sampling dates under all treatments**, reflecting a consistent and homogeneous expansion of plant size along the minor axis. Temporal patterns remained comparable under opaque panels, semi-transparent panels, and open-field conditions, suggesting that plants followed a similar structural development trajectory regardless of radiation treatment. Finally, at harvest (Figure 3.31), minimum plant diameter at harvest showed similar values across treatments, with no statistically significant differences detected among radiation conditions. Lettuce grown under opaque and semi-transparent panels reached comparable final values to those observed in the open-field control, indicating that agrivoltaic shading did not substantially affect plant compactness or symmetry by the end of the cycle. This behavior is consistent with that observed for maximum diameter (Figure 3.29), where plants also converged to similar final values across treatments. Taken together, both variables indicate that panel coverage did not alter the final canopy structure, neither in terms of overall size (maximum diameter) nor in its lateral symmetry (minimum diameter), reinforcing the stability of plant architectural development under agrivoltaic conditions.

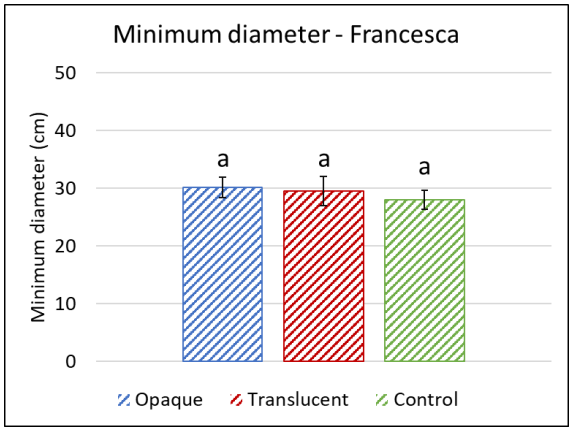

Figure 3.31 Mean minimum diameter at the end of the autumn cycle for Lettuce (cv. Francesca) under opaque panels (blue), semi-transparent panels (red), and open-field conditions (green). Bars express standard deviations. Letters indicate homogeneous groups obtained by the Tukey's test ($p < 0.05$).

Morphological proportion

During the **summer** cycle, **the ratio between maximum diameter and plant height did not show statistically significant differences among radiation treatments at harvest** (Figure 3.32). Plants grown under opaque panels, semi-transparent panels, and open-field conditions exhibited comparable diameter-to-height ratios, indicating a consistent plant architecture across treatments. This pattern is consistent with the observations for both maximum and minimum diameter, as well as plant height, where no significant differences were detected at harvest. Taken together, these results could suggest that the balance between lateral expansion and vertical development was maintained across radiation conditions. This could suggest that plant architectural traits were primarily governed by intrinsic growth regulation rather than by the microclimatic differences associated with panel coverage. In this context, lettuce plants could have adjusted their growth dynamics under modified light environments, allowing them to maintain a stable proportional structure by the end of the crop cycle.

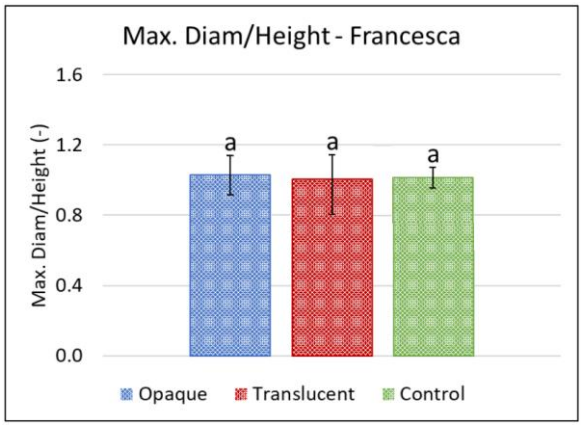

Figure 3.32 Mean ratio between the maximum diameter and height at the end of the summer cycle for Lettuce (cv. Francesca) under opaque panels (blue), semi-transparent panels (red), and open-field conditions (green). Different letters indicate significant differences between sampling dates within the same treatment (Tukey's test, $p < 0.05$).

During the **autumn** cycle (Figure 3.33), **minimum plant diameter at harvest showed comparable values across treatments, with no statistically significant differences among radiation conditions**. Lettuce grown under opaque and semi-transparent panels reached final values similar to those observed in the open-field control, indicating that agrivoltaic shading did not alter plant compactness or symmetry by the end of the cycle. Earlier in the cycle, minimum diameter increased progressively under all treatments, reflecting a consistent expansion of plant size along the minor axis. Growth followed a similar temporal pattern across radiation conditions, with a steady enlargement from early stages towards the final phase, suggesting that structural development proceeded in a comparable manner regardless of panel coverage. This behavior is in line with that observed for maximum diameter (Figure 3.30), where plants also converged to similar final canopy sizes across treatments. Likewise, it is consistent with plant height responses (Figure 3.19), which showed limited treatment effects at harvest.

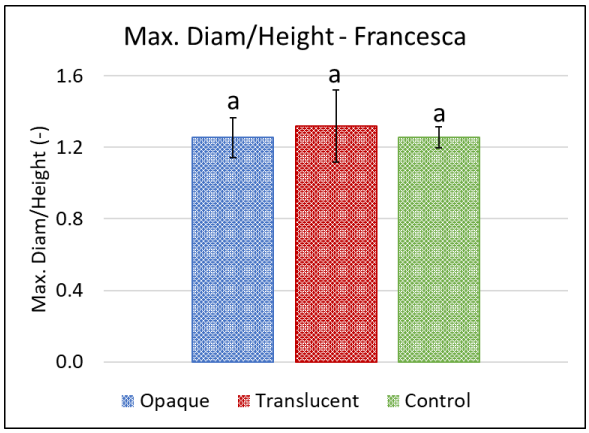

Figure 3.33 Mean ratio between the maximum diameter and height at the end of the autumn cycle for Lettuce (cv. Francesca) under opaque panels (blue), semi-transparent panels (red), and open-field conditions (green). Different letters indicate significant differences between sampling dates within the same treatment (Tukey's test, $p < 0.05$).

From an agronomic perspective, the observed data indicated that agrivoltaic conditions do not appear to compromise final crop morphology, maintaining canopy structure at harvest. The maintenance of both maximum and minimum diameters, together with plant height, suggested that canopy architecture seemed balanced, which is directly linked to marketable quality in lettuce. However, further trials under different environmental conditions are needed to confirm these findings.

Compactness index

The compactness index of lettuce (cv. Francesca) at the end of the **summer** cycle (Table 3.3) presented **very close values across treatments**, with variations lower than 5 % between radiation conditions. Earlier in the cycle, compactness values were already relatively high under opaque and semi-transparent panels and increased slightly towards harvest, reflecting stable canopy development. Under open-field conditions, lower initial values were observed, followed by a more pronounced increase over time, eventually reaching levels comparable to those under panel coverage. Final compactness exceeded 90% in all cases, indicating a well-developed and uniform canopy structure at harvest under both agrivoltaic and open-field conditions. At the agronomic level, these results show that agrivoltaic conditions do not appear to negatively affect canopy compactness or structural quality at harvest. The similar final values across treatments reflect a consistent canopy configuration under both panel-covered and open-field conditions. However, further trials under different climatic conditions are required to confirm the consistency of this response.

Table 3.3 Mean crop compactness index of the Lettuce (cv. Francesca) cultivar by treatment and sampling time at the end of the summer cycle.

Section	***Compactness index (%)***
Opaque	93.1
Translucent	93.1
Control	92.9

During the **autumn** cycle, the compactness index of lettuce (cv. Francesca) at the end of the autumn cycle (Table 3.4) **fell within a narrow range across treatments**, with no clear separation between radiation conditions. Final values ranged within a relatively narrow interval, indicating a consistent canopy structure at harvest under both agrivoltaic and open-field conditions. This behaviour is consistent with that observed for the diameter-to-height ratio (Figure 3.34), where plant architecture also followed a similar pattern across treatments at harvest. Together, checking these results seemed that agrivoltaic conditions did not influence the structural configuration of the crop, leading to consistent architectural outcomes regardless of panel coverage. Values also pointed out that agrivoltaic conditions did not appear to compromise canopy compactness or crop performance.

Table 3.4 Mean crop compactness index of the Lettuce (cv. Francesca) cultivar by treatment and sampling time at the end of the autumn cycle.

Section	***Compactness index (%)***
Opaque	85.7
Translucent	81.1
Control	82.9

3.8.2.2. Lettuce (cv. Maravilla)

Maximum diameter

During the **summer** cycle, maximum plant diameter of lettuce (cv. Maravilla) **increased progressively across sampling dates under all radiation conditions** (Figure 3.34). Significant differences were observed between early and late sampling stages within each treatment, indicating a continuous lateral expansion of the plants throughout the crop cycle. Intermediate stages showed more moderate increases, consistent with a gradual growth pattern. Across treatments, similar temporal trends were observed under opaque panels, semi-transparent panels, and open-field conditions. At harvest, maximum diameter values were comparable among treatments, suggesting that the presence of photovoltaic panels did not substantially constrain final lateral development. This behavior is consistent with the patterns observed at the beginning of the cycle, where plant growth followed a similar trajectory across radiation conditions, with no clear separation among treatments.

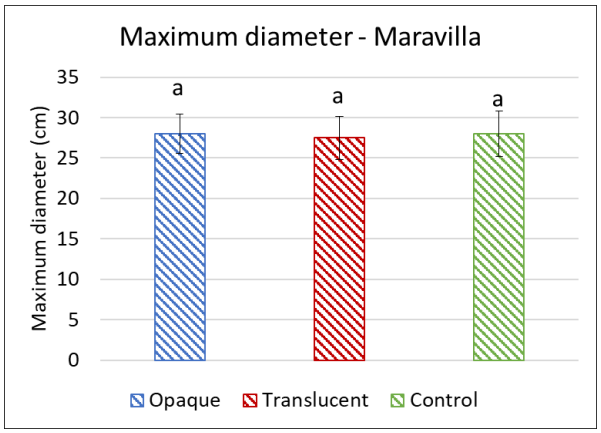

Figure 3.34 Mean maximum diameter at the end of the summer cycle for Lettuce (cv. Maravilla) under opaque panels (blue), semi-transparent panels (red), and open-field conditions (green). Bars express standard deviations. Letters indicate homogeneous groups obtained by the Tukey's test ($p < 0.05$).

During the **autumn** cycle, starting the cycle**, maximum diameter increased progressively across sampling dates under all treatments**, reflecting a steady lateral expansion of the plant. Growth followed a similar temporal pattern under opaque panels, semi-transparent panels, and open-field conditions. Minor variations were observed during intermediate stages, but the overall trajectory remained consistent across radiation regimes. At harvest fell within a near range across treatments, with no clear separation between radiation conditions (Figure 3.35). Plants grown under opaque and semi-transparent panels reached final diameters

close to those observed in the open-field control, indicating that lateral plant size at harvest was not constrained by panel coverage. Although panel-induced microclimatic conditions could be affecting growth rates during specific phases, plants resulted in similar final canopy dimensions at the end of the season.

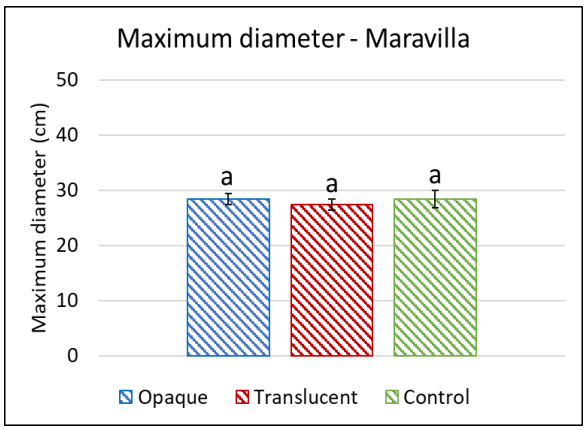

Figure 3.35 Mean maximum diameter at the end of the autumn cycle for Lettuce (cv. Maravilla) under opaque panels (blue), semi-transparent panels (red), and open-field conditions (green). Bars express standard deviations. Letters indicate homogeneous groups obtained by the Tukey's test ($p < 0.05$).

Minimum diameter

During the **summer** cycle, minimum plant diameter of lettuce (cv. Maravilla) **did not show statistically significant differences among radiation treatments at harvest** (Figure 3.36). Plants grown under opaque panels, semi-transparent panels, and open-field conditions exhibited comparable values at the end of the cycle, indicating that development along the minor axis was not substantially altered by the different light environments. This pattern is consistent with that observed for maximum diameter (Figure 3.34), where no significant differences among treatments were also detected at harvest. Taken together, both variables could indicate that plant architecture was maintained across radiation conditions, with no clear evidence of alterations in canopy compactness or lateral symmetry under agrivoltaic shading.

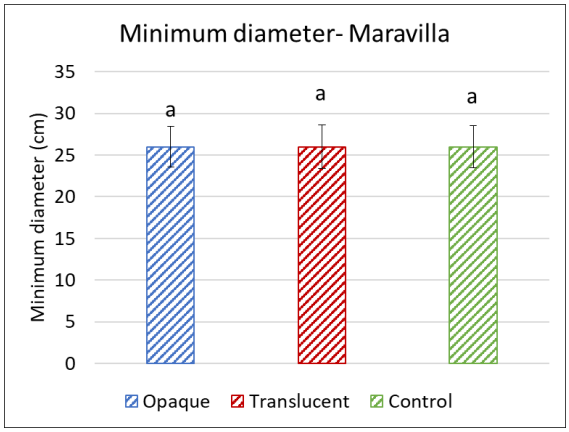

Figure 3.36 Mean minimum diameter at the end of the summer cycle for Lettuce (cv. Maravilla) under opaque panels (blue), semi-transparent panels (red), and open-field conditions (green). Bars express standard deviations. Letters indicate homogeneous groups obtained by the Tukey's test ($p < 0.05$).

During the **autumn** cycle, the evaluated parameter at harvest **showed values within a narrow range across treatments**, with no clear separation between radiation conditions (Figure 3.37). Lettuces evoluted under opaque and semi-transparent panels reached final values close to those observed in the open-field control, indicating that this trait was not constrained by panel coverage at the end of the cycle. At the beginning, the parameter growed progressively under all treatments, following a consistent temporal pattern from early development stages to harvest. Changes over time were gradual, with only minor deviations at intermediate stages, and no clear divergence among radiation regimes. This reflects a stable developmental trajectory under both agrivoltaic and open-field conditions. In comparison with maximum plant diameter (Figure 3.35), a similar trend was observed, with both variables showing convergence at harvest despite small differences during earlier stages. This could reinforce the idea that agrivoltaic conditions did not substantially modify the overall growth pattern of the crop during the autumn cycle, although more field assays are necessary.

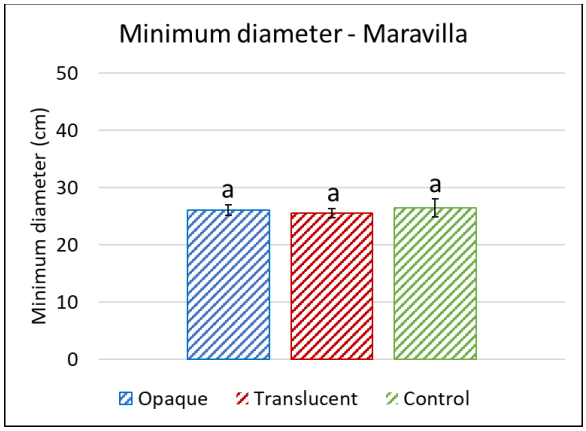

Figure 3.37 Mean minimum diameter at the end of the autumn cycle for Lettuce (cv. Maravilla) under opaque panels (blue), semi-transparent panels (red), and open-field conditions (green). Bars express standard deviations. Letters indicate homogeneous groups obtained by the Tukey's test ($p < 0.05$).

Morphological proportion

During the **summer** cycle, the **ratio between maximum diameter and plant height of lettuce (cv. Maravilla) did not show statistically significant differences among radiation treatments at harvest** (Figure 3.38). Values under opaque panels, semi-transparent panels, and open-field conditions were grouped within the same significance class, indicating comparable morphological proportions at the end of the cycle. This trend is consistent with the patterns observed for plant height and both maximum and minimum diameters (Figures 3.21, 3.34, and 3.36) in cv. Maravilla, where no significant differences among treatments were detected at harvest. Taken together, these results could suggest that the balance between vertical and lateral development was maintained across radiation conditions. The slightly higher mean ratio observed under opaque panels could indicate a tendency towards relatively greater lateral expansion compared to plant height under reduced radiation conditions, although this difference was not statistically significant. Overall, these findings could indicate that agrivoltaic shading did not substantially modify plant architecture, and that morphological proportions at harvest were largely governed by intrinsic growth patterns rather than by differences in light environment.

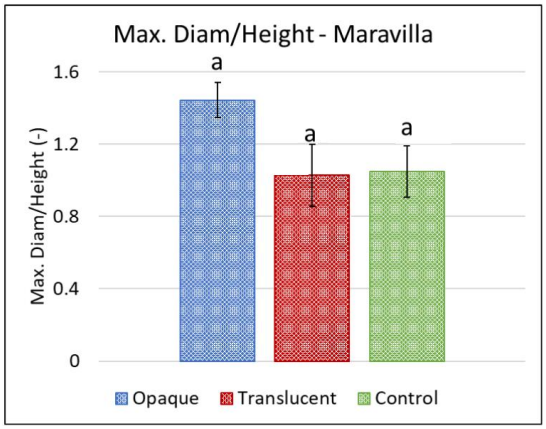

Figure 3.38 Mean ratio between the maximum diameter and height at the end of the autumn cycle for Lettuce (cv. Maravilla) under opaque panels (blue), semi-transparent panels (red), and open-field conditions (green). Bars express standard deviations. Letters indicate homogeneous groups obtained by the Tukey's test ($p < 0.05$).

During the **autumn** cycle (Figure 3.39), **the ratio between maximum diameter and plant height at harvest fell within a narrow range across treatments**, with no clear separation between radiation conditions. Lettuce grown under opaque and semi-transparent panels reached proportions close to those observed in the open-field control, showing that final plant morphology was not altered by panel coverage. Earlier in the cycle, the ratio decreased progressively under all treatments, reflecting a shift in plant architecture as growth advanced, with a gradual transition from a more expanded canopy to a more vertically developed structure. This temporal pattern was consistent across radiation regimes, with only slight deviations during intermediate stages. In relation to maximum diameter (Figure 3.35), where final canopy size converged across treatments, and plant height (Figure 3.23), which also showed convergence at harvest, the ratio confirms that both dimensions evolved in coordination, leading to similar morphological proportions at the end of the cycle regardless of radiation conditions. From an agronomic standpoint, this characterizes that agrivoltaic systems do not appear to disrupt plant architectural development, allowing crops to reach typical morphological

proportions at harvest. Nevertheless, additional trials under different climatic conditions are required to verify the stability of this response.

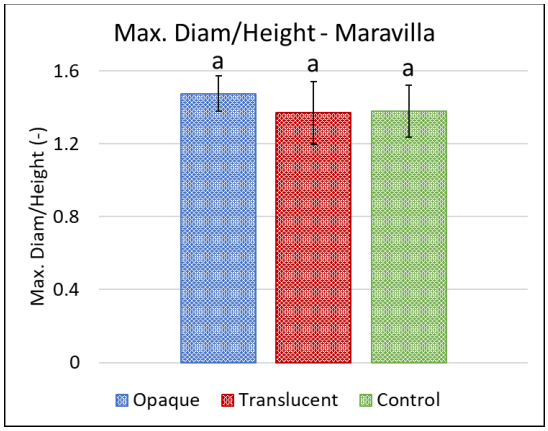

Figure 3.39 Mean ratio between the maximum diameter and height at the end of the autumn cycle for Lettuce (cv. Maravilla) under opaque panels (blue), semi-transparent panels (red), and open-field conditions (green). Bars express standard deviations. Letters indicate homogeneous groups obtained by the Tukey's test ($p < 0.05$).

Compactness index

During the **summer** cycle, the compactness index of lettuce (cv. Maravilla) at harvest (Table 3.5) **fell within a narrow range across treatments**, with no clear separation between panel conditions. Final values were above 90% in all cases, reflecting a well-developed canopy structure under both agrivoltaic and open-field conditions. Earlier in the cycle, lower compactness values were observed at the initial stages, particularly under open-field conditions, followed by a progressive increase as the crop developed. This reflects a gradual consolidation of canopy structure over time, with plants becoming more compact as they approached harvest. The temporal evolution followed a similar pattern, with only small deviations during intermediate stages. At harvest, the slight differences (less than 5 %) calculated between treatments did not translate into distinct structural outcomes. Data did not appear to be affected at the end of the cycle, allowing plants to reach typical levels of development. Further trials under different climatic conditions will be required to confirm the consistency of this first observation.

Table 3.5 Mean crop compactness index of the Lettuce (cv. Maravilla) cultivar by treatment and sampling time at the end of the summer cycle.

Section	***Compactness index (%)***
Opaque	92.9
Translucent	94.5
Control	92.9

During the **autumn** cycle, the compactness index of lettuce (cv. Maravilla) at harvest (Table 3.6) **remained within a narrow range across treatments**, with no clear separation between radiation conditions. Final values

were consistent under opaque panels, semi-transparent panels, and open-field conditions, indicating that canopy compactness at harvest was not affected by panel coverage. This behavior is coherent with the pattern observed for the diameter-to-height ratio (Figure 3.40), where plant architecture also converged at harvest across treatments. Both variables point to a stable structural development, with plants reaching similar morphological proportions and canopy organization regardless of microclimate conditions. At the agronomic level, this suggested that agri-PV parameters could be not affecting canopy compactness at harvest.

Table 3.6 Mean crop compactness index of the Lettuce (cv. Maravilla) cultivar by treatment and sampling time at the end of the autumn cycle.

Section	***Compactness index (%)***
Opaque	92.1
Translucent	93.2
Control	93.5

Broccoli

Maximum diameter

During the **autumn** cycle (Figure 3.40), maximum plant diameter of broccoli at harvest **was lower under opaque and semi-transparent panels than under open-field conditions**. The open-field control showed significantly higher values than both panel-covered treatments, whereas no differences were detected between opaque and semi-transparent panels. Under the conditions of this study, this pattern could reflect a reduction in lateral canopy expansion under agrivoltaic cover. From an agronomic perspective, broccoli grown beneath the panels would still complete its development, although with a somewhat smaller final canopy diameter than plants cultivated in open-field conditions. Besides this, future assays should be conducted during the harvest at different time points for open-field and panel-covered treatments, as plants grown under agrivoltaic conditions may require a longer period to reach their full development.

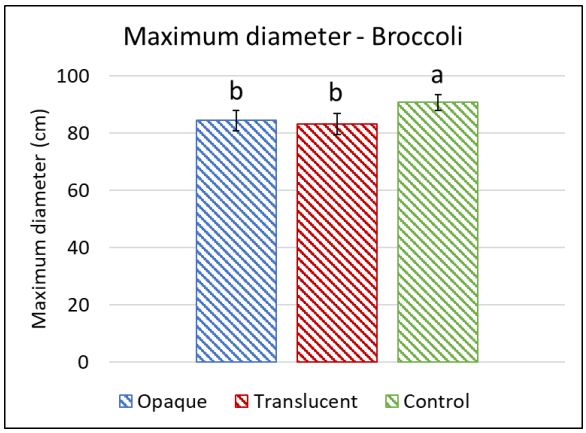

Figure 3.40 Mean maximum diameter at the end of the autumn cycle for broccoli under opaque panels (blue), semi-transparent panels (red), and open-field conditions (green). Bars express standard deviations. Letters indicate homogeneous groups obtained by the Tukey's test ($p < 0.05$).

Minimum diameter

For the **autumn** cycle (Figure 3.41), **maximum plant diameter of broccoli at harvest was higher in the open-field control than under opaque and semi-transparent panels**. The open-field control differed significantly from the opaque treatment, whereas the semi-transparent treatment did not differ from either of them. This pattern could indicate that minimum canopy expansion was partly reduced under opaque cover, while semi-transparent panels allowed an intermediate response. From an agronomic perspective, these observations could suggest that the degree of shading could influence the final lateral development of broccoli, although additional trials under different climatic conditions would be needed to confirm this behavior. In this context, it would also be valuable to relate these results to the sensor data in order to better understand the underlying causes of the observed patterns. Future analyses will consider integrating these datasets to further explore the influence of microclimatic conditions on crop development.

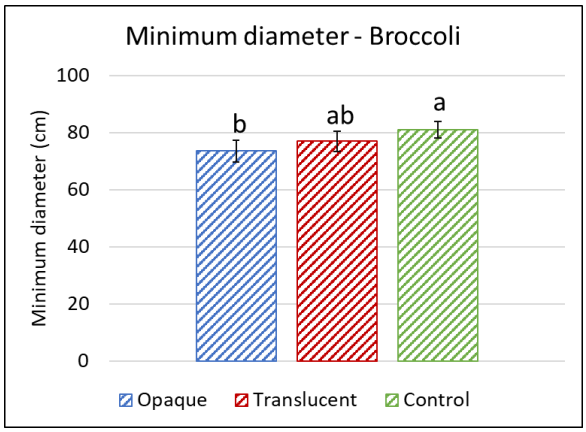

Figure 3.41 Mean minimum diameter at the end of the autumn cycle for broccoli under opaque panels (blue), semi-transparent panels (red), and open-field conditions (green). Bars express standard deviations. Letters indicate homogeneous groups obtained by the Tukey's test ($p < 0.05$).

Morphological proportion

During the **autumn** cycle (Figure 3.42), **the ratio between maximum diameter and plant height of broccoli at harvest fell within a narrow range across treatments,** with no clear separation between radiation conditions. Values under opaque, semi-transparent, and open-field conditions were closely aligned, and the grouping letters indicate no statistical differences among treatments. This pattern suggested that the proportional relationship between lateral expansion and vertical growth was maintained regardless of panel coverage. In line with the behaviour observed for maximum and minimum diameters, as well as plant height, the overall plant architecture at harvest followed a consistent configuration across radiation regimes. These valorations point to a stable morphological development under agrivoltaic conditions, where plants achieved proximal structural proportions at harvest.

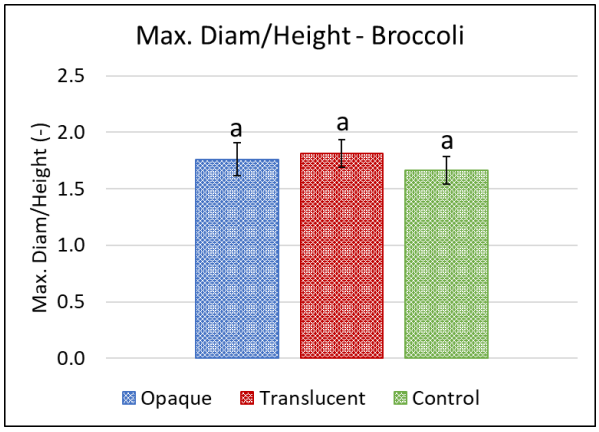

Figure 3.42 Mean ratio between the maximum diameter and height at the end of the autumn cycle in autumn cycle for broccoli under opaque panels (blue), semi-transparent panels (red), and open-field conditions (green). Bars express standard deviations. Letters indicate homogeneous groups obtained by the Tukey's test ($p < 0.05$).

Compactness index

During the **autumn** cycle, the compactness index of broccoli at the end of the season (Table 3.7) presented **values within a relatively narrow range across treatments**, with no clear separation between crop conditions. While some variability was observed during intermediate stages, the overall temporal pattern was consistent across radiation regimes. At harvest, the observed variations did not translate into distinct structural outcomes. From an agronomic perspective, these observations show that agrivoltaic conditions did not seem to induce broccoli head compactness at the end of the cycle. However, further trials under different climatic conditions are required to confirm the consistency of this response.

Table 3.7 Mean crop compactness index of the broccoli cultivar by treatment and sampling time during the autumn cycle.

Section	***Compactness index (%)***
Opaque	87.2
Translucent	92.6
Control	89.2

Biomass production

Biomass at harvest

At harvest, lettuce biomass showed **no statistically significant differences** among the three light treatments for either cultivar during the **summer** cycle (Figure 3.43). Both Maravilla and Francesca reached comparable final biomass values across treatments, as indicated by the same significance letter within each cultivar. Although slight numerical differences were observed, with marginally higher mean values under translucent panels and control conditions, these variations were within the experimental variability and cannot be attributed to a clear treatment effect. Overall, the results indicate that the presence of agrivoltaic panels, regardless of their optical properties, did not negatively affect lettuce biomass accumulation at harvest. This suggests that, under the studied conditions, lettuce plants were able to compensate for differences in light environment throughout the growing cycle, maintaining similar final yields across all treatments.

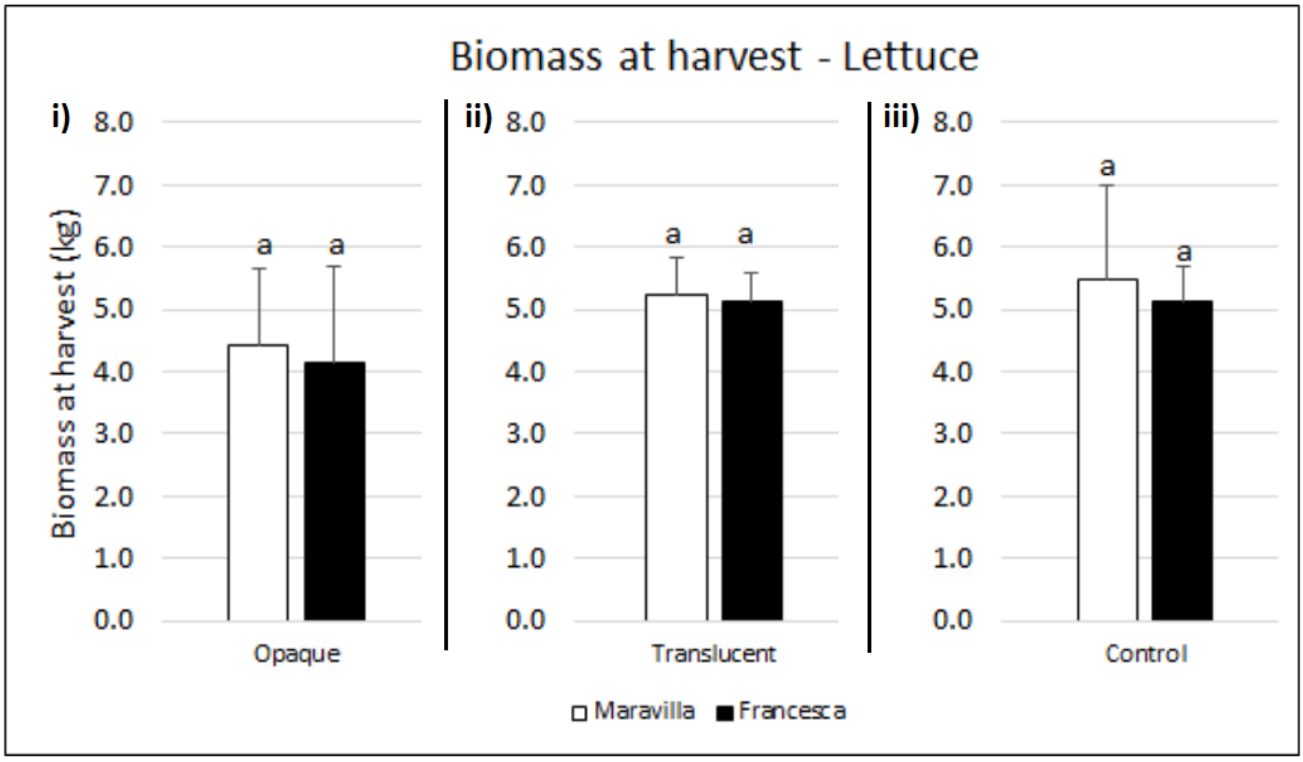

Figure 3.43 Biomass at harvest of lettuce cultivars under the different radiation treatments evaluated during the summer cycle, shown separately for each treatment (i: opaque, ii: translucent, iii: open-field) for Maravilla (white) and Francesca (black). Values represent the mean biomass per group of ten lettuce plants. Bars express standard deviations. Letters indicate homogeneous groups obtained by the Tukey's test ($p < 0.05$).

During the **autumn** cycle (Figure 3.44), lettuce biomass at harvest did **not show statistically significant differences** between Maravilla and Francesca within any of the radiation treatments, indicating a similar biomass production at the end of the crop cycle under each light condition. From a numerical perspective, a gradual increase in biomass can be observed from opaque to control conditions for both cultivars, although this trend is more pronounced in Francesca. Maravilla shows a more moderate response across treatments, with smaller differences between radiation conditions. Despite these tendencies, the variability within each treatment prevents establishing clear statistical differences between cultivars. These observations would be consistent with a relatively stable biomass production under agrivoltaic conditions, although the slightly stronger response of Francesca under open-field conditions could point to a higher sensitivity to increased light availability. Further experiments under different environmental conditions would be needed to confirm whether these trends are maintained.

.

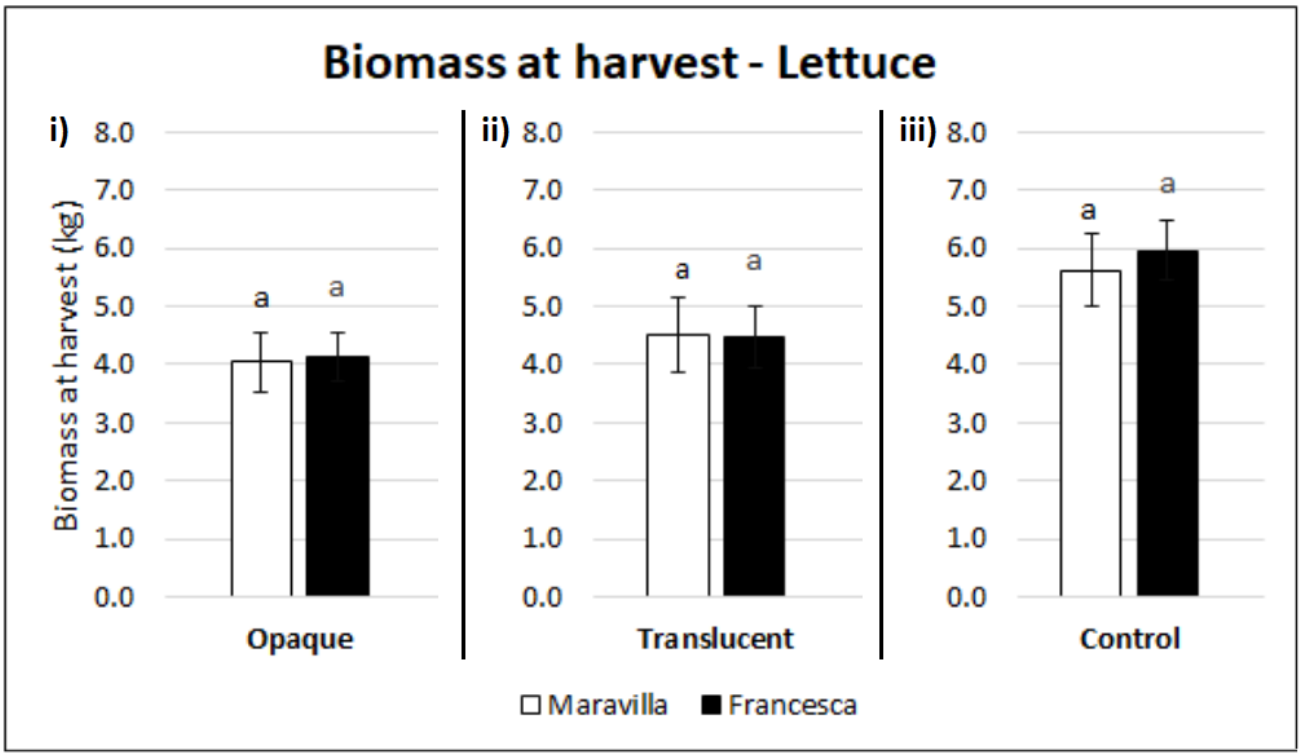

Figure 3.44 Biomass at harvest of lettuce cultivars under the different radiation treatments evaluated during the autumn cycle, shown separately for each treatment (i: opaque, ii: translucent, iii: open-field) for Maravilla (white) and Francesca (black). Values represent the mean biomass per group of ten lettuce plants. Bars express standard deviations. Letters indicate homogeneous groups obtained by the Tukey's test ($p < 0.05$).

Fresh weight

The fresh weight at harvest for the **summer** cycle (Figure 3.45) showed a **clear cultivar-dependent response to radiation conditions**. Under opaque panels, Maravilla and Francesca exhibited very similar fresh weight values, indicating a comparable performance under the most restrictive light environment. In contrast, under translucent panels and open-field conditions, Maravilla consistently reached higher fresh weight than Francesca, pointing to a stronger positive response of this cultivar to increased radiation availability. From a global perspective, Maravilla displayed a marked increase in fresh weight from opaque to control conditions, with values approaching nearly a twofold rise, highlighting a strong sensitivity to light availability. In contrast, Francesca showed a more moderate variation across treatments, with a less pronounced increase towards open-field conditions. This more contained response suggests that Francesca could maintain a more stable biomass production under reduced radiation, whereas Maravilla appeared to benefit more from higher light inputs. Taken together, these patterns would indicate that Francesca could be better adapted to agrivoltaic conditions, maintaining relatively consistent fresh weight under shading, while Maravilla would be more responsive to full radiation environments, achieving higher biomass under open-field conditions. In practical terms, this could have implications for cultivar selection depending on the intended balance between productivity and stability under agrivoltaic systems.

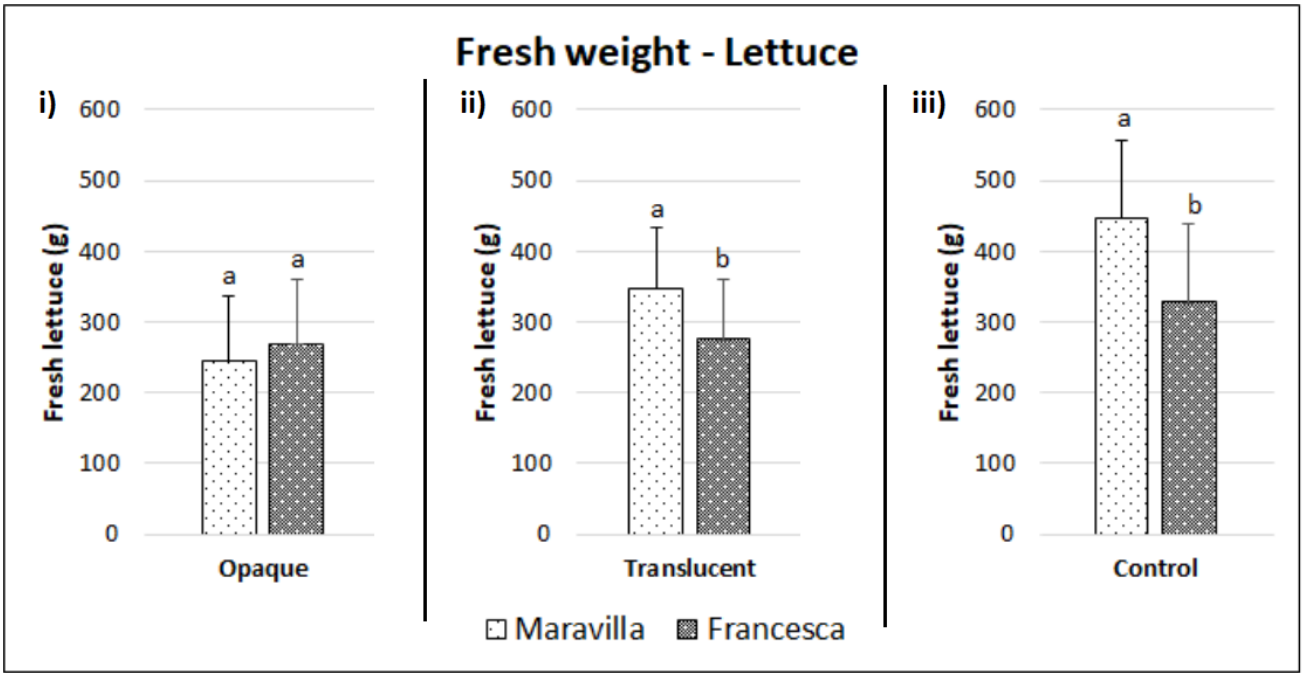

Figure 3.45 Fresh weight of lettuce cultivars under the different radiation treatments evaluated during the summer cycle, shown separately for each treatment (i: opaque, ii: translucent, iii: open-field) for Maravilla (white) and Francesca (black). Bars express standard deviations. Letters indicate homogeneous groups obtained by the Tukey's test ($p < 0.05$).

During the **autumn** cycle (Figure 3.46), fresh weight at harvest **did not show statistically significant differences** between Maravilla and Francesca within any of the radiation treatments. Under opaque panels, semi-transparent panels, and open-field conditions, both cultivars were assigned to the same significance group according to Tukey's test ($p < 0.05$), indicating a similar fresh biomass at the end of the crop cycle within each light environment. Fresh weight values were slightly higher under open-field conditions for both cultivars, while opaque and semi-transparent treatments showed lower but relatively close values. The increase from agrivoltaic to open-field conditions appears more noticeable in Francesca, whereas Maravilla shows a more moderate variation across treatments. However, the observed variability prevents establishing statistical differences between cultivars within each treatment. These results are consistent with a stable fresh biomass production under agrivoltaic conditions. The similar response of both cultivars under opaque and semi-transparent panels suggests that reduced radiation did not substantially limit biomass accumulation, although additional trials under different climatic conditions would be necessary to confirm these patterns.

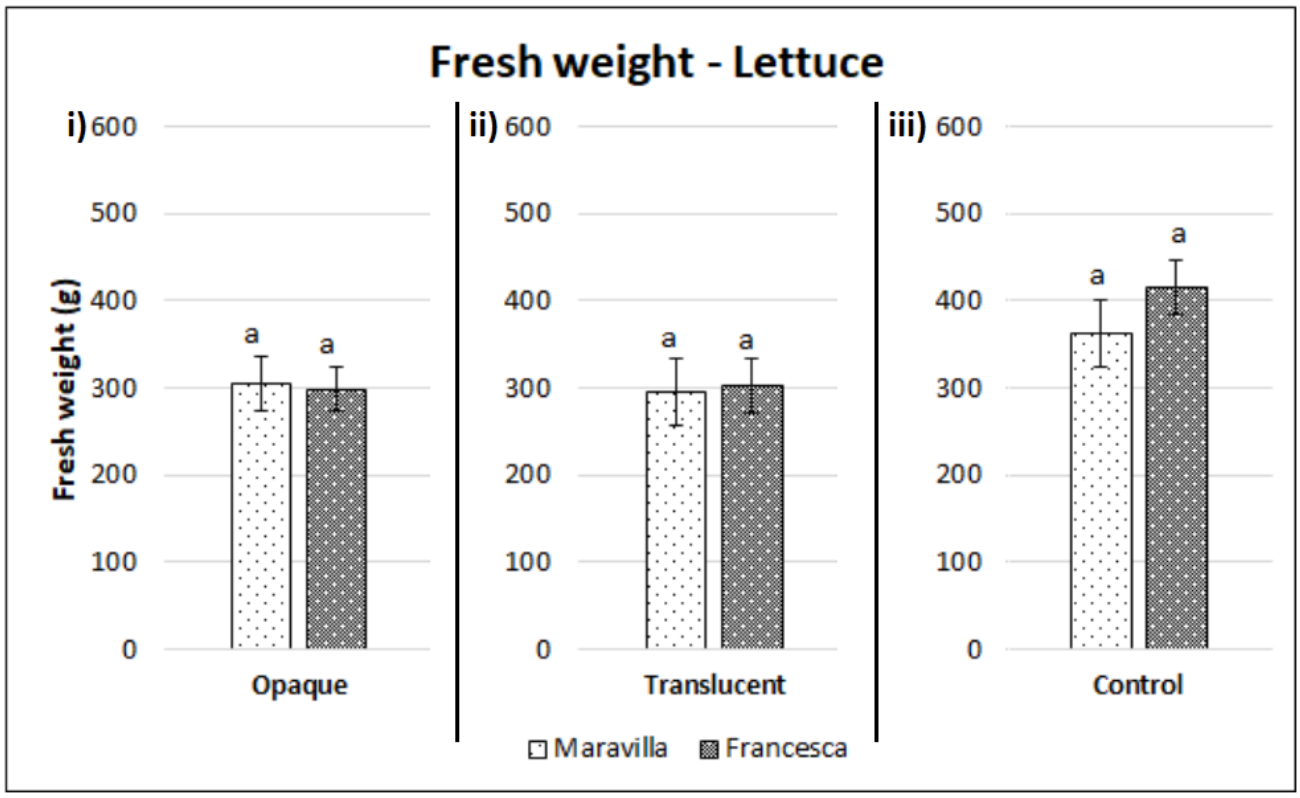

Figure 3.46 Fresh weight of lettuce cultivars under the different radiation treatments evaluated during the autumn cycle, shown separately for each treatment (i: opaque, ii: translucent, iii: open-field) for Maravilla (white) and Francesca (black). Bars express standard deviations. Letters indicate homogeneous groups obtained by the Tukey's test ($p < 0.05$).

During the **autumn** cycle (Figure 3.47), fresh weight of broccoli **showed clear differences among treatments**. The open-field control exhibited significantly higher fresh weight compared with both agrivoltaic treatments, as indicated by the different significance letter. Mean fresh weight under control conditions was markedly greater, reflecting more favorable growth conditions in the absence of shading. In contrast, broccoli grown under opaque and translucent panels showed lower fresh weight values, and no statistically significant differences were detected between these two treatments. Both shaded conditions were grouped within the same significance class, suggesting that, under autumn conditions, the type of panel (opaque or translucent) did not differentially affect broccoli fresh biomass. The strong response observed in the control treatment highlights the higher sensitivity of broccoli to reduced radiation during the autumn cycle, when ambient light availability is already limited. Under these conditions, additional shading imposed by agrivoltaic structures appears to constrain fresh biomass accumulation. It could suggest that unlike lettuce, broccoli fresh weight in autumn is significantly affected by agrivoltaic shading, with open-field conditions provided a clear advantage in terms of yield when they were collected at the same time.

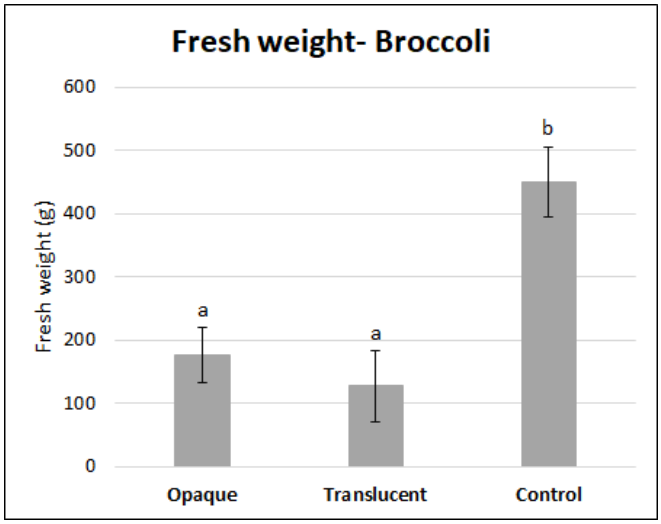

Figure 3.47 Fresh weight of broccoli cultivars under the different control treatments evaluated during the autumn cycle (grey bars). Bars express standard deviations. Letters indicate homogeneous groups obtained by the Tukey's test ($p < 0.05$).

3.8.3.2. Dry matter

During the **summer** cycle (Table 3.8), dry matter content **differed between cultivars and showed some variation among light treatments**. In general, Francesca presented higher dry matter percentages than Maravilla across all treatments, indicating intrinsic varietal differences in tissue composition and water content. For Francesca, open-field conditions tended to promote slightly higher dry matter accumulation compared with shaded treatments, although differences among panel types were moderate. In the case of Maravilla, dry matter content appeared more sensitive to the light environment, with shaded conditions showing some reduction compared to open-field growth.

Table 3.8 Mean dry matter values of the lettuce cultivar by treatment and sampling time during the summer cycle.

Section	*Monitoring*	*Dry matter (%)*
Francesca	Opaque	4.75
	Translucent	4.88
	Control	5.41
Maravilla	Opaque	4.15
	Translucent	3.20
	Control	3.51

During the **autumn** cycle (Table 3.9), dry **matter content showed clear differences between crops** and, to a lesser extent, among light treatments. Broccoli consistently exhibited substantially higher dry matter content than lettuce, reflecting inherent crop-specific differences in biomass composition and tissue structure. Within lettuce, both cultivars displayed relatively similar dry matter levels across treatments, with only minor variations associated with the light environment. No strong or systematic effect of panel type was observed,

suggesting that under autumn conditions dry matter accumulation in lettuce was mainly driven by cultivar traits rather than shading. For broccoli, dry matter content was generally high under all treatments, with only moderate differences between shaded and open-field conditions. This indicates that broccoli dry matter accumulation during the autumn cycle was relatively stable and less sensitive to changes in light regime.

Table 3.9 Mean dry matter values of the lettuce and broccoli cultivar by treatment and sampling time during the autumn cycle.

Section	***Monitoring***	***Dry matter (%)***
Francesca	Opaque	4.12
	Translucent	4.25
	Control	4.26
Maravilla	Opaque	4.23
	Translucent	4.04
	Control	4.31
Broccoli	Opaque	8.49
	Translucent	9.26
	Control	8.24

3.3. Conclusion and Perspectives

The results obtained from the Barcelona agri-PV demonstrator during the first year of operation show that **lettuce crops developed under different radiation conditions** (opaque panels, semi-transparent panels, and open-field control) followed comparable growth trajectories and reached similar final values at harvest. Across the evaluated parameters, including plant height, maximum and minimum diameters, biomass, and derived architectural indicators, no consistent statistically significant differences were observed among treatments at the end of the crop cycle.

Although some differences were observed during intermediate stages of development, these were not maintained at harvest, suggesting a convergence in plant growth regardless of radiation conditions. This behaviour could indicate that, within the range of conditions evaluated, agrivoltaic shading did not substantially alter crop development patterns or final plant architecture.

From a physiological perspective, these results could reflect that lettuce maintained its growth dynamics under modified light environments, likely due to its capacity to adjust leaf expansion and light-use efficiency within non-limiting radiation ranges. This could allow plants to compensate for differences in incident radiation during specific growth stages, leading to similar structural outcomes at harvest.

In terms of potential commercial quality, the absence of differences in key morphological traits such as plant size, diameter, and architectural balance could suggest that marketable characteristics were not negatively

affected under agrivoltaic conditions. The maintenance of canopy structure and proportional development across treatments could be associated with a consistent product appearance at harvest.

Future work should aim to relate these agronomic observations with the microclimatic data collected by the sensor network, in order to better understand the interactions between radiation, temperature, and crop response. In addition, further experimental campaigns under different seasonal and climatic conditions will be required to assess the robustness and reproducibility of these findings.

4. Agri-PV demonstrator - Scalea (IT)

4.1. Site description and experimental design

The demonstrator is located in Scalea (Italy) and was already built by EF Solare Italia S.p.A. and feature characteristics suitable for fulfilling the objectives of the Symbiosyst project. Within the scope of this initiative, the tracking system was upgraded—through EF Solare's own budget, independent from the Symbiosyst funding thanks to the installation of new, more efficient and higher-power bifacial photovoltaic modules.
This report refers to the period from October 2024 to February 2025 and describes the operation of the **tracker-based agrivoltaic system**, with particular attention to the system's energy production and the comparison between crops grown beneath the structures and those grown in the adjacent open field.
Data were collected on electrical parameters and energy production from the photovoltaic system, along with agronomic data related to crops both beneath the trackers and in open-field conditions. The agrivoltaic system consists of photovoltaic modules mounted on singleaxis trackers (new high efficiency bifacial modules installed in July 2024). An inverter capable of managing both battery charging and discharging was selected.
Due to the impossibility of obtaining a grid connection within the schedule and cost constraints of the experimentation, the photovoltaic system was designed as an off grid installation, equipped with a battery storage system and a custom "smart" dissipator capable of activating resistive loads whose power consumption varies according to the real time production of the agrivoltaic system. The inclusion of this "smart" dissipator allows the PV system to remain in operation continuously throughout the day. Without it, once the batteries reached a sufficient state of charge to supply the small connected loads, the photovoltaic generation would automatically drop to zero, as there would be no grid to absorb excess power.
Although the dissipator is itself a prototype, this configuration allowed the off grid photovoltaic system to operate regularly and simulate a variety of user load profiles.

Experimental design

Eletrical data collection

The photovoltaic system built for the agrivoltaic installation is capable of providing a wide range of information, both through **dedicated sensors and through the inverter's built-in monitoring functions,** which allow the acquisition of several electrical parameters of the system.
Below is a summary of the **energy-related quantities available** from the system (Table 4.1).

Table 4.1 Summary of the energy related quantities in SCALEA demonstrator.

	Measure of interest	Note
Agri_PV plant	Power Charging (in the batteries)	
	Power generated (by the PV modules)	
	Exported Power	Zero as the PV plant is not grid-connected
	Imported Power	Zero as the PV plant is not grid-connected
	Power Discharged	
	Energy Charging (in the the batteries)	
	Energy generated (by the PV modules)	
	Exported Energy	Zero as the PV plant is not grid-connected
	Imported Energy	Zero as the PV plant is not grid-connected
	Energy Discharged	

Through the inverters, several electrical parameters of the photovoltaic generator can also be acquired (Table 4.2).

Table 4.2 Electrical parameters acquired through the inverters.

Electrical Quantity	Notes
Input currents to the inverter MPPTs	These represent the sum of the currents from all strings connected to an MPPT input
MPPT voltages	Voltage measured at the string input terminals

Agronomic management

EF Solare involved a local and long-standing partner for agriculture activities that thanks to its expertise carried out of the management of the tracker-based agrivoltaic prototype into the Scalea greenhouse facility.
Agricultural management involves the execution of the **standard annual cultivation operations**. With regard to the trees in the two monitored fields (with PV modules and the control), it is confirmed that they are well maintained and developing regularly.
Since planting, the main agronomic operations performed on the trees have included **canopy shaping and containment pruning**, aimed at promoting the development of a "globe-shaped" canopy. Height is particularly controlled to avoid any contact with the photovoltaic modules positioned above the trees.

Each year, the canopies undergo:

Structural (wood) pruning — March–April

This operation removes unproductive parts of the canopy, such as old woody branches, and branches turning inward, in order to stimulate the growth of new shoots and favour proper canopy aeration.

Green pruning — multiple interventions throughout the season

These operations promote lateral growth and control overall canopy height. They include the removal of suckers and water sprouts originating from woody-pruning cuts, and shortening cuts intended to regulate canopy volume and encourage the emission of new lateral shoots.

Soil Management

No shallow tillage is performed. A tilled soil surface would be uneven, complicating the passage of self-propelled lifting platforms used for PV module inspections and electrical maintenance.
Instead, the soil has been sown with white clover (*Trifolium repens*) and perennial ryegrass (*Lolium perenne)*, which are periodically mulched. The resulting plant residue is left on the soil, where it forms:

- a natural mulch,
- an organic-matter reserve,
- a protective layer that stabilizes soil moisture.

Irrigation Management

Irrigation is performed through a low-flow dripline system, using self-compensating buried drip lines located at a depth of 20 cm, as well as an over-canopy sprinkler system.
Irrigation management is automated, with irrigation cycles triggered based on soil-moisture levels measured by humidity sensors and matric-potential sensors.
The automation system (Dream 2) activates irrigation when soil-moisture levels fall below thresholds critical for the crop, and stops irrigation once optimal moisture levels are detected by the sensors.

Crop Protection Management

Monitoring and control of pest and disease pressure are carried out according to the principles of integrated pest management (IPM)**:**

- interventions are performed only after careful evaluation of infestation levels;
- priority is given to mechanical, agronomic, or biological control methods;
- if chemical products are required, only authorised, selective, and low-persistence products are used;
- treatments are applied using low-volume sprayers**,** minimising operator exposure and environmental impact;
- natural antagonists are preserved as part of a sustainable ecological approach.

It is also noted that:

- Spraying operations do not encounter obstacles from the structures; machinery moves easily between the rows.
- Liquids reach the plants without interfering with the elevated PV modules.
- As modules and electrical components are positioned significantly above canopy height, they are not wetted by water or chemical products.

Lavender Plantation (November 2024)

In November 2024, **lavender plants (***Lavandula angustifolia***)** were planted both under the agrivoltaic prototype and in the open field (Figure 4.1).
A total of 80 plants were installed across 10 rows (8 plants per row). Lavender was selected as a research-relevant species because the partial shading provided by the elevated PV modules may extend the flowering period and increase essential-oil content and being a melliferous plant, it attracts bees and pollinators, serving as a biological indicator of environmental health. All lavender plants successfully rooted, and during the 2025 growing season they developed vigorous shrubs. Some produced flower spikes, offering

important resources for pollinators. At the end of autumn, they were pruned to restore a compact spherical form.



Figure 4.1 Lemon trees and lavender plants in the scalea demonstrator.

Agronomic data collection

Agronomic data for both the crops under the tracking system and for those in the open field are collected through dedicated sensors indicated in Table 4.3 that measure the following variables.

Table 4.3 Agronomic sensor installed in the Scalea demonstrator.

Sensor installed and unit of measure
Matric Potential (kPa)
Soil Temperature (Teros) (°C)
Dendrometer (mm)
Soil Moisture at 10 cm (%)
Soil Moisture at 20 cm (%)
Soil Moisture at 40 cm (%)
Soil Temperature (°C)
PAR (Photosynthetically Active Radiation) (µmol m^{-2} s^{-1})
External Air Temperature (°C)
Air Humidity (%)
Dew Point (°C)

Has been collected also meteorological data from the weather station installed close to the demonstrator. The environmental parameters collected are summarize in the Table 4.4.

Table 4.4 Envrionemntal parameters collected with the meteorological station in the Scalea demonstrator.

AS25 – Precipitation (mm)
AS26 – Solar Radiation (W/m²)
AS27 – High-precision Air Temperature (°C)
AS28 – Relative Humidity (%)
AS29 – Wind Direction
AS30 – Wind Speed (m/s)
AS40 – Evapotranspiration (mm)

4.2. Results of the first year of activity

Behaviour of the Agrivoltaic System from the Electrical and Energy Perspective

On days where some of the relevant data were unavailable due to malfunctions in devices, sensors, communication systems, or data loggers, **missing values were reconstructed** using EF Solare's internal databases. This was possible because the company operates several other photovoltaic plants in direct proximity to the Scalea demonstrator, allowing robust cross-comparison and gap-filling.
Below are the daily energy-production graphs for the October–November–December quarter (Figure 4.2).

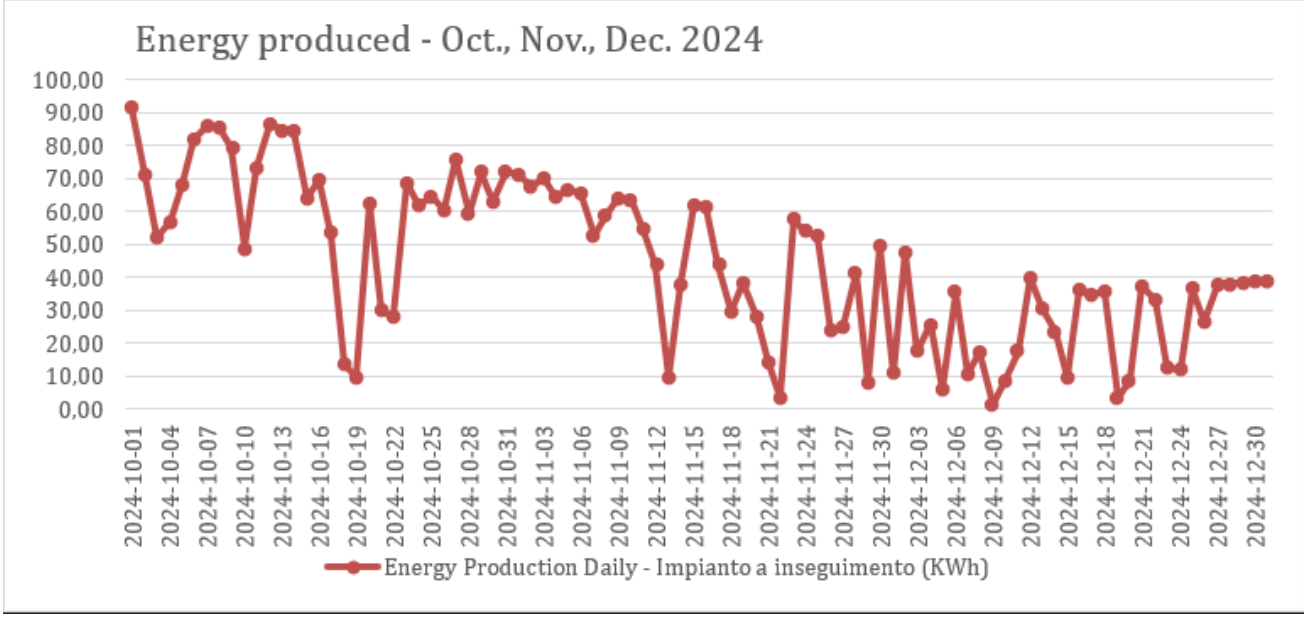

Figure 4.2 Daily energy-production in the months October, November and December 2024.

Taking into account the photovoltaic tracking configuration described in the previous section, the following Figure 4.3 shows:

- Power output from the inverters,
- Battery charging behaviour,
- Battery discharging behaviour onto the loads.

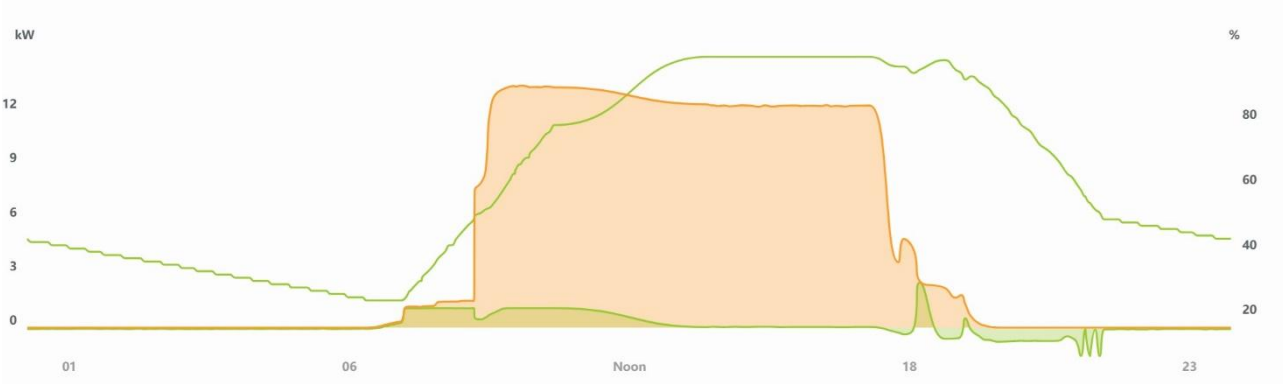

Figure 4.3 Power output from the inverters, battery charging behaviour and battery discharging behaviour onto the loads.

Key observations are:

The system's production curves **show very steep rise and fall slopes in the morning and afternoon**, respectively. This is a direct result of the **tracker's** ability to optimise module orientation throughout the day. Since the system includes electrochemical storage, the maximum output power delivered by the inverters depends on:

- the battery state of charge,
- the maximum consumption set by the resistive-load simulator ("power waster"),
- the real loads connected to the system.

In the graphs, this is visible as extended power plateaus during periods of strong irradiance, where the inverter output stabilises at a fixed power level for several hours.
The green line representing the state of charge is particularly informative, showing how the battery charges rapidly in the morning and discharges steadily according to programmed load behaviour.
The load-discharge curves illustrate how the batteries supplement or replace generation depending on environmental and operational conditions.

Agricultural results

Photosynthetically active radiation – PAR

When comparing the trees positioned beneath the trackers with those in the open field, it is observed that they exhibit a very similar and homogeneous vegetative structure.
Although the agronomic and environmental sensor data will be analysed in greater depth in upcoming studies conducted by the research group, some preliminary considerations can already be made regarding one of the

most important agronomic parameters of the experimentation: **PAR (Photosynthetically Active Radiation)**, measured by sensors that detect the sunlight used for photosynthesis.
PAR sensors record the number of photosynthetically active photons emitted by the sun, expressed in µmol m^{-2} s^{-1} (PPFD). They provide a quantitative measure of the light available to the plant for photosynthesis within the 400–700 nm wavelength range.
In the Scalea prototype, two sensors were installed:

- **PAR1** — positioned at mid-canopy height within one of the tracker rows of the agrivoltaic system
- **PAR2** — positioned in the open field adjacent to the agrivoltaic installation

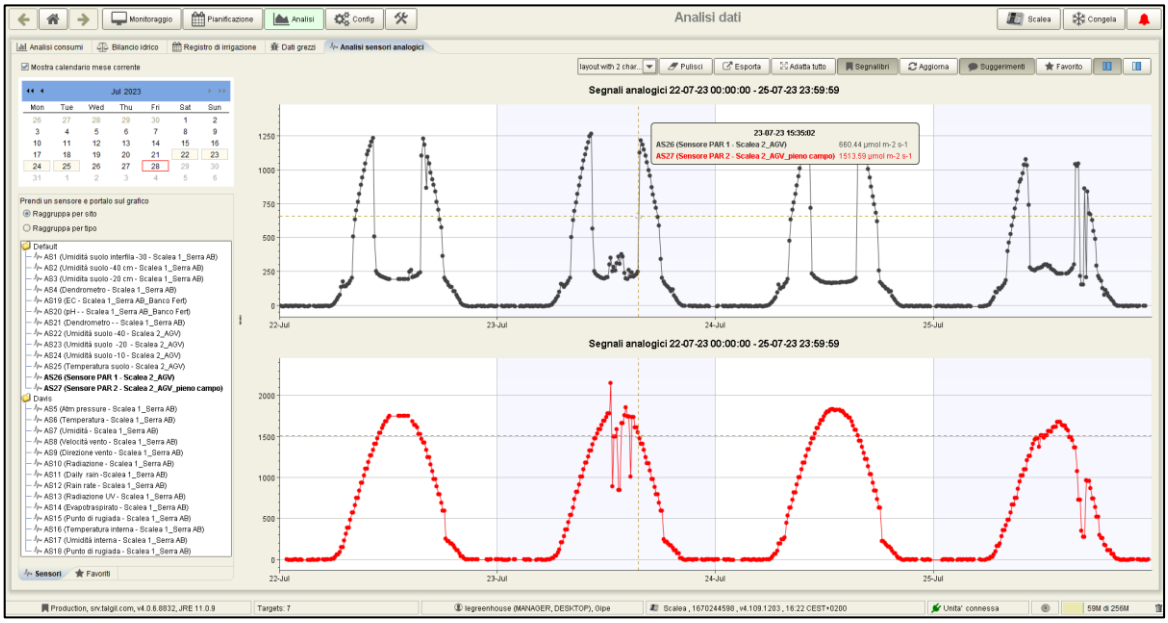

Figure 4.4 PAR1 sensor installed close to trackers; Graph below - PAR2 Sensor in open field close to the demonstrator.

Analysis of the PAR1 and PAR2 graphs for selected reference days shows that (Figure 4.4):

- Under **clear-sky** conditions, the sensor positioned below the tracker receives direct irradiation in the morning and afternoon, similarly to the open-field sensor.
- During **midday hours**, however, radiation beneath the tracker is less intense due to shading from the elevated modules.
- Nevertheless, across the **entire day**, total irradiance remains **sufficient to sustain photosynthesis** in the observed crops.

Light Propagation and Canopy Development

The elevated tracker-mounted PV modules form a north–south shadowing structure, ensuring:

- Direct light availability during certain hours of the day
- Progressive increases in canopy volume over the third and fourth year of plant development
- With proper pruning, the outer canopy continues to receive direct sunlight for most of the day
- The **5.20 m spacing** between tracker rows provides:

- Good light penetration
- Adequate airflow
- Suitable conditions for crop development even under partial shading

Climate Change Considerations and Protective Effects

Given the increasing climatic variability—characterised by extreme weather events, intense heat waves, hailstorms, and heavy rainfall—the presence of photovoltaic modules provides **protective benefits**, including:

- Mitigation of climatic stress on vegetation
- Reduced damage from hail, frost, and excessive rain
- Reduced soil erosion
- Moderation of excessive heat loads
- Dampening of strong winds

Visual Observations and Physiological Measurements

Although the trees grown under the agrivoltaic system and those in the open field appear similar in overall growth, closer inspection reveals **meaningful differences**:

- Leaves beneath the modules are larger and darker green
- Some branches exhibit longer internodes, an adaptive response to partial shading
- These qualitative observations were confirmed by scientific field measurements conducted with researchers from a highly reputable Italian university specialised in agronomy

Key measured parameters (summirized in Table 4.6):

- **Leaf number per growing shoot** — similar in both systems
- **Average leaf surface area** — significantly larger under the agrivoltaic system
- **Stomatal conductance** — higher under shading conditions (improved water status)
- **Leaf water potential** — significantly less negative beneath the modules, indicating better hydration
- **Photosynthetic efficiency (Fv/Fm)** — similar in both conditions

Table 4.6 Key physiological measured parameters.

Treatment	Leaves (n.)	Leaf Area (cm^2)	Stomatal Conductance ($mmol\ m^{-2}\ s^{-1}$)	Leaf Water Potential (MPa)	Fv/Fm
Under PV Modules	21	45	266	–1.3	0.77
Open Field	21	32	149	–1.8	0.76
Significance	ns	*0.04*	*0.007*	*0.001*	ns

These results demonstrate that reduced incident radiation does **not** necessarily have harmful effects on crop performance.

Instead, plants often adapt by improving their light-capture efficiency, especially when water conditions are more favourable.

Soil Moisture, Precipitation, and Microclimate

Controlled or spontaneous ground cover provides **multiple sustainability benefits** (Figure 4.5):

- reduces soil evaporation and therefore irrigation needs,
- limits soil dust that would otherwise settle on PV modules,
- reduces water demand for module cleaning,
- enhances biodiversity.

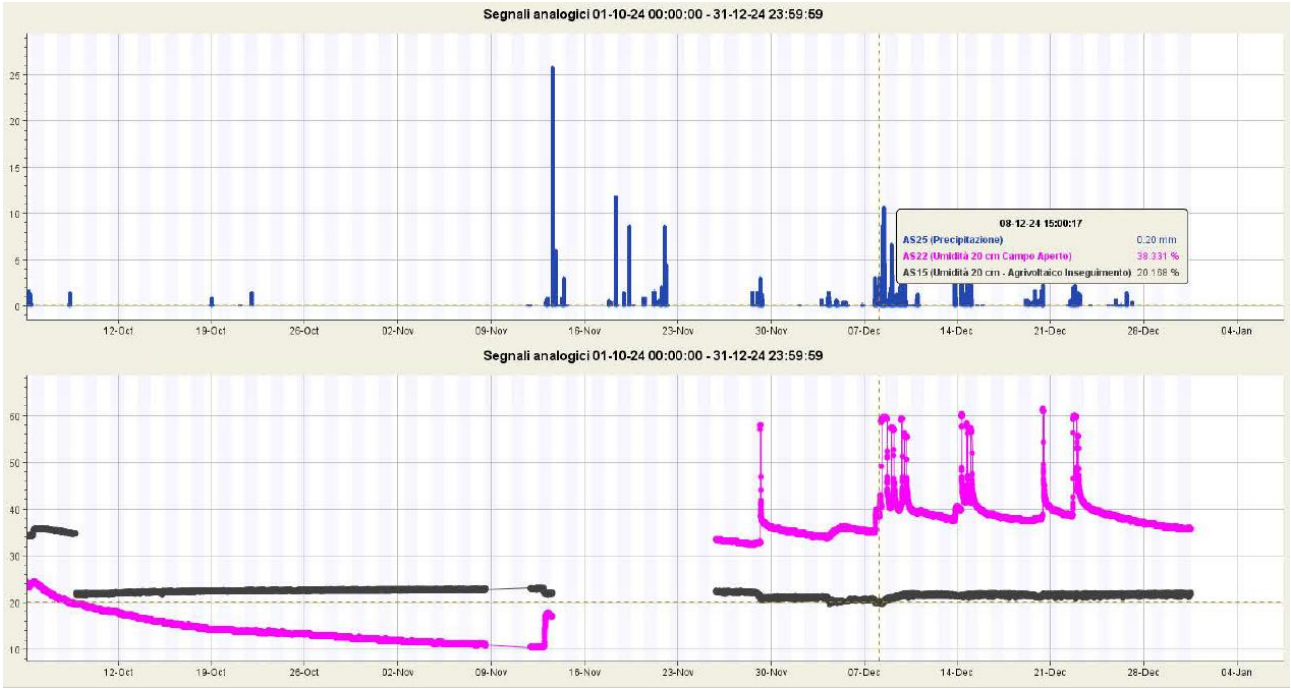

Figure 4.5 Rainfall (blue lines) and moisture level at – 20 cm depth in the tracker based agri-PV demo (black line) and in the free filed area (purple line) (October – December 2024).

Thanks to ground cover (mulching effect) and the protective presence of PV modules (Figure 4.6):

- rainfall alone was sufficient to maintain **optimal soil moisture levels**,
- irrigation demand was reduced or entirely avoided.

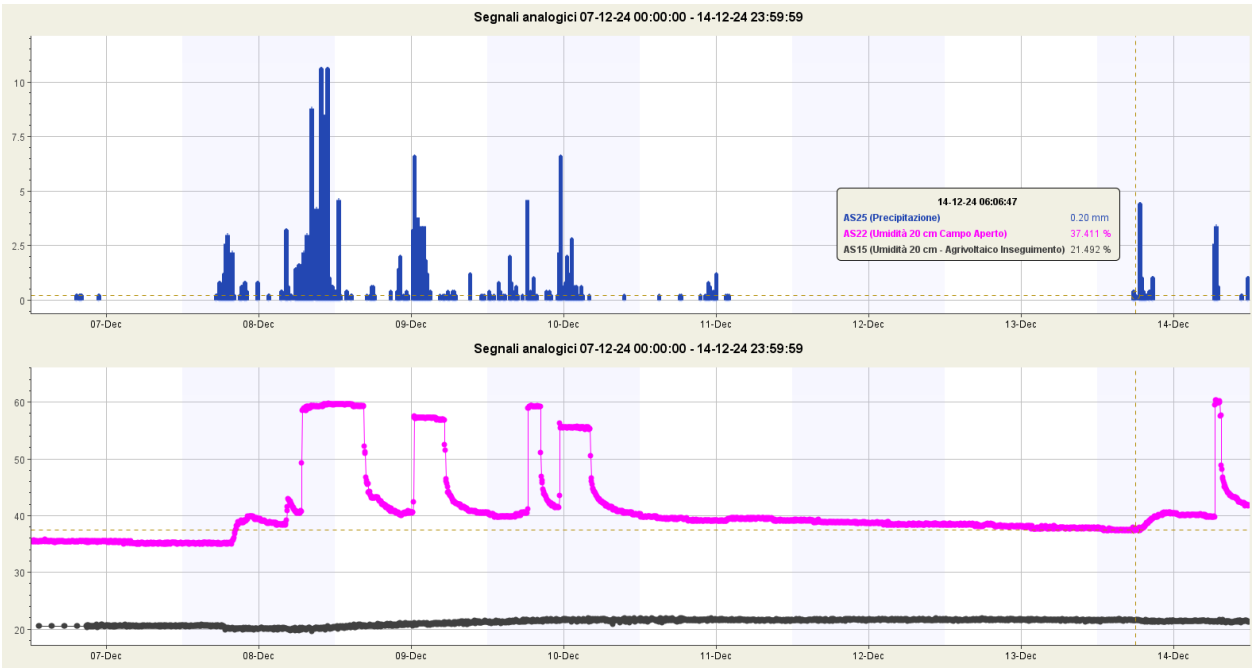

Figure 4.6 Rainfall (blue lines) and moisture level at – 20 cm depth in the tracker based agri-PV demo (black line) and in the free filed area (purple line) (7thto 14th December 2024).

In the **open field**, soil moisture at 20 cm fluctuates sharply depending on rainfall

In the **agrivoltaic system**, soil moisture remains **stable**, unaffected by precipitation patterns

Horizontal tracker positioning during rain promotes even water runoff and prevents harmful puddling beneath the modules

During prolonged heat periods (summertime):

- The agrivoltaic system reduces **evapotranspiration**,
- Maintains a **more stable and humid microclimate**,
- Moderates temperature fluctuations between day and night,
- Reduces wind exposure,
- And slightly cools PV modules, improving **electrical performance** by reducing thermal losses.

Irrigation Management Using Matric-Potential Sensors

During 2025, irrigation of the lemon trees cultivated both under the tracker-based agrivoltaic system and in the open field was managed using **soil matric-potential data** measured by dedicated sensors installed at a depth of approximately 30 cm.
The **matric potential** is the most significant soil-water parameter because it describes the extent to which water adheres to soil surfaces. As water drains from the soil, the amount of air-filled pore space increases and water binds more tightly to soil particles, thereby reducing matric potential.

It represents (at atmospheric pressure) the soil matrix's tendency to draw water molecules towards itself. This tendency corresponds to the average force acting on the least-bound water molecules. In conditions of maximal hydration, this force is nearly zero.
Matric potential arises from hydrogen bonding, Van der Waals forces, capillary interactions.
Since soil is composed of small particles providing large surface areas, water adhesion depends on soil type. For example:

- **Sandy soil**: large particles, fewer binding sites → higher matric potential, greater water availability
- **Silty soil**: smaller particles, more binding sites → lower matric potential, much less water availability

Matric potential is always **negative or zero**, because it lowers water potential and decreases water's chemical activity. It is measured in **Pascal (Pa)** or **meters of water column (m H_2O)**.
In the field, matric potential was measured using **two dielectric matric-potential sensors**, one installed in the open field and one in the agrivoltaic system.
The sensor measures the charge-storage capacity of a ceramic disc to determine its moisture content and subsequently converts this value into water potential.
For matric potential:

- Values close to **0 kPa** indicate excellent conditions
- Many crops tolerate values of **–50 to –80 kPa**
- Some species can tolerate values as low as **–200 to –300 kPa**
- More negative values indicate higher stress for the plant and reduced growth and productivity

During the irrigation season, data from both sensors were analysed, and a monthly irrigation-control schedule was defined based on matric-potential thresholds.

Irrigation Activation Thresholds (kPa):

- April: from –50 kPa to –10 kPa
- May: from –60 kPa to –10 kPa
- June: from –50 kPa to –10 kPa
- July: from –50 kPa to –10 kPa
- August: from –40 kPa to –10 kPa
- September: from –60 kPa to –10 kPa

Applying this protocol improved overall water-use efficiency, ensuring that irrigation supplied only the quantities needed to satisfy the specific water requirements of the lemon cultivar.

4.3. Conclusion and Perspectives

The results obtained at the Scalea agrivoltaic demonstrator during the period October 2024 – February 2025 confirm the technical feasibility and agronomic value of a tracker-based agrivoltaic system, even in an off-grid configuration. The single-axis tracking system with high-efficiency bifacial modules demonstrated consistent energy production, with steep morning and afternoon power ramps reflecting the tracker's effectiveness in

maximising solar capture throughout the day. The integration of battery storage and a smart resistive dissipator proved to be a practical solution in the absence of a grid connection, allowing continuous system operation. A formal grid connection, currently under evaluation with the distributor ENEL, is expected to further simplify operational management from 2026 onward.

From an agronomic perspective**, crops cultivated beneath the trackers showed no signs of reduced productivity or physiological stress compared to the open field**. On the contrary, **key indicators such as leaf area, stomatal conductance, and leaf water potential all pointed to improved plant water status under partial shading, while photosynthetic efficiency remained comparable between the two systems.** Soil moisture dynamics further highlighted the stabilising role of the agrivoltaic canopy, with moisture levels beneath the modules remaining more consistent and less sensitive to precipitation variability than in the open field. This effect, combined with the automated matric-potential-based irrigation protocol, contributed to a measurable improvement in water use efficiency across the growing season.

Overall, the Scalea demonstrator provides solid early evidence that tracker-based agrivoltaic systems can simultaneously deliver renewable energy, improved crop performance, and enhanced climate resilience — representing a promising land-use strategy for Mediterranean agricultural contexts.

5. Agri-PV demonstrator - Schipluiden (NL)

5.1. Site description and experimental design

During the first operational year of the closed Agri-PV demonstrator at the Lotsweg greenhouse, KUBO successfully completed a full cycle of data collection. The hardware was installed in an earlier phase, monitoring activities were running since September 2024, and the data structuring was done to bring information in an organized way to the partners in the consortium. During this first-year analysis and validation of the light levels coming into the greenhouse were done. The demonstrator consists of a **greenhouse retrofitted with photovoltaic modules and equipped with a high-resolution PAR (Photosynthetically Active Radiation) monitoring grid and integrated data logging systems**.

The aim of the Netherlands demonstrator is to quantify:

(i) effective light entering the greenhouse under different PV densities.
(ii) spatial distribution of radiation across zones.
(iii) effects of glass type (coated vs. clear) on light uniformity.
(iv) temporal shading patterns.
(v) expected agronomic impacts based on DLI-based crop models.
(vi) LED supplementation required to compensate PV-induced shading.
(vii) validation of WP2 models.

Demonstrator Setup (Lotsweg Greenhouse)

The KUBO demonstrator consists of **144 photovoltaic panels distributed across six zones, representing PV surface coverages of 0%, 6.25%, and 12.5%,** implemented on both coated and clear glass roof sections.

Crop-level light conditions are monitored through a calibrated grid of 96 PAR sensors installed at the crop plane. In addition, a dedicated weather station provides measurements of ambient radiation and key climatic variables, while the photovoltaic system is continuously monitored on both the AC and DC sides. All monitoring and measurement systems have been fully operational since September 2024, enabling the collection of continuous and long-duration datasets.

The demonstrator has been designed to quantify real-world reductions in PAR as a function of PV density, to evaluate radiation uniformity and temporal fluctuations within the greenhouse, and to generate empirical validation data for the models developed in WP2. Furthermore, it supports scenario analyses related to lighting, climate, and crop modelling, and provides the basis for multi-season monitoring activities.

Monitoring, Data Collection & Methodology

The sensor network implemented at the KUBO demonstrator consists of **96 PAR sensors arranged in a fixed grid** across six measurement zones (Figure 5.1), each characterized by a specific combination of PV density and glass type.

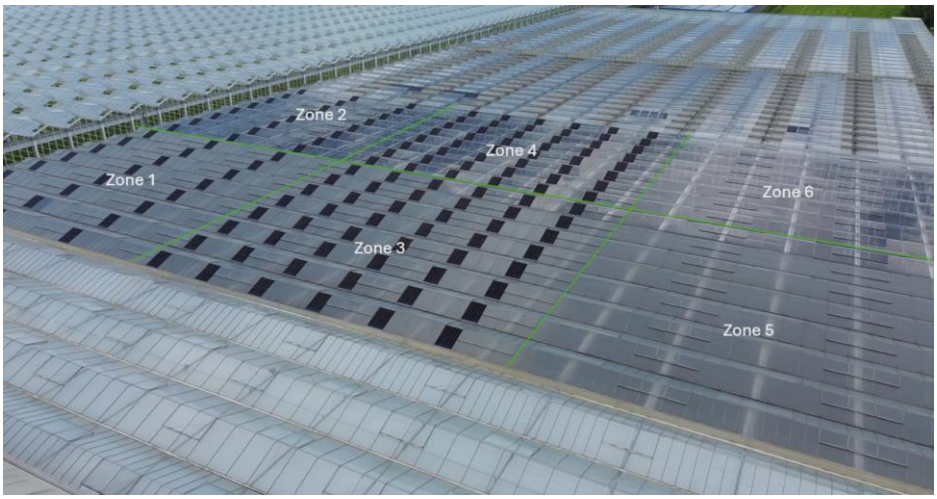

Figure 5.1 Six control zones in the greenhouse

This network is complemented by an integrated weather station providing an external reference for ambient radiation and climatic conditions, as well as by continuous logging of PV system AC/DC output. Each PAR sensor operates at high temporal resolution, enabling detailed analyses of light penetration, radiation stability, and shading dynamics within the greenhouse environment.

The monitoring activities cover **two main measurement domains:**

- Solar and photosynthetically active radiation (PAR) analysed both at point level and aggregated by zone.
- Photovoltaic system performance, including DC and AC outputs with precise timestamp correlation.

Data acquisition is based on high-frequency sampling combined with systematic time alignment, structured data storage, and consortium-compatible data export formats. At the start of the analysis, a dedicated pre-

processing workflow was applied, including outlier removal, alignment with external radiation measurements, sensor drift verification, and aggregation of the datasets into 15-minute, hourly, and daily summaries.
Data analysis is carried out using **Python-based scripts** developed to support data merging, zonal averaging, computation of variability indices, radiation mapping, detection of shading events, and correlation analyses between radiation patterns and PV production. These analyses are further complemented by the integration of 3D greenhouse geometry inputs, which are used for light simulation purposes and for the validation of the modelling approaches developed in WP2.

5.2 Results of the first year of activity

Light Entry Analysis (First-Year Results)

The analysis of incoming radiation **indicates that photovoltaic modules reduce PAR in proportion to their surface coverage.** Diffuse glass improves light uniformity across the crop area, whereas clear glass allows higher absolute PAR levels but is associated with stronger temporal and spatial fluctuations. The zones without PV coverage (0%) serve as the reference condition, while the 6.25% and 12.5% PV zones exhibit predictable and reproducible shading behaviour.
A comparison between diffuse and clear glass shows that diffuse glass effectively reduces radiation peaks while increasing overall homogeneity, whereas clear glass results in more direct light beams and higher variability. Temporal dynamics are characterised by clear morning and afternoon gradients and a strong dependence on solar angle, with diffuse glass producing flatter and more stable daily radiation curves.
Increasing PV density leads to a higher average reduction in PAR, however, it also improves the predictability of radiation distribution patterns within the greenhouse.
The comparison of radiation conditions between the different zones is illustrated in Figure 5.2, Figure 5.3, and Figure 5.4.

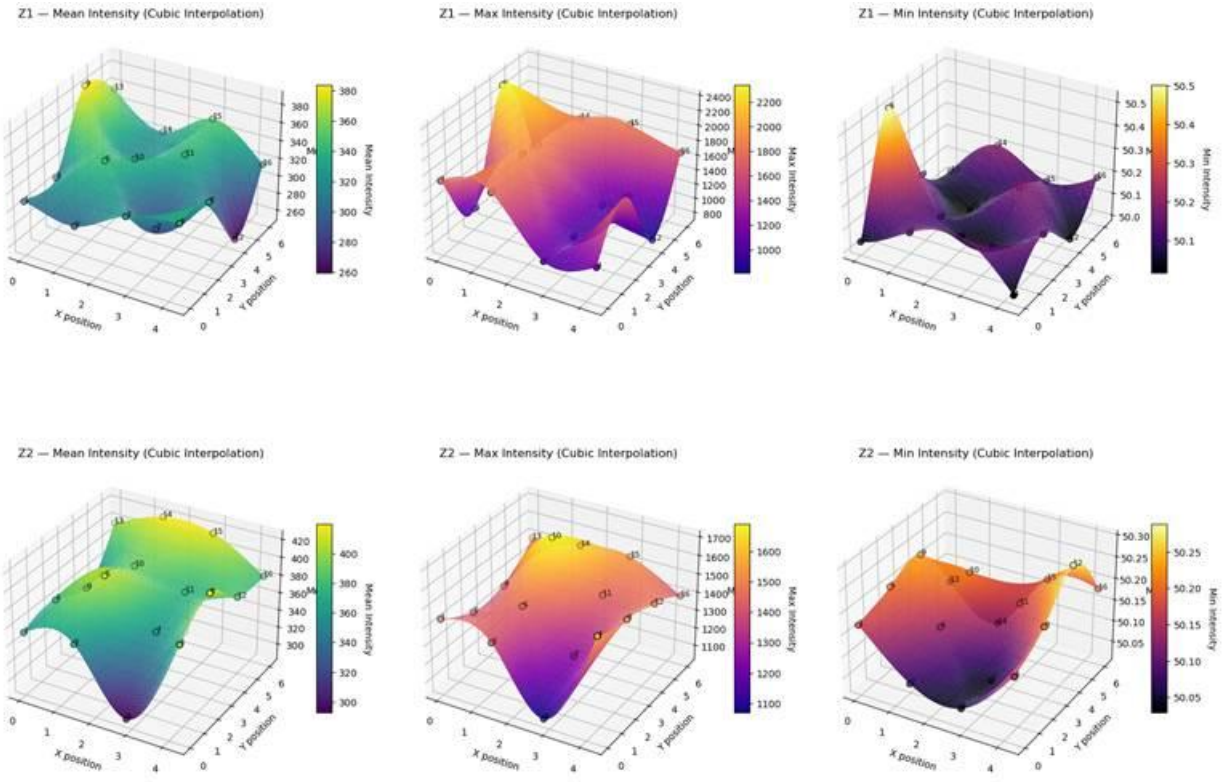

Figure 5.2 Comparison between zone 1 and zone 2.

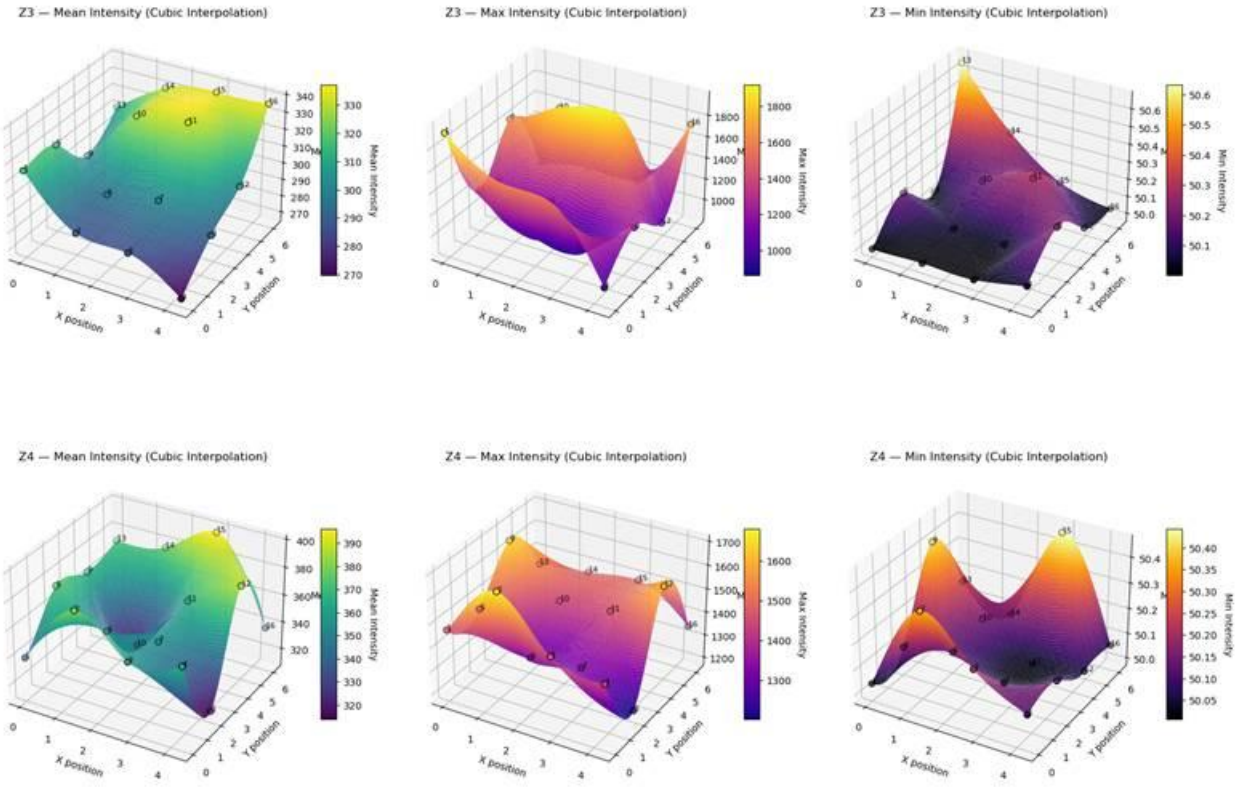

Figure 5.3 Comparison between zone 3 and 4.

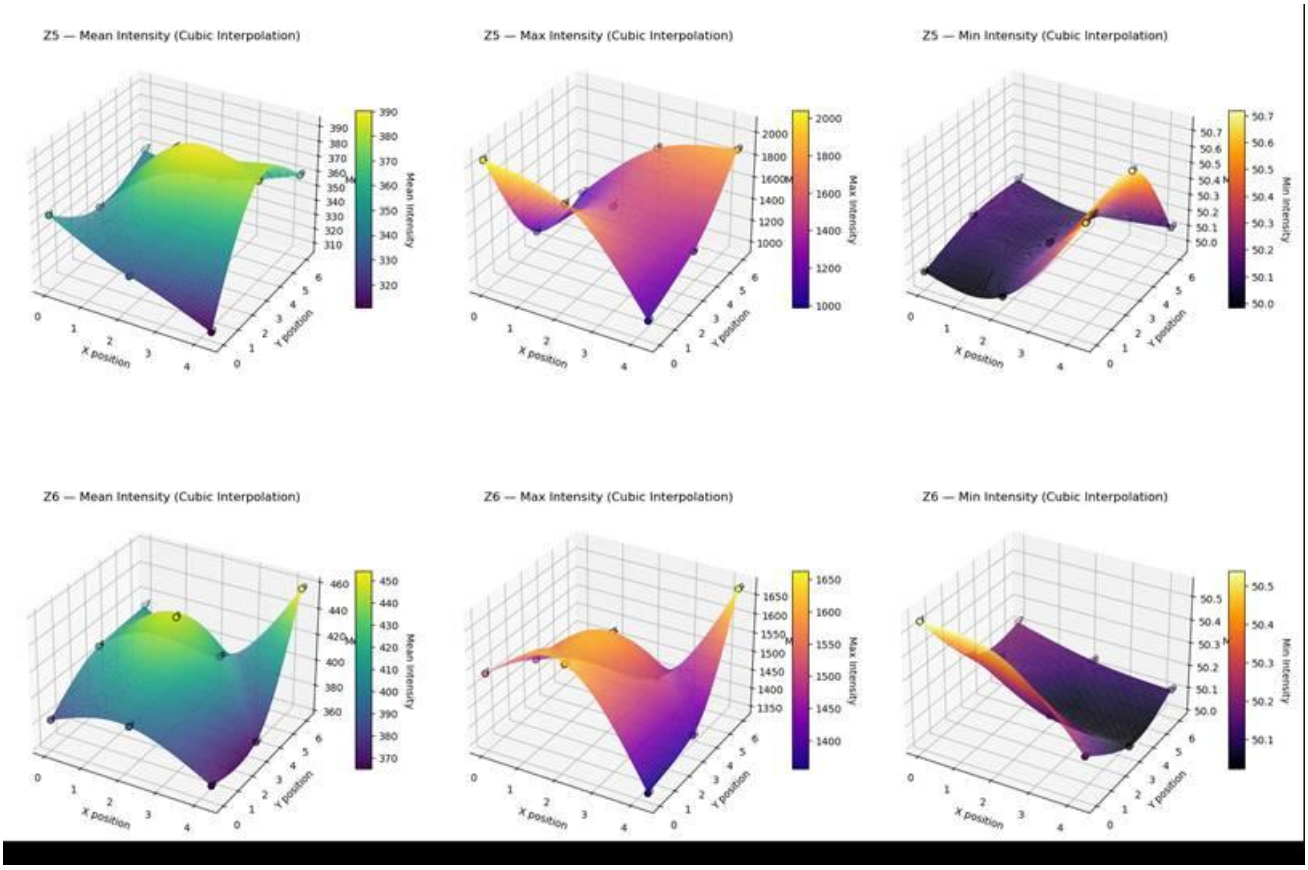

Figure 5.4 Comparison between zone 5 and 6.

Spatial Radiation Distribution (Zone-Based Analysis)

The 96-sensor grid enables detailed radiation mapping at zonal level, supporting the calculation of light uniformity and the detection of fine-scale shading micro-patterns. Here below some example of various PV configurations are provided.

In the 6.25% PV coverage configuration, **clear differences emerge between zones**:

- The diffuse zone (Z1) exhibits lower variability and smoother radiation gradients
- the clear-glass zone (Z2) shows higher variability, with pronounced peaks and troughs closely linked to solar angle dynamics.

Under the 12.5% PV configuration, the same spatial patterns persist but with amplified effects. In this case, diffuse glass continues to stabilise the spatial distribution of radiation, despite a larger average reduction in PAR associated with the higher PV density.

In the control configuration without PV modules (0% PV), the comparison between diffuse coating and clear glass further highlights the uniformity benefits of diffuse glass, demonstrating improved radiation homogeneity even in the absence of photovoltaic shading.

The results are illustrated in Figures 5.5 and Table 5.1 below.

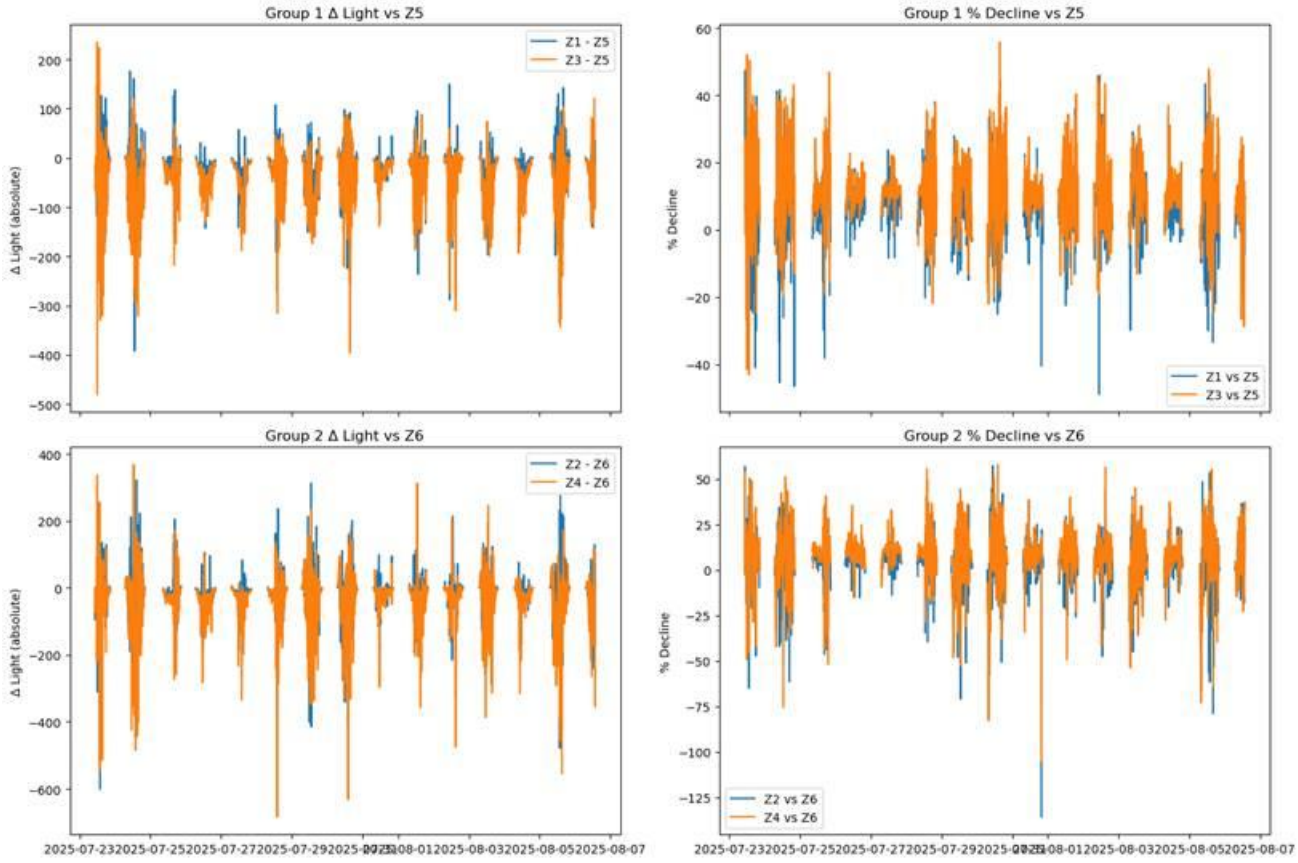

Figure 5.5 Radiation difference & percentage decline.

Zone	Glass Type	PV Density	Avg % Decline	Median % Decline	Std % Decline
Z1	Fotoniq	6.25%	7.27	7.60	9.48
Z3	Fotoniq	12.5%	11.82	11.53	9.59
Z2	Clear	6.25%	4.51	6.06	14.46
Z4	Clear	12.5%	8.34	10.22	14.99

Table 5.1 Radiation difference & percentage decline table with results.

Crop Impact and Modelling Approach

The **first year of monitoring** at the Netherlands Agri PV demonstrator provides a scientifically robust basis for analysing the impact of PV integration on greenhouse crop performance. As no crops were cultivated within the demonstrator, **all agronomic assessments are fully model-driven.**

Modelling Framework

The crop impact analysis integrates **measured PAR datasets from the Lotsweg demonstrator at different temporal and spatial resolutions**, including hourly, daily, and spatially resolved measurements.

These data are combined with literature-based DLI requirements for representative crops and with the light interception and modelling approaches developed in WP2.
The analysis includes explicit scenario comparisons across different PV surface densities (0%, 6.25%, and 12.5% of PV coverage) and different glass types (diffuse versus clear).
Hourly PAR values are also aggregated into daily light integrals (DLI), after which differences between control and PV scenarios (ΔDLI) are calculated. These DLI reductions are subsequently translated into expected yield impacts using established literature elasticities, typically assuming a yield reduction of 0.7–1.0% per 1% loss in DLI. The modelling framework excludes CO_2 interactions, crop acclimation processes, and LED supplementation—which is addressed separately—and assumes a homogeneous crop canopy with a direct mapping between light reduction and yield response.

Key Insights from Radiation and Modelling

The first-year radiation and modelling results highlight several key insights:

- **Diffuse glass** was found to significantly improve light uniformity within the greenhouse, thereby stabilising crop light conditions;
- **Clear glass** maximises total PAR but introduces substantially higher spatial and temporal variability;

PV shading effects scale linearly with PV density, with a 12.5% coverage resulting in approximately 1.7 times the light reduction observed at 6.25% coverage.
In general, the results demonstrate that light uniformity is at least as critical as total PAR in ensuring modelling accuracy. Overall, the dataset provides a robust empirical basis that is well suited for WP2 model calibration and for scenario evaluation within WP7.

Modelled Crop Impact

Based on the obtained results from the scenario analyses it is possible to observe clear crop-dependent responses to PV-induced light reduction. The magnitude of the expected yield impact varies significantly as a function of crop light requirements, seasonal radiation availability, and the interaction between DLI reduction and light variability. Crops with higher light demand are expected to have a stronger sensitivity to both absolute DLI losses and fluctuations in light distribution, whereas low-light crops are expected to remain largely resilient within the investigated PV density ranges.

For **high-light crops, such as tomato, cucumber, pepper, and eggplant**, the modelling indicates a pronounced response to agrivoltaic shading:

- At a PV coverage of 6.25%, the expected yield reduction ranges from approximately 4% to 8%
- At a PV coverage of 12.5% the expected yield reduction ranges from approximatively 8 to 15.

These crops are highly sensitive not only to reductions in total DLI, but also to increased spatial and temporal variability in incident radiation, making light management and uniformity critical factors for maintaining yield stability.

Medium-light crops, exemplified by strawberry, show an intermediate response. The expected yield reduction typically falls within a range of approximately 5–10%, with a strong dependence on seasonal light availability.
In these crops, the interaction between PV-induced shading and background climatic conditions plays a key role, meaning that yield impacts may vary substantially across seasons and locations.

In contrast, **low-light crops, such as lettuce and herbs**, appear largely tolerant to the investigated levels of PV integration. The expected yield impact remains in the order of 0–5%, generally falling within acceptable agronomic tolerance ranges. This resilience reflects both lower intrinsic light requirements and a greater capacity to maintain productivity under reduced and diffuse radiation conditions.

Across all crop categories, diffuse glass emerges as a critical design element, as it DLI and moderates physiological stress, even when total light levels are slightly reduced. By improving light uniformity and reducing short-term radiation variability, diffuse glass contributes to more predictable crop responses.

Seasonal Effects

Seasonality emerges as a dominant factor in determining the magnitude of PV-induced impacts on crop performance.

- During **winter and shoulder seasons**, background radiation levels are inherently low, making crops particularly sensitive to additional light deficits introduced by photovoltaic shading. Under these conditions, even moderate reductions in DLI can translate into proportionally larger impacts on crop development and yield.
- In contrast, during **summer**, the high absolute availability of solar radiation substantially reduces the relative impact of PV integration. Elevated DLI levels allow crops to better tolerate partial shading, resulting in a smaller relative yield penalty for the same PV density.
- The **spring and autumn periods** represent transitional phases characterised by increasing variability in radiation availability. During these seasons, crop responses are more heterogeneous and strongly influenced by short-term fluctuations in weather conditions, solar angle, and day length. This increased variability amplifies uncertainty in crop.

As a consequence, crop simulations and impact assessments must be evaluated **on a seasonal basis rather than using annual averages**, as aggregated annual metrics risk masking critical periods of sensitivity and may underestimate agronomic risks during low-radiation phases.

LED Supplementation and Compensation Strategies

To mitigate PV-induced light reduction, LED supplementation is implemented as a core strategy within the Agri-PV greenhouse concept. The objective of this approach is to compensate for reductions in DLI caused by photovoltaic shading while maintaining stable crop growth conditions and aligning energy consumption with on-site renewable energy production, as exposed in the subsections below.

Modelling Approach

LED performance is modelled using photometric IES files generated by ENGIE and integrated into KUBO's parametric 3D modelling environment. This framework allows a physically consistent representation of light distribution from artificial sources and enables the simulation of combined PV shading and LED supplementation scenarios.

The compensation model follows four sequential steps:

1. First, the **DLI deficit is determined** for each zone by comparing PV scenarios with the corresponding control conditions (ΔDLI).
2. Second, the **DLI deficit is converted into the required supplemental PAR provided by LEDs (PAR_LED)** on an hourly basis.
3. Third, the **LED fixture configuration is optimised** in terms of spacing, mounting height, overlap, and light uniformity to ensure effective and homogeneous compensation at crop level.
4. Finally, the **energy balance between LED electricity consumption and PV energy production is evaluated.**

Together, these steps enable a dynamic assessment of light compensation strategies under different design and operational conditions.

First-Year Compensation Results

First-year modelling results show that the level of LED supplementation required increases with PV density. More in detail, results can be summarized as follows based on PV density:

- At a PV coverage of 6.25%, the simulated DLI deficit ranges approximately between 4% and 8%, corresponding to a required LED contribution of about 15–25 µmol m^{-2} s^{-1}.
- At a PV coverage of 12.5%, the DLI deficit increases to approximately 8–15%, requiring higher supplemental light levels in the range of 30–45 µmol m^{-2} s^{-1}.

Across all analysed scenarios, diffuse glass plays a critical role in reducing LED demand by stabilising natural light distribution and lowering peak DLI deficits. In contrast, clear glass configurations require higher levels of LED compensation due to increased spatial and temporal variability in incident radiation and more localised shading patterns.

Energy Considerations

The **energy balance associated with LED supplementation** is strongly season-dependent:

- During **winter** periods, LED demand often exceeds on-site PV production, resulting in a net energy deficit that must be supplied externally.
- Conversely, during **summer**, PV overproduction can partially or fully offset LED electricity consumption.

As a result, the net energy balance of the system is both crop- and season-specific.

Overall, LED supplementation emerges not merely as a technical solution, but as an optimisation problem that requires balancing crop yield preservation, energy use, and system design. Effective integration of LEDs within agrivoltaic greenhouses therefore depends on coordinated optimisation of PV density, glazing properties, crop selection, and seasonal operating strategies.

5.2. Conclusions and Perspectives

Key Conclusions

The results of the first-year monitoring and modelling activities confirm that **PV-induced shading** is measurable, predictable, and scales linearly with PV density.

The analyses demonstrate that **diffuse glass** significantly improves light uniformity within greenhouse environments, enhancing modelling reliability and stabilising crop light conditions. In contrast, **clear glass** configurations maximise total PAR but introduce undesirable spatial and temporal variability, which increases uncertainty in crop response.

DLI-based modelling indicates expected yield reductions in the range of 4–15%, depending on crop type and PV surface coverage, with high-light crops being the most sensitive. At the same time, the results show that **LED supplementation can fully compensate DLI deficits** when properly configured, restoring target light levels at crop level.

Overall, the dataset generated during the first operational year provides high-quality validation input for WP2 model calibration and WP7 scenario evaluation.

Design Implications

The findings indicate that **PV surface densities in the range of 6–12% are technically feasible** within greenhouse systems. However, the range of applicable configurations remains limited, and structural implications—such as load distribution, roof design, and integration constraints—must be carefully assessed during the design phase.

Based on the results, **diffuse glass** is strongly recommended due to its stabilising effect on both light distribution and crop response.

Furthermore, **LED supplementation strategies must be crop-specific**, particularly for high-light crops, where sensitivity to DLI reductions is greatest.

Finally, **energy consumption trade-offs must be evaluated on a seasonal basis** and within the context of an overall business case, as the balance between PV production and LED demand varies significantly throughout the year.

Outlook

Future challenges of work will be to focus on extending the current findings through **multi-season dataset expansion**, allowing seasonal effects and inter-annual variability to be assessed more robustly. The integration of crop-specific DLI requirements will be essential to further refine system design and ensure that greenhouse agrivoltaic solutions are appropriately tailored to different crop categories.

In parallel, **integration of the modelling framework into the early-stage design tool providing** a feasibility check, can support informed decision-making in a greenhouse sector that remains highly cautious about reducing light availability.

Additional efforts will target the **replication of scenarios across different climatic contexts**, as well as the further **optimisation of LED supplementation strategies**.

Based on the current measurements and available data, a well-founded decision can already be made on the application of Agri-PV in greenhouse systems without the need for full-scale crop trials, as the effects of light reduction on crop performance are well understood and can be reliably captured through combined measurement-and-modelling approaches.